HELLENIC REPUBLIC
National and Kapodistrian University of Athens
EST. 1837

Inter-Institutional MSc in

"Oceanography and Management of the Marine Environment"

MASTER THESIS

Oil spill forecasting systems uncertainty assessment in the Aegean Sea

---

Konstantinos Kampouris

(21815)

Supervisor: Sarantis Sofianos, Assoc. Prof.

Athens, October 2020

Abstract

The Aegean Sea is one of the world's busiest waterways, combined with complex and intense weather and sea current patterns with strong seasonality, complicated coastline and bathymetry. Therefore, the uncertainty assessment of the oil spill forecasting systems in this region is of great interest. The purpose of this study is to evaluate the impact of the uncertainty of the atmospheric forcing on the performance of the oil spill modelling and the dispersion of the pollutants in the marine environment. Ensemble simulations were carried out using the ECMWF Ensemble Prediction System and the oil spill model MEDSLIK II. The Aegean Sea was chosen as the study area performing ensembles of 50 members with seven days forecast lead time, during different seasons. Three types of oil were chosen representing lighter, medium and heavier oil spills, covering also a wide range of oil densities. The oil spill duration and the spill rate were chosen taking into account significant accidents of the past like for instance the Prestige case. Results suggest that the model errors in the oil spill trajectories are sensitive to the atmospheric forcing uncertainties. An ensemble approach assuming model errors in the atmospheric forcing shows great potential for predicting several possible pathways of oil spill transport, which could provide important information for the control and mitigation strategies, in the event of an oil spill accident.

Keywords: Aegean Sea, MEDSLIK II, oil spill, ensemble simulation, uncertainty

Περίληψη

Το Αιγαίο είναι ένας από τους πιο πολυσύχναστους θαλάσσιους διαύλους του κόσμου, συνδυάζοντας πολύπλοκη και έντονη ατμοσφαιρική και θαλάσσια κυκλοφορία με έντονη εποχικότητα, περίπλοκη ακτογραμμή και βαθυμετρία. Επομένως, η εκτίμηση της αβεβαιότητας των συστημάτων πρόγνωσης διασποράς πετρελαιοκηλίδων στην περιοχή αυτή έχει μεγάλο ενδιαφέρον. Σκοπός της παρούσας μελέτης είναι να εκτιμηθεί το αντίκτυπο της αβεβαιότητας των ατμοσφαιρικών δράσεων στην απόδοση του μοντέλου διασποράς πετρελαιοκηλίδας και στην διασπορά των ρύπων στο θαλάσσιο περιβάλλον. Πραγματοποιήθηκαν προσομοιώσεις τύπου «ανσάμπλ» χρησιμοποιώντας δεδομένα του ECMWF Ensemble Prediction System και το αριθμητικό μοντέλο MEDSLIK II. Το Αιγαίο Πέλαγος επιλέχθηκε ως περιοχή μελέτης όπου πραγματοποιήθηκαν «ανσάμπλς» 50 μελών, διάρκειας 7 ημερών σε διαφορετικές εποχές. Επιλέχθηκαν τρεις τύποι πετρελαίου που αντιπροσωπεύουν ελαφρές, μεσαίες και βαρύτερες πετρελαιοκηλίδες, καλύπτοντας επίσης ένα ευρύ φάσμα πυκνοτήτων πετρελαίου. Η διάρκεια και ο ρυθμός διαρροής του πετρελαίου επιλέχθηκαν λαμβάνοντας υπόψη τα σημαντικά ατυχήματα του παρελθόντος, όπως το ατύχημα του Prestige. Τα αποτελέσματα υποδεικνύουν ότι τα σφάλματα του μοντέλου στις τροχιές της πετρελαιοκηλίδας είναι ευαίσθητα στην αβεβαιότητα των ατμοσφαιρικών δράσεων. Μία προσέγγιση τύπου «ανσάμπλ» που θεωρεί σφάλματα του μοντέλου στις ατμοσφαιρικές δράσεις παρουσιάζει μεγάλες δυνατότητες για την πρόβλεψη πολλών πιθανών «μονοπατιών» μεταφοράς πετρελαίου, τα οποία θα μπορούσαν να παρέχουν σημαντικές πληροφορίες για τις στρατηγικές ελέγχου και μετριασμού, σε περίπτωση ενός ατυχήματος πετρελαιοκηλίδας.

Λέξεις-κλειδιά: Αιγαίο Πέλαγος, MEDSLIK II, πετρελαιοκηλίδα, προσομοίωση «ανσάμπλ», αβεβαιότητα

Acknowledgments

First and foremost, I would like to thank my professor and supervisor, Sarantis Sofianos, for the opportunity of working on such an interesting subject and for providing guidance and feedback throughout this thesis. I would also like to thank Vasileios Vervatis and Ioannis Karagiorgos for their assistance and dedicated involvement in every step throughout the process of researching and writing this thesis. Finally, I must express my very profound gratitude to my colleagues, friends, and family, whose continuous support and encouragement have been invaluable during the last year.

Contents

List of Figures

1. Introduction

1.1. Introduction

Although unintentional oil pollution caused by ships is declining over the years, increased oil shipments may pose an increased risk. In the event of an oil spill, oil spill modelling predictions serve as the initial/forefront tools to assist regional and national contingency plans (Zodiatis et al., 2017). The behavior of some environmental variables may alter the physical and chemical processes acting on oil spills. Uncertainties related to parameters like met-ocean conditions, influence the transportation and weathering of oil and the accuracy of oil spill modelling predictions. Thus, the identification of such factors, the analysis of their sensitivity and the validation of the oil spill models are necessary for the improvement of oil spill forecasts.

Wind is a major error source of oil spill transport modelling, especially for long time simulations. Incomplete knowledge of the initial conditions of the atmosphere and unavoidable simplifications of the equations used to describe the complexity of the weather, due to limitations in computer power, are the major sources of uncertainty in numerical weather predictions. A good method to overcome this problem and improve the accuracy of oil spill modelling is to follow an alternative approach shifting from a deterministic to a probabilistic approach, using an ensemble of wind predictions. The basic idea of ensemble-based forecasts is the representation of the atmospheric state, by a number of different, but equally possible model forecasts, created by perturbed initial conditions and/or state variables. The ensemble spread can be regarded as a proxy of the model uncertainties in the forecast. A large spread indicates large model errors in the prediction and yields several forecast predictions increasing the possibility some of them to be closer to the true (unknown) state (fig. 1.1).

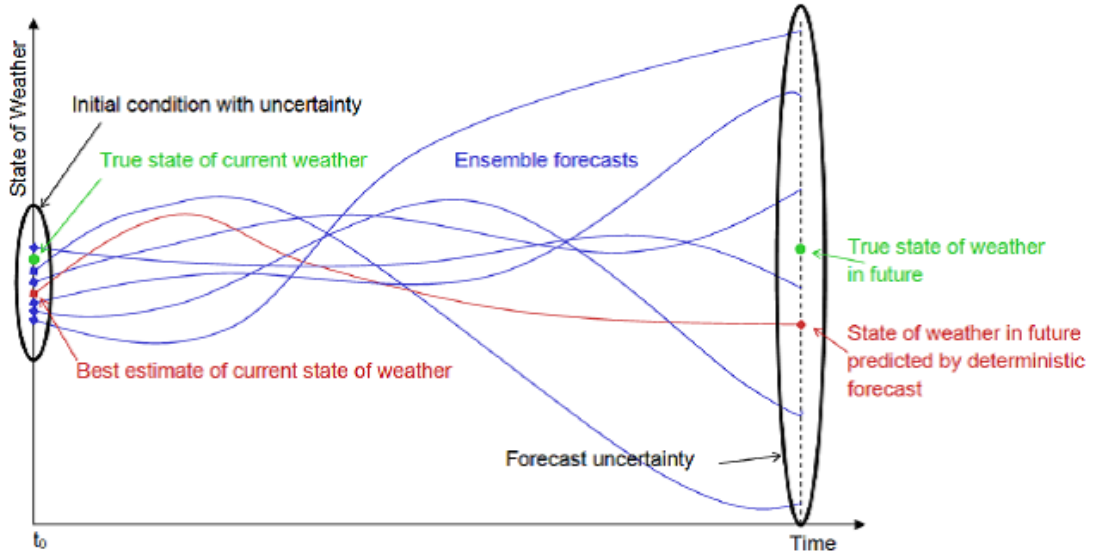

Figure 1.1: Uncertainty captured in an Ensemble Weather Forecast. Reprinted from "Recommendations on trajectory selection in flight planning based on weather uncertainty" by Cheung et al. (2015), SESAR Innovation Days.

Ensemble oil spill simulations have been used in the past mainly to access the risk of oil spills and their potential environmental impacts. Hazard mapping was used to quantify this risk by Sepp Neves et al. (2020), Al Shami et al. (2017), Sepp Neves et al. (2016), Liubartseva et al. (2015), Goldman et al. (2015), Jiménez Madrid et al. (2016), Price et al. (2003), Olita et al. (2019), Amir-Heidari et al. (2019). Perturbed forcing fields have been used to assess the impact of forcing errors in an oil spill forecasting system by Jorda et al. (2007), while a stochastic approach has been used for the forecast of the transport and transformations of a point mass oil spill by B.J. Snow et al. (2014). Furthermore, important work has been done, to demonstrate the potential of ocean ensemble forecasting, using the ensemble approach for the atmospheric forcing for the Deep Water Horizon oil spill case, in the Gulf of Mexico (Khade et al., 2017).

1.2. Study area

1.2.1. Risk of marine oil pollution in the Aegean Sea

Maritime transport is a major source of pollution from oil and polycyclic aromatic hydrocarbons (PAHs) in the Mediterranean Sea, and it has been shown that the distribution of oil spills is associated with the major shipping routes (UNEP/MAP, 2012) (fig. 1.2 & 1.3). The total activity of vessels in the Mediterranean has been steadily increasing in recent years and is expected to continue over the next decade. Increasingly larger merchant vessels operate within and through the Mediterranean, transporting more goods. As seen in fig. 1.3, the main oil transport route (90% of the total traffic), extends from the eastern to the western Mediterranean and connects the passages of the Dardanelles Strait and the Suez Canal, with the Straits of Gibraltar.

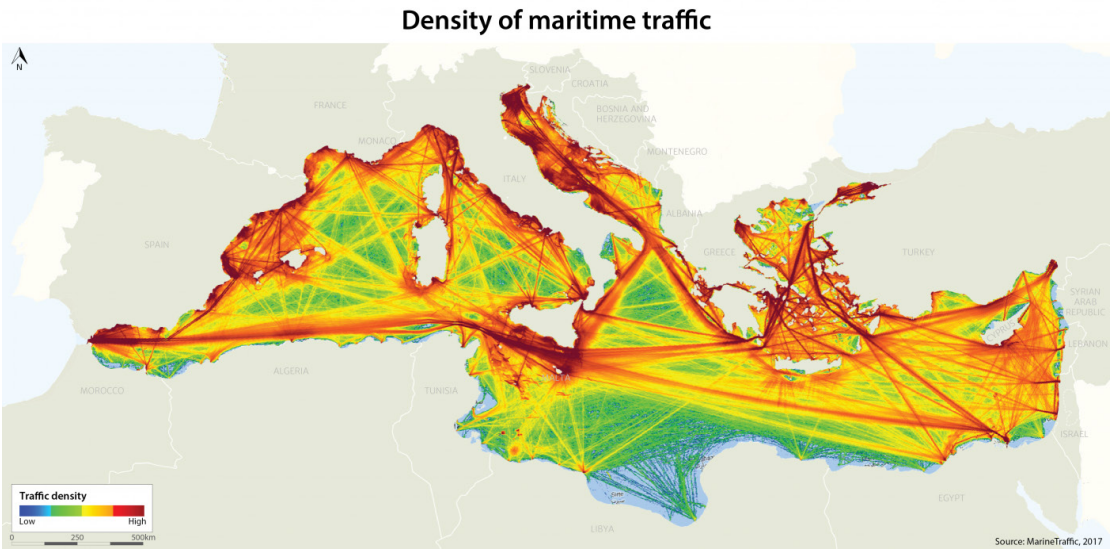

Figure 1.2: Density of maritime traffic in the Mediterranean Sea (Source: MarineTraffic, 2017). Reprinted from "Environment Programme, Mediterranean Action Plan Barcelona Convection".

The Aegean in particular, as one of the world's busiest waterways, has a relatively high probability of occurrence of significant oil spills. It is also important here to mention the large number of maritime accidents in relation to other areas of the Mediterranean (EMSA, 2019) (fig. 1.4). Kafireas Strait, which was chosen as the study area, is a channel for one of the main traffic routes in the Mediterranean, especially for the transportation of crude oil from Novorossiysk in the Black Sea, to destinations in the Mediterranean Sea, through the straits of the Dardanelles.

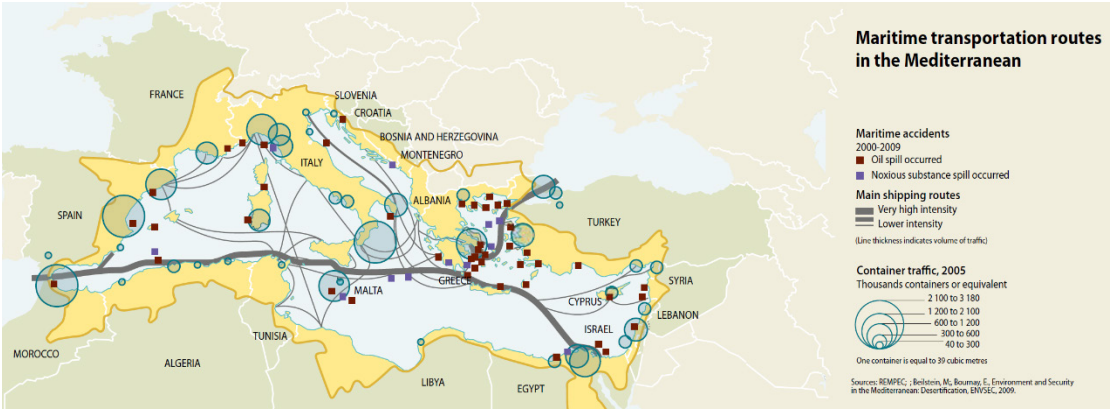

Figure 1.3: Maritime transportation routes in the Mediterranean. Reprinted from "UNEP/MAP: State of the Mediterranean Marine and Coastal Environment", UNEP/MAP – Barcelona Convention, Athens, 2012.

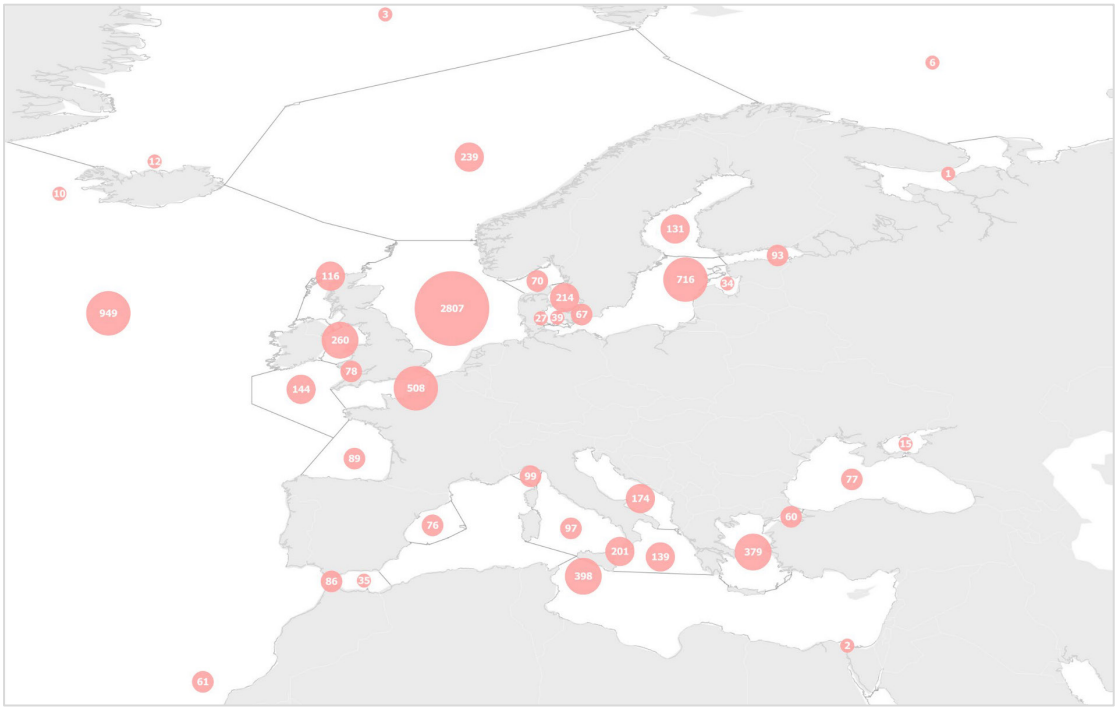

Figure 1.4: Distribution of marine casualties and incidents within sub-sea areas around EU waters for 2011-2018. Reprinted from "Annual Overview of Marine Casualties and Incidents 2019", by European Maritime Safety Agency (EMSA).

1.2.2. Physical properties and geography of the Aegean Sea

The Aegean Sea is located in the Northeastern part of the Mediterranean and is bordered to the west and north by the coasts of Greece, to the east by the coasts of Turkey and to the south by the island of Crete. The Aegean Sea is connected through the straits of the Dardanelles and Bosporus to the Marmara and Black Seas. It is a basin with complex and intense weather and sea current patterns with strong seasonality, complicated coastline and bathymetry (fig. 1.5). Therefore, the uncertainty assessment of the oil spill forecasting systems in this region is of great interest.

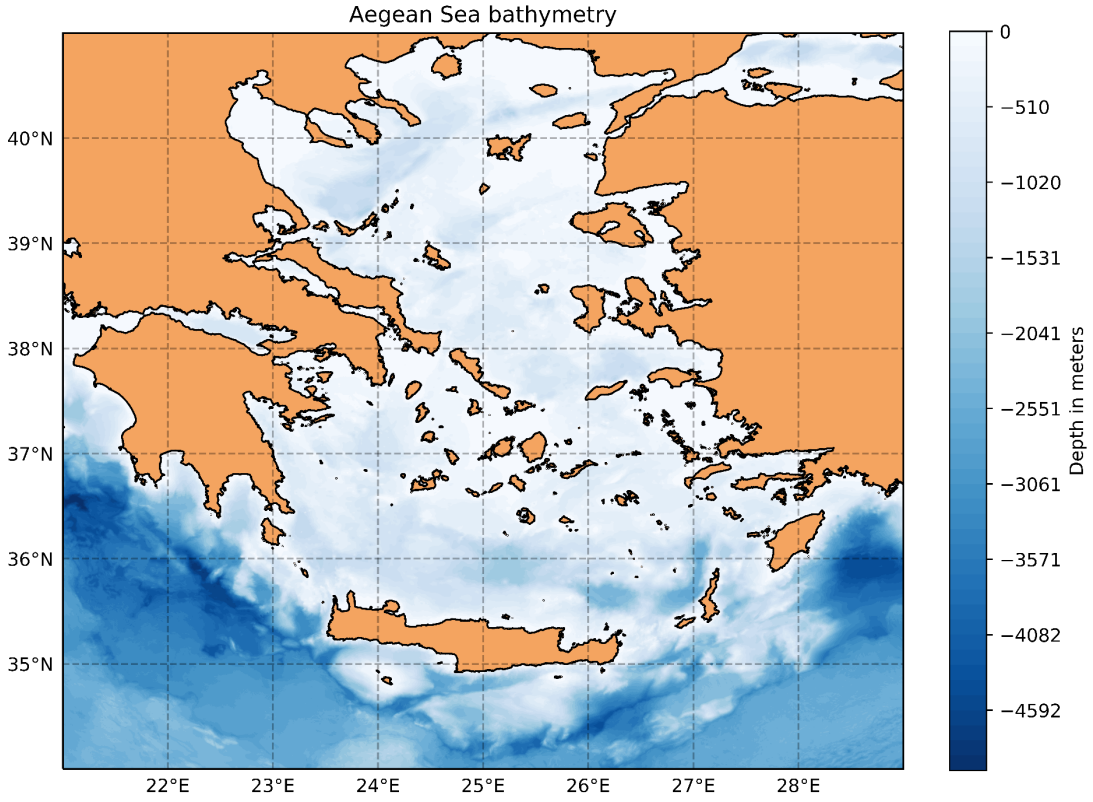

Figure 1.5: Bathymetry and coastlines of the Aegean Sea.

The surface water circulation of the Aegean Sea (fig. 1.6) is characterized by a generally cyclonic circulation on the scale of the basin, cyclonic and anticyclonic mesoscale gyres and transient eddies. Seasonal changes in meteorological conditions, the complex topography and bathymetry of the area, the inflow of lower temperature and salinity water from the Black Sea and the outflow of rivers in Greece and Turkey create a complex circulation that changes temporally and seasonally. Perhaps the most important feature of the circulation is the low salinity waters of the Black Sea (BSW)

that enter the Aegean through the straits of the Dardanelles. After its entry into the Aegean, this water mass generally follows a cyclonic course. From the Dardanelles it continues in a westerly direction, passing North of Lemnos, south of Halkidiki and then southwestward moving along the island of Euboea, as it finally enters the south Aegean through the strait of Kafireas and the strait of Mykonos-Ikaria.

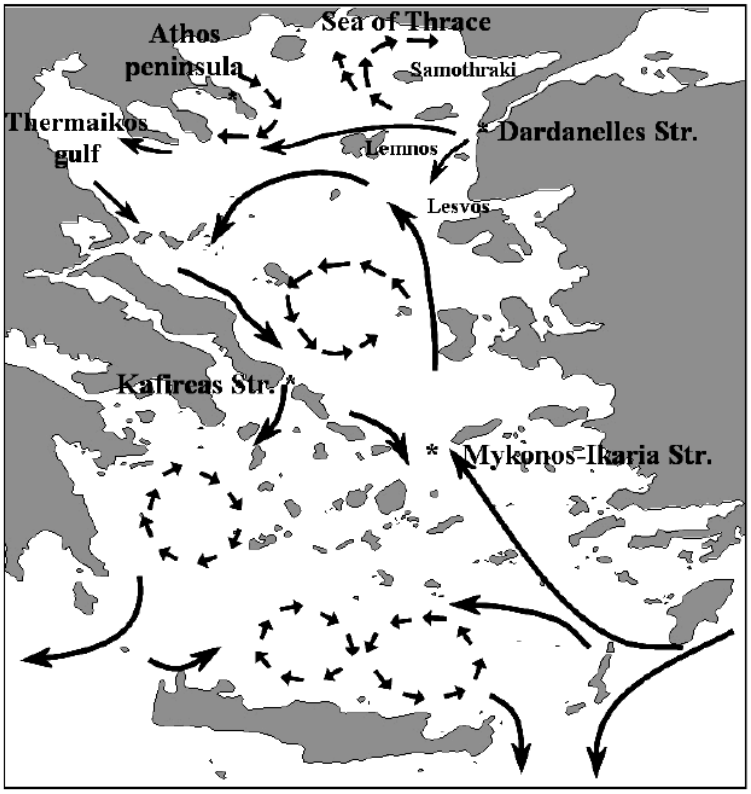

Figure 1.6: Schematic representation of the Aegean Sea upper circulation. Reprinted from "Circulation and hydrological characteristics of the North Aegean Sea: a contribution from real-time buoy measurements" by NITTIS, K., & PERIVOLIOTIS, L. (2002), Mediterranean Marine Science.

The wind field of the Aegean Sea is dominated mainly by north winds with average monthly values ranging from 3 m/s to > 7.5 m/s. These north winds show an annual fluctuation with two maximums: one in winter during the period from December to February and one in summer from July to August. During the winter, strong, cold and dry north winds blow over the Aegean Sea, while occasionally south winds may occur. During the warm season, the wind field is dominated by the Etesian Winds, a system of strong and dry north winds (Poulos et al., 1997).

1.3. Objectives

The purpose of this study is to evaluate the impact of the atmospheric forcing uncertainty on the performance of the oil spill modelling and the transport of the pollutants in the marine environment. To that end, we use a probabilistic approach for the simulation of the oil spill by using an ensemble of wind predictions (based on the ECMWF EPS) and generate an ensemble of oil spill forecasts. Finally, after evaluating this impact, we try to answer if the ensemble approach for the oil spill prediction can provide additional information with respect to a deterministic approach, providing the decision-makers with a picture of several equally possible outcomes, to better plan the mitigation procedures in the event of an oil spill.

2. Methodology

2.1. Model description

The numerical model MEDSLIK II (De Dominicis et al., 2013a), (De Dominicis et al., 2013b), is a freely available community model, which is based on its precursor the oil spill model MEDSLIK (Lardner et al. 1998, Lardner et al. 2006, Zodiatis et al. 2005, Zodiatis et al. 2008). It is designed to predict the transport and weathering of an oil spill, caused by complex physical processes occurring at the sea surface, using a Lagrangian representation of the oil slick. This numerical representation requires the following different state variables: the oil slick, the particle and the structural state variables, which are all used for different calculations. The transformation and movement of an oil slick depend on many factors, the main ones being: meteorological and oceanographic conditions at the air-sea interface, the marine currents in the oil spill area as well as the chemical characteristics, the initial volume and the rate of oil release.

A brief description of the basic equations used by MEDSLIK II is given below based on De Dominicis et al. (2013a), De Dominicis et al. (2013b) and Zodiatis et al. (2017), and a schematic representation of the model's solution procedure methodology can be seen in fig. 2.1. Over time, as the oil moves, its concentration changes due to physical and chemical processes also known as "weathering", e.g. evaporation, emulsification, dispersion in the water column and viscosity changes. The general equation for calculating the oil concentration C (x, y, z, t) in the marine environment is:

$$\frac{\partial C}{\partial t} + \boldsymbol{U} \cdot \nabla C = \nabla \cdot (\boldsymbol{K} \nabla C) + \sum_{j=1}^{M} r_j(\boldsymbol{x}, C(\boldsymbol{x}, t), t) \qquad (1)$$

where $\partial C/\partial t$ is the time rate of oil concentration change, **U** is the sea current mean field with components (U, V, W), **K** is the diffusivity tensor which parameterizes the turbulence and $r_j(C)$ are the number of M transformation rates that change the oil concentration due to physical and chemical transformation processes.

The solution of the above equation and the calculation of the evolution of the oil concentration based on a Lagrangian formalism, is based on the following fundamental assumptions:

- Water hydrodynamics and other processes generally are not influenced by the constituent particles.
- The constituent particles behave like water parcels, moving through infinitesimal displacements with the absence of inertia and with no interaction among themselves.
- Physical and chemical processes modify the volume associated with each particle, by acting on the entire slick rather than on the properties of every single particle.

Based on these assumptions, Eq. 1 is divided into two components:

1. The transformation equation due to "weathering":

$$\frac{\partial C_1}{\partial t} = \sum_{j=1}^{M} r_j(\boldsymbol{x}, C_1(\boldsymbol{x}, t), t) \tag{2}$$

where C_1 is the concentration of oil due to "weathering" processes. The transformation processes act on the total volume of the oil slick and the oil slick state variables are defined. The "weathering" processes are calculated through Mackay et al. (1980) fate algorithms. In order to be used, the surface volume of the oil slick is divided into a thin part, V_{TN}, at the edges of the oil slick, and a thick part, V_{TK}, near its center.

2. The advection-diffusion equation:

$$\frac{\partial C}{\partial t} = -\mathbf{U} \cdot \nabla C_1 + \nabla \cdot (\boldsymbol{K} \nabla C_1) \tag{3}$$

where the oil slick is discretized into a large number of particles, transported by sea currents, wind, waves and diffusion processes, with associated particle state variables, some of which are deduced from the oil slick state variables. Concentration C is subdivided into its following components, called structural state variables: The surface oil concentration, C_S, subsurface C_D, adsorbed on the shore, C_C and in bottom sediments C_B.

Finally, to fully solve the problem of advection-diffusion and transformation, of the general equation for calculating concentration (Eq. 1), a numerical grid must be determined where the particles can be measured and the concentration calculated.

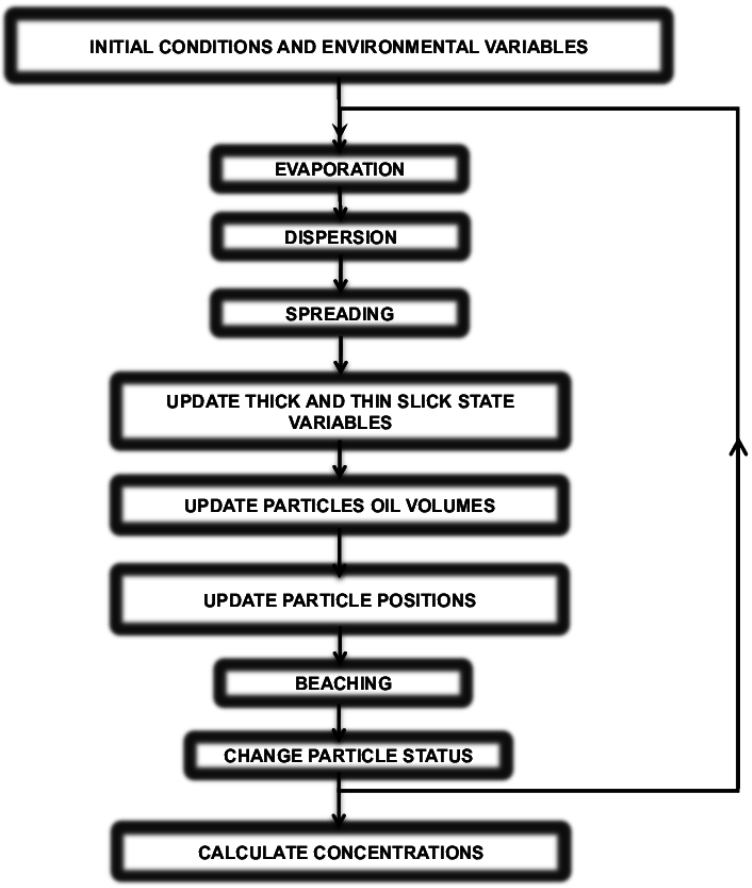

Figure 2.1: MEDSLIK-II model solution procedure methodology. Reprinted from "MEDSLIK-II, a Lagrangian marine surface oil spill model for short-term forecasting – Part 1: Theory" by M. De Dominicis et al. (2013), Geoscientific Model Development.

2.2. Model inputs – Data

As mentioned above, MEDSLIK-II requires the input of data on atmospheric winds, sea surface temperature, marine currents and information about the oil spill, in order to calculate the oil transport and transformation processes.

2.2.1. Oceanic forcing

For the oceanic forcing, daily three-dimensional currents were used (velocity and temperature), covering the area 18 ° E to 32 ° E and 32 ° N to 43 ° N, with depths from 1.0181 m up to 153.43 m. We selected two periods of seven-day simulations, the one in winter (mid-January 2017) and the other in spring (mid-May 2017). The input currents were interpolated to 1 h time step, which is used by the oil spill model MEDSLIK II.

The data were provided by the physical component of the Mediterranean Forecasting System (Med-Currents), a coupled hydrodynamic-wave model, whose outputs are freely available on the Copernicus Marine Environment Monitoring Service (CMEMS) portal (marine.copernicus.eu). The model covers the entire Mediterranean with a horizontal grid resolution of 1/24° (approximately 4 km) and 141 unevenly distributed vertical levels. Hydrodynamics is provided by NEMO v3.6 while the wave component is provided by Wave Watch-III.

Figures 2.2 and 2.3 present the rose diagrams of the daily surface sea current velocity, for a point near the starting position of the oil slick. Figure 2.2 shows the speed and direction of the surface sea current for the period from 2017-01-10 to 2017-01-16 (winter), while fig. 2.3 for the period from 2017-05-10 to 2017-05-16 (spring). The prevailing direction of the surface sea currents is south-southwest for both time periods, which is in agreement with the bibliography about the surface water circulation of the Aegean Sea, with values ranging from 0.1 to 0.4 m/s in winter and 0 to 0.5 m/s in spring.

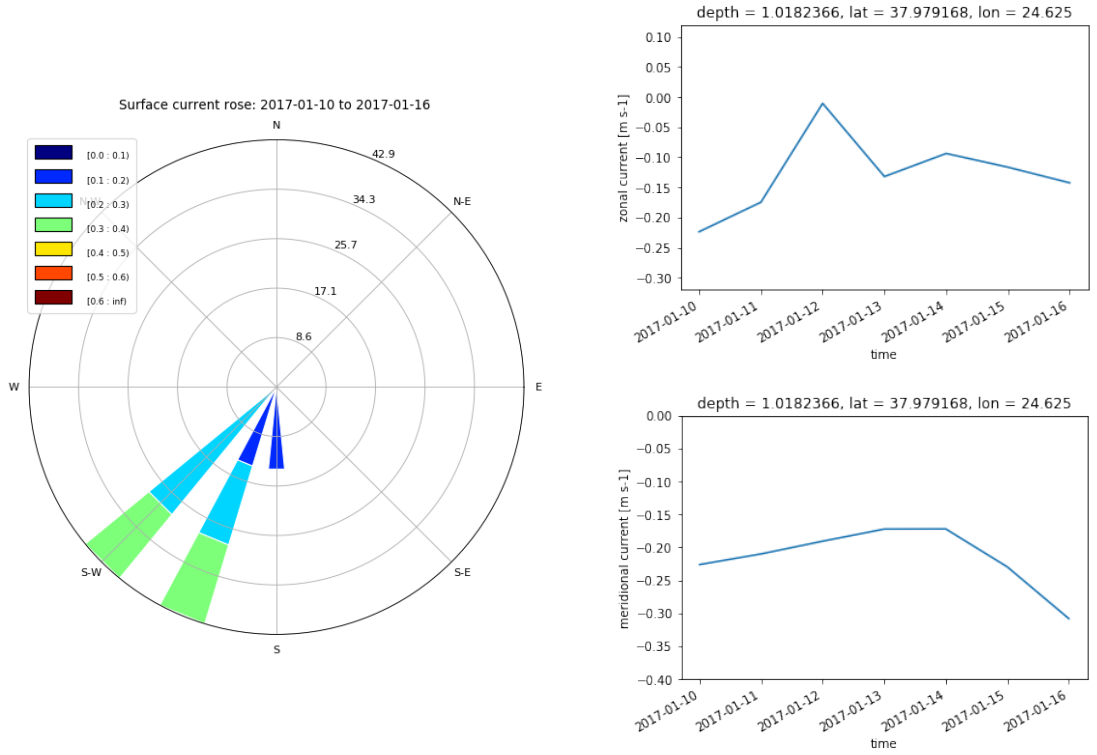

Figure 2.2: Surface current speed rose of the deterministic simulation for the time period: 2017-01-10 to 2017-01-16.

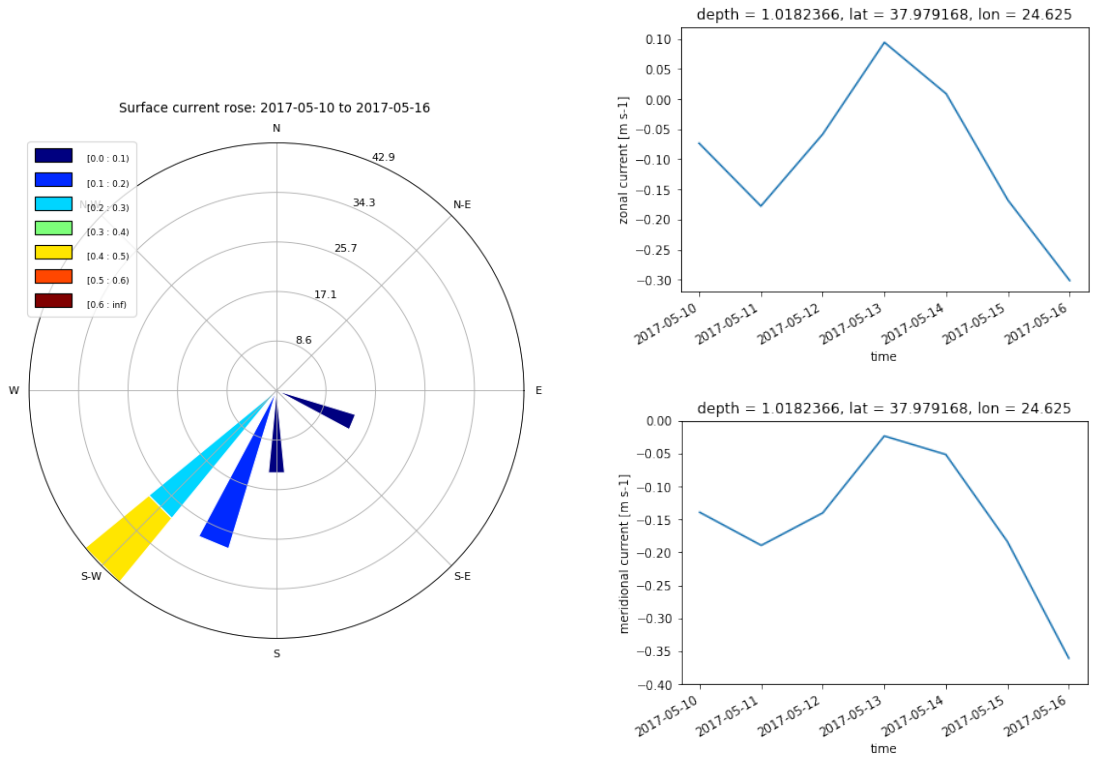

Figure 2.3: Surface current speed rose of the deterministic simulation for the time period: 2017-05-10 to 2017-05-16.

.

2.2.2. Wind forcing

For the wind forcing, 50 ensemble members of 3-h wind velocities were used, covering the area of 18 ° E to 32 ° E and 32 ° N to 43 ° N and a horizontal grid resolution of 9 km for the deterministic and 18 km for the ensemble members. Two periods of seven-day simulations were selected (mid-January 2017 and mid-May 2017). The input winds, like the three-dimensional currents, were also interpolated to 1 h time step, which is used by the oil spill model MEDSLIK II. The ensembles, which are used as a product in this study, were generated via the ECMWF Ensemble Prediction System (ECMWF EPS), a system used for the generation of probabilistic weather forecasts.

Figures 2.4, 2.5, 2.6 and 2.7 present the wind roses of the 3-h wind velocity at 10 m for a point near the starting position of the oil slick. Figure 2.4 shows the wind speed and direction of the deterministic simulation for the period from 2017-01-10 to 2017-01-16 (winter), while fig. 2.5 shows the total values of the wind speed and direction of the 50 ensemble members for the same time period. The prevailing wind direction is north-northeast, nearly opposite to the currents in the area, with a maximum value above 12 m/s for both wind roses. The total ensemble wind displays a larger variability of wind directions, as a result of the spread of the ECMWF ensembles.

Likewise, fig. 2.6 and 2.7, present the wind speed and direction of the deterministic simulation and the total ensemble values of the wind speed and direction of the 50 members respectively, for the period from 2017-05-10 to 2017-05-16 (spring). The prevailing wind direction is to the south, with a maximum value between 8 to 10 m/s. In spring, the intensity of the wind is lower than the winter and the prevailing wind direction is closer to that of the currents in the area. Also, the differences between the deterministic and the total ensemble, as well as the spread of the wind velocity values, are lower than the winter case.

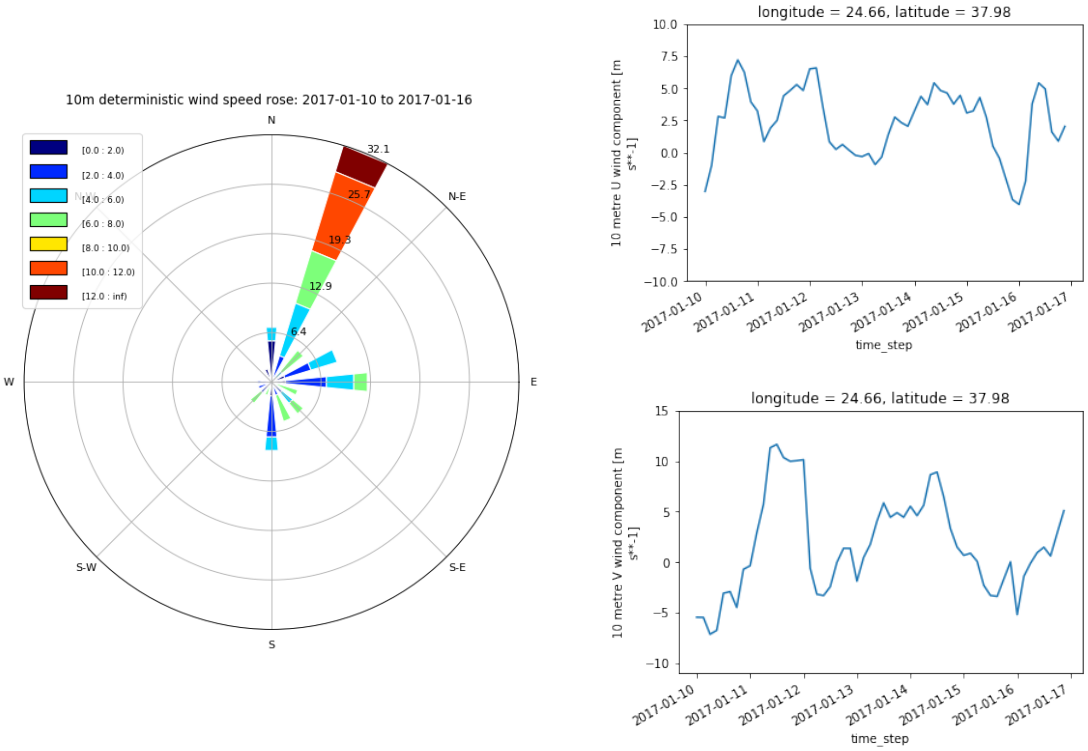

Figure 2.4: Wind speed rose at 10m of the deterministic simulation for the time period: 2017-01-10 to 2017-01-16.

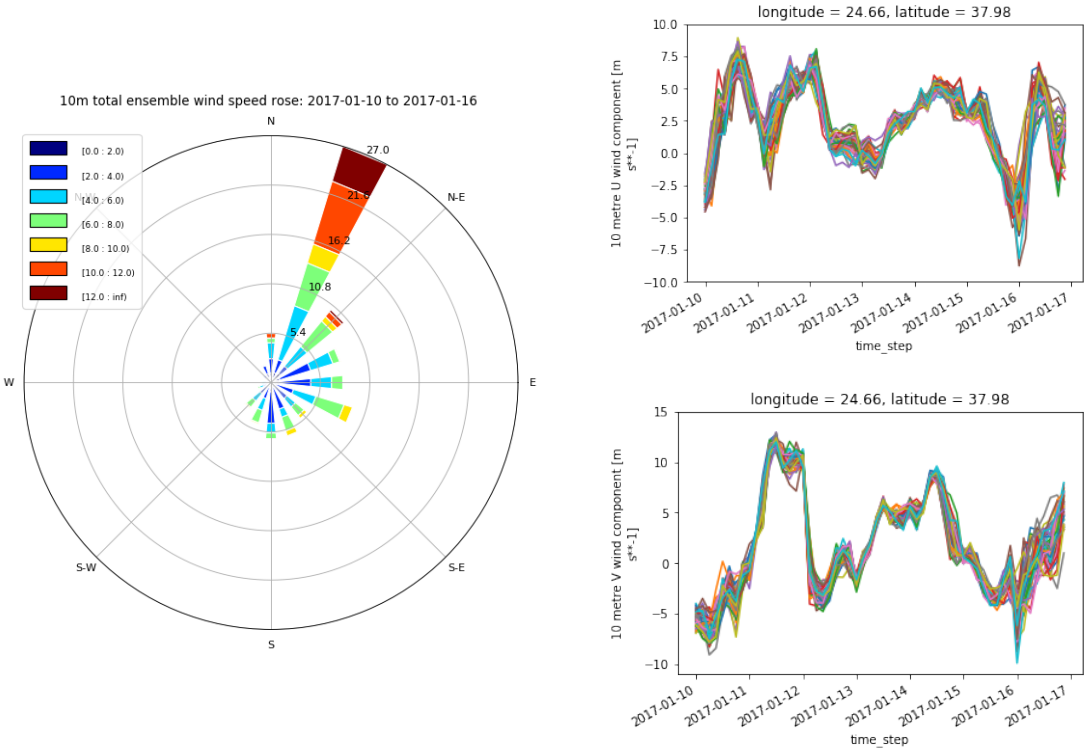

Figure 2.5: Wind speed rose at 10m of the total ensemble for the time period: 2017-01-10 to 2017-01-16.

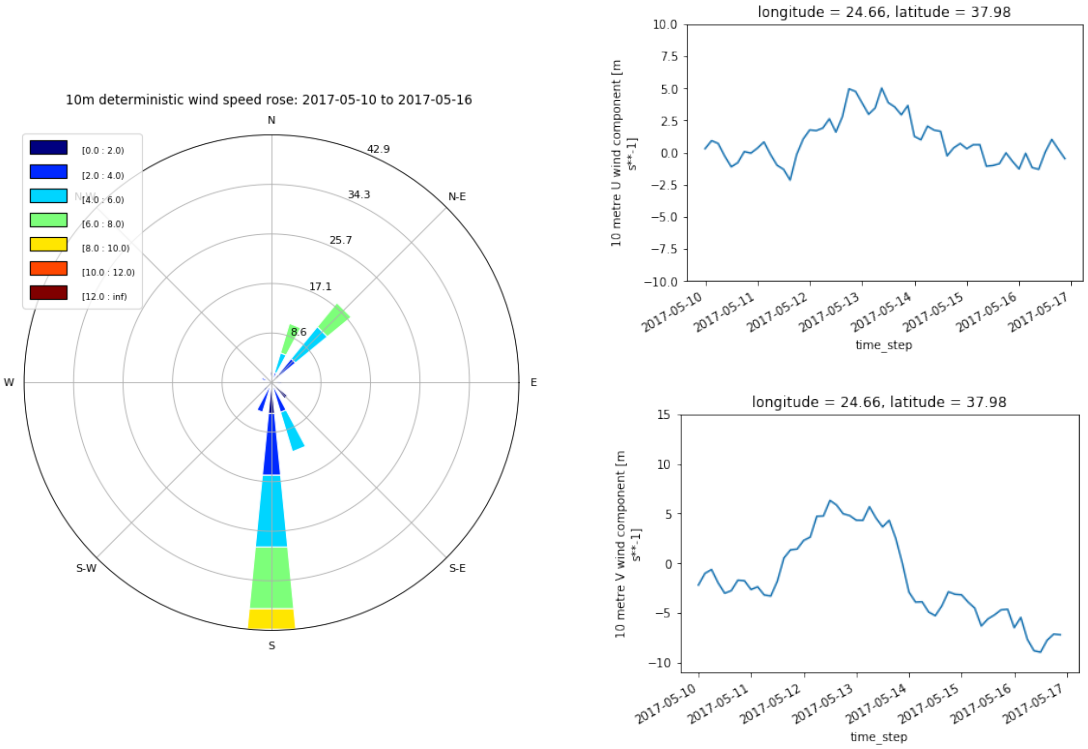

Figure 2.6: Wind speed rose at 10m of the deterministic simulation for the time period: 2017-05-10 to 2017-05-16.

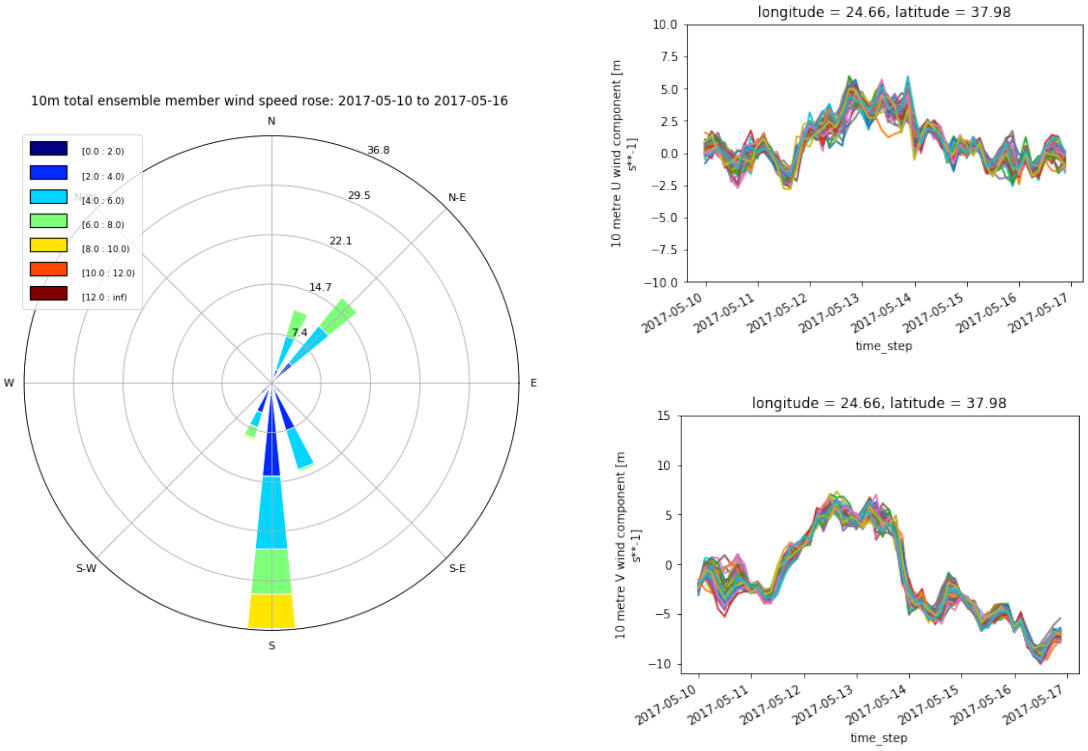

Figure 2.7: Wind speed rose at 10m of the total ensemble for the time period: 2017-05-10 to 2017-05-16.

The sudden changes of the wind in the winter, as shown in fig. 2.8a, especially between 50 to 75 hours and 125 to 168 hours, indicate the high variability of the atmosphere during the period under investigation and potentially a higher uncertainty in the forecasts if phase errors are present in the ECMWF system. In spring the lower wind intensity and the gradual change of the wind, as shown in fig. 2.8b, indicate a less variable wind pattern and potentially smaller phase errors and uncertainty.

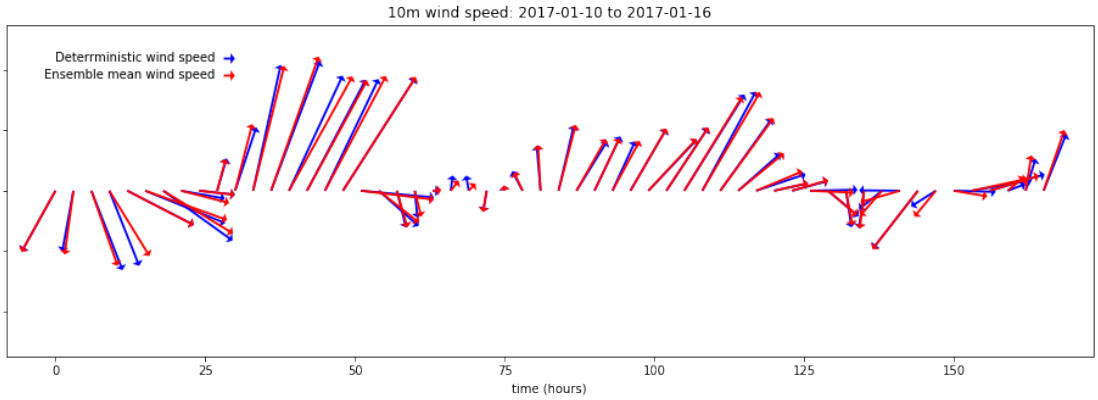

(a)

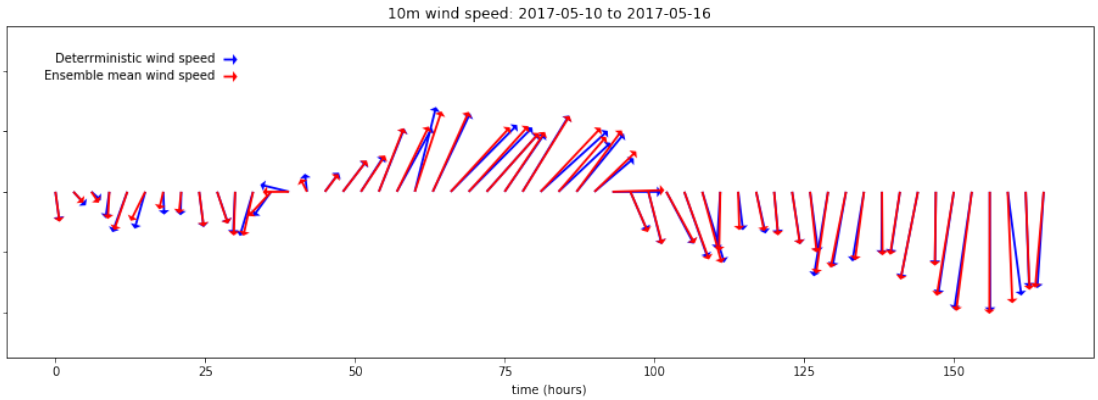

(b)

Figure 2.8: 10m wind speed of deterministic and ensemble mean for (a) winter and (b) spring.

2.2.3. Bathymetry and Coastlines

Bathymetry used in the MEDSLIK II simulations was obtained from the General Bathymetric Chart of the Oceans (GEBCO). The data set GEBCO_2014, a global grid at 30 arc-second intervals, was used for the defined study area (from 23 ° E to 26 ° E and 36 ° N to 39 ° N). For coastlines, version 2.3.7 of the high-resolution GSHHG geographic data set was used. In addition to the MEDSLIK II simulations, this data set was also used in the creation of the maps displaying the surface/dispersed and beached oil, for greater consistency. Figure 2.9 presents the bathymetry and the coastlines of the study area, along with the names of the locations and the starting point of the oil spill (shown as a red cross in the map).

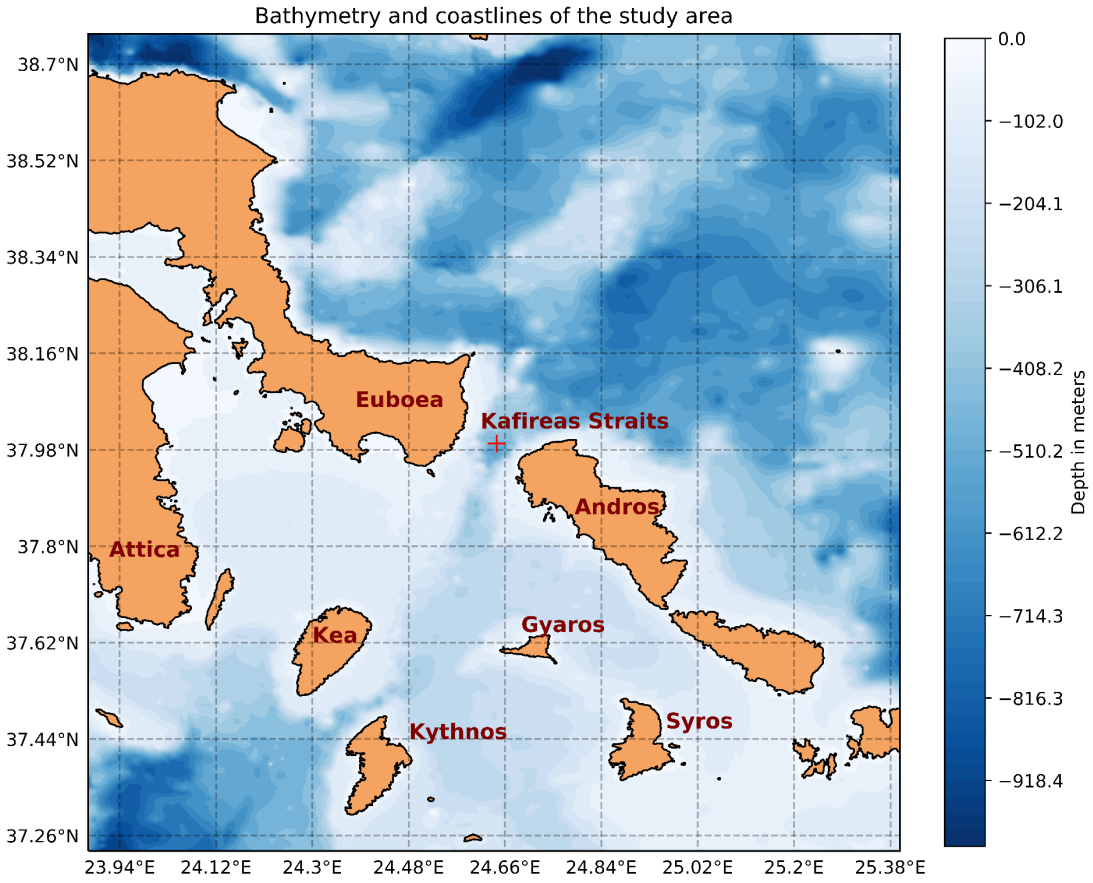

Figure 2.9: Bathymetry, coastlines and names of the locations in the study area, as well as the starting point of the oil spill.

2.3. Ensemble experiment setup

A single oil release point was used performing simulations of 7 days forecast lead time, with continuous oil release and a rate of spillage of 5 tons per hour. The oil spill duration and the spill rate were chosen, taking into account significant accidents of the past, like for instance the Prestige case (Portman, 2016), (Sepp Neves et al., 2016). The number of parcels, used in the simulations to calculate diffusion and dispersion and to estimate the concentration of oil in the oil slick, was 10^5, while the values of horizontal and vertical diffusions remained constant during experiments and the default model values were used. Stokes drift was taken into account in the calculation of oil transport, and the depth of the mixing layer for the periods January 2017 and May 2017 was set at 50 m and 10 m respectively, according to the oceanographic data used.

The range of experiments performed included:

- An atmospheric forcing of 50 ensembles of hourly (1h) wind speed values at 10 m as well as the ECMWF-HRES deterministic simulations for the time period of January 2017 and May 2017 (a total of 50+1 simulations per experiment/period).
- The corresponding oceanographic data (marine current velocity and temperature) for the above two periods and for depths of 0 m, 10 m, 30 m, 120 m.
- 3 types of oil: API 12, API 31 and API 38 representing heavier, medium and lighter oil spills, covering also a wide range of oil densities (Sepp Neves et al., 2016).

A total of 306 simulations were performed for a period of 168 hours (i.e. 7 days) shown in Schematic 2.1.

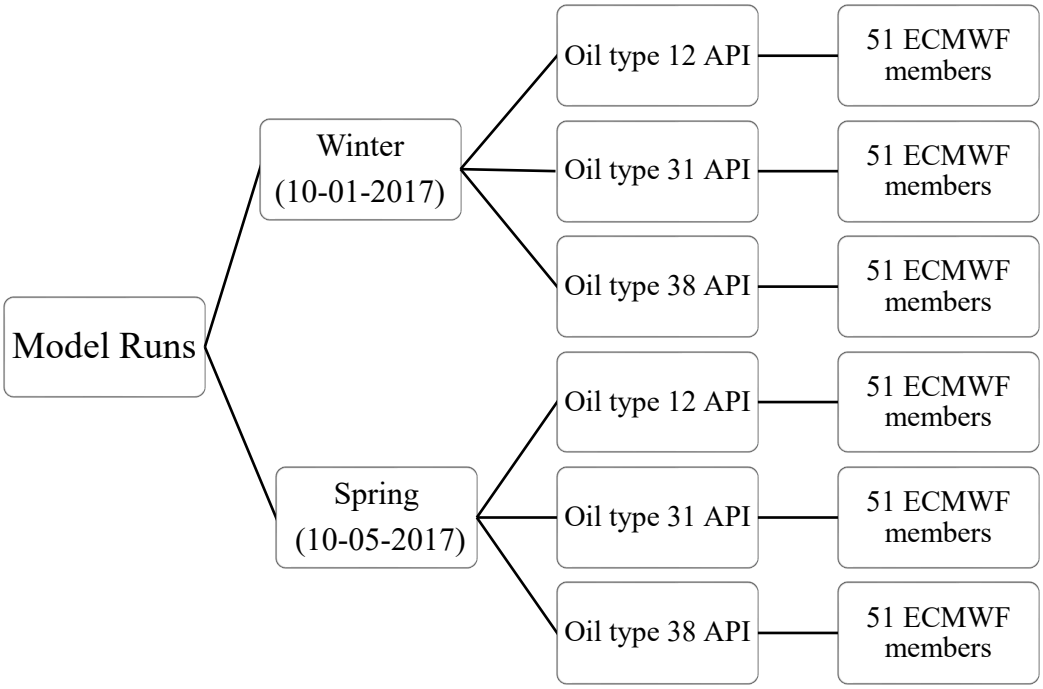

Schematic 2.1: Experimental design.

As an example of the oceanic and wind forcing used in the experiment, we present for winter and spring in fig. 2.10 and fig. 2.11 respectively, the state of the wind field, according to the deterministic simulations, and the surface marine currents for four different times. The oceanic and the wind forcing are used by MEDSLIK II for the simulation of the deterministic oil spills for the corresponding times.

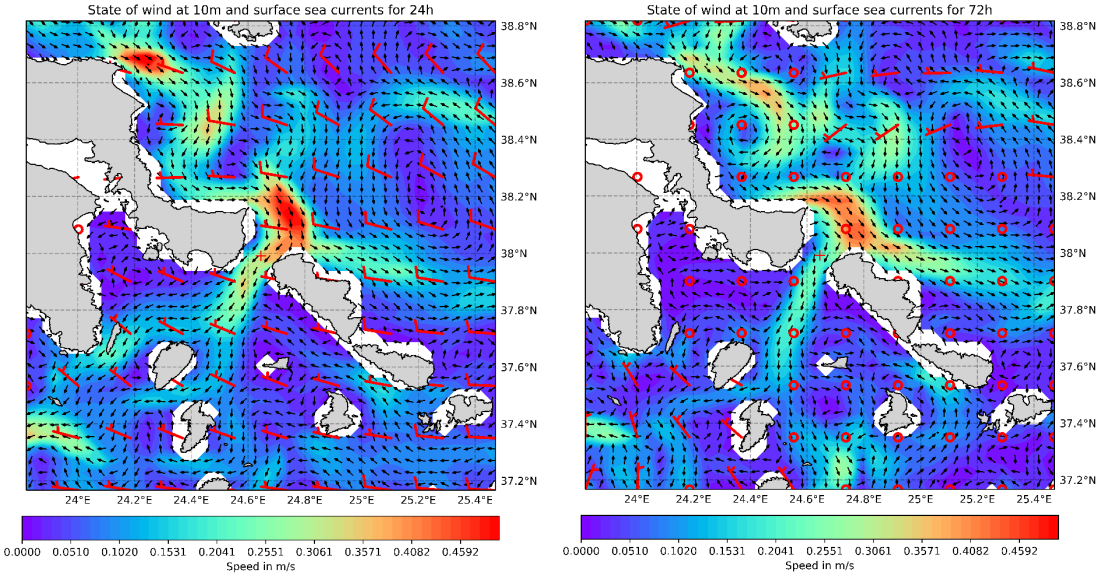

(a) (b)

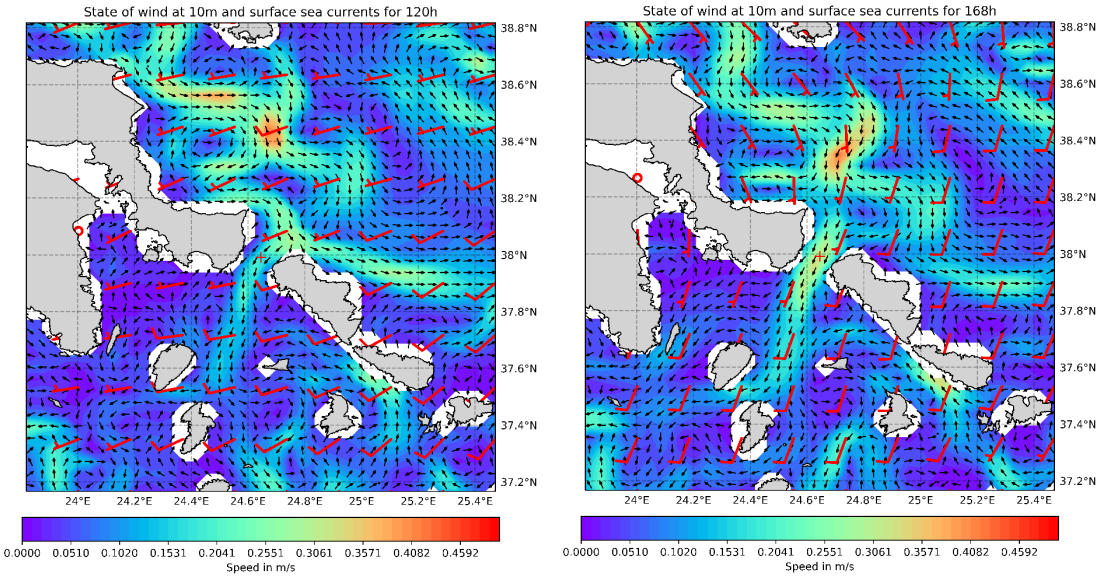

(c) (d)

Figure 2.10: State of wind field (according to the deterministic simulation) and surface marine currents for winter and: (a) 24, (b) 72, (c) 120 and (d) 168 hours.

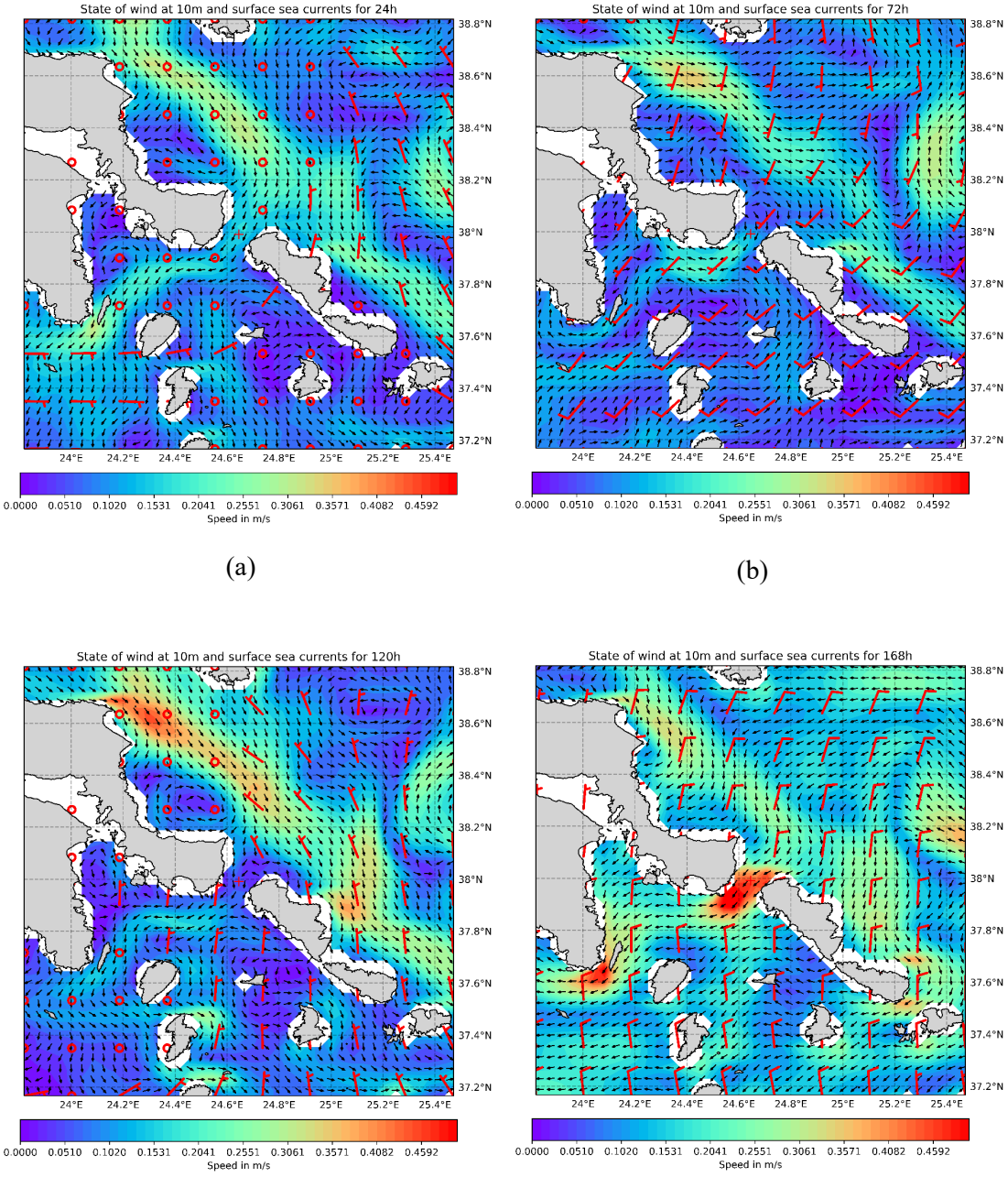

Figure 2.11: State of wind field (according to the deterministic simulation) and surface marine currents for spring and: (a) 24, (b) 72, (c) 120 and (d) 168 hours.

2.4. Metrics

2.4.1. Convex hull area

The convex hull of a given set of oil spill particle positions in the area of interest is defined as the smallest convex polygon that contains all positions in the set of modelled particles. In this study convex hull is used to examine the spreading, transport and dispersion of the simulated oil spills and evaluate the uncertainty of the area affected by the oil particles simulated by the deterministic and the ensemble members. An example of a convex hull of a set of points as they spread in time is presented in fig. 2.12.

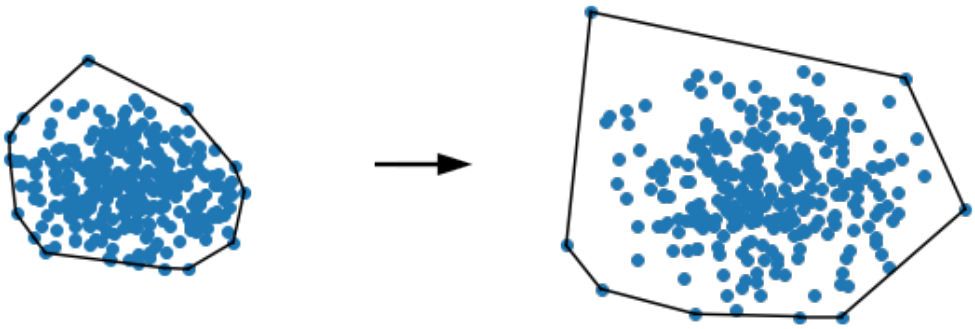

Figure 2.12: Example of convex hull of a set of points as they spread in time.

In addition, we use the convex hull to compute two more metrics, A_{exceed} and DA. A_{exceed} denotes the area of the deterministic convex hull that exceeds the area of one ensemble member's convex hull, while DA denotes the difference in the size between the deterministic convex hull and the convex hull of the combined ensemble oil spills. We use the A_{exceed} metric to compare the differences between the deterministic and each ensemble member convex hull as well as the differences between the convex hulls of the ensemble members, using as the area of reference the extent of the deterministic convex hull. An example of the A_{exceed} metric is presented in fig. 2.13. A_{exceed} is depicted as the hatched area.

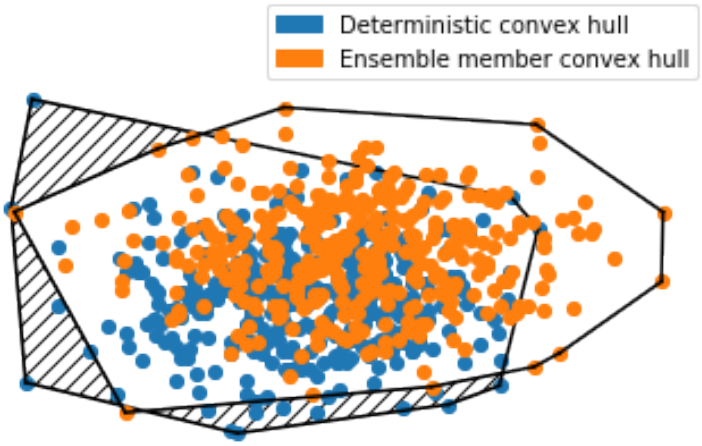

Figure 2.13: Area of deterministic that exceeds the area of the ensemble member convex hull (A_{exceed}).

Furthermore, apart from the DA metric, we use percentage change to calculate the percentage increase (or decrease) between the deterministic convex hull and the convex hull of the combined ensemble oil spills (total ensemble convex hull). Namely, to calculate the percentage of how much bigger (or smaller) is the total ensemble convex hull, in comparison to the deterministic and to quantify in a way how much more (or less) information it provides. We define the percentage change as:

$$Percentage\ change(\%) = \frac{DA}{\begin{matrix} Deterministic \\ convex\ hull\ area \end{matrix}} * 100\% \qquad (4)$$

2.4.2. RMSE

The root mean square error (RMSE) of the ensembles is estimated with respect to the deterministic simulation, calculating the separation distance between the deterministic and the ensemble means of oil spill Lagrangian trajectories, as a function of the forecast lead time (De Dominicis et al., 2013b). In this study, the Lagrangian trajectory definition refers to the mean trajectory geographically weighted by the number (and subsequently concentration) of the released oil spill particles.

$$RMSE(t_i) = \sqrt{\frac{\sum_{s=1}^{S} d_i\left(x_s(t_i), x_0(t_i)\right)^2}{S}} \quad (5)$$

where d_i is the distance between the deterministic, x_0, and the ensemble, x_s, mean positions respectively, at a given forecast lead time t_i following the mean trajectories after the initial release of particles, and S is the total number of the ensemble members.

2.4.3. Uncertainty index s

The non-dimensional index s according to De Dominicis et al. (2013b) and Liu & Weisberg (2011) is defined as:

$$s(t_i) = \frac{1}{S}\sum_{s=1}^{S} \frac{\sum_{t=t_0}^{t_i} d_i\left(x_s(t), x_0(t)\right)}{\sum_{t=t_0}^{t_i} l_{0i}\left(x_0(t_0), x_0(t)\right)} \quad (6)$$

where d_i and S have already been defined in Eq. 5 and l_{oi} is the length of the simulated deterministic mean trajectory at a given forecast lead time t_i, following the mean trajectories after the initial release of particles at time t_0. As seen by the above equation, the average of the separation distances between the simulated deterministic and ensemble members is weighted by the length of the deterministic trajectory, aiming at the reduction of possible evaluation errors that could arise by using only the Lagrangian separation distance (as in RMSE). For this reason, the uncertainty index s is used alongside the RMSE as it provides a more accurate quantification of the uncertainty in the oil spill trajectories. A trajectory model skill score (ss) can also be defined, using this index.

In most studies, RMSE and index s (and subsequently skill score ss) are used in the comparison between observed and simulated trajectories, as negative oriented metrics, in order to evaluate the modelling system's capability in reproducing the observed trajectories (predictability of the trajectories). The lower the RMSE and s values, the better the performance and predictability of the model simulations, with 0 indicating a perfect fit between observation and simulation. In this study, we use RMSE and index s, as positive oriented metrics, to compare the deterministic with the ensemble trajectories. Higher RMSE and s values indicate more significant differences between

the deterministic and ensemble trajectories and consequently the importance of the uncertainty generated by the ensemble simulations.

2.4.4. Oiling probability

The description of oiling probability is presented by Amir-Heidari et al. (2019) and Goldman et al. (2015). In the event of an oil spill, the oiling probability for a receptor (e.g. the coastline in our case) indicates the chance of the receptors' exposure to oil. The traditional approach for the calculation of oiling probability is based on a binary philosophy, i.e. oil spill events counted as "0" for nonexistent concentrations of oil in the beach or "1" for measured concentration regardless the amount of oil. The oiling probability for a total of n oil spill scenarios, with one source and one receptor only is according to Amir-Heidari et al. (2019):

$$P = \frac{\sum_{i=1}^{N} B_i}{N} \tag{7}$$

where Bi equals "1" or "0" if during the i simulation we measure oil concentrations or not, and N is the total number of simulations.

3. Results

In this section we present the results of MEDSLIK II simulations and quantify, using the metrics discussed in section 2.4, the uncertainty generated in the oil spill forecasting by the wind forcing (ECMWF EPS) ensembles and their possible use in concert with the deterministic simulation. This chapter presents the results for oil API: 31 which represents the most common type of oils (medium oils) and a middle case scenario for our study, while the results for the other two types are presented only briefly here (section 3.3) and in the appendices. Each oil slick was represented by 10^5 independent Lagrangian particles in the simulations.

Section 3.1, presents the surface oil maps of the ensemble oil spill simulations for seven days forecast lead time in the chosen study area (Kafireas strait), and the use of the previously mentioned metrics i.e. the convex hull, the trajectory of the oil spill mean point, the RMSE and the uncertainty index s, to quantitatively assess the uncertainty. Section 3.2, presents the beached oil maps of the ensemble oil spill simulations and the use of metrics like oiling probability, to quantify the uncertainties in beached oil forecasting.

3.1. Oil trajectory – spreading

3.1.1. Surface oil concentration maps

The direction of spreading and transportation of surface oil is greatly controlled by the direction of the wind, as seen in fig. 3.1, 3.2, 3.3 and 3.4, in conjunction with the wind field changes, presented previously in fig. 2.4 - 2.8. The concentrations of the ensemble oil spills, as simulated by the model, are constant, but there are variations in the transport and the evolution of the shape and size of the oil spills between members solely because of the wind spread.

Figure 3.1 illustrates the surface oil concentrations and spreading of the deterministic simulation for winter and for 24, 72, 120 and 168 hours. Different colors represent the different concentrations of particles. On the first day of the simulation, the oil slick is transporting southwest, following the direction of the marine currents and the wind, as seen in fig. 3.1a. Between 24 to 72 hours, the sudden changes in the wind field are responsible for the spread of the oil slick, observed in fig. 3.1b. Afterwards, the oil slick spreads mainly in the downwind direction and is transporting northeast while beginning to interact with the coast of Andros (fig. 3.1c). Finally, in the following days of the

simulation, the oil slick spreads further in the area, as seen in fig. 3.1d, once again as a result of the sudden changes in the wind. As can be seen in fig. 3.2, although the prevailing transport of the ensemble oil spill members is also downwind and similar to the deterministic oil spill, there are considerable differences in the shapes of the oil slicks. These differences in the direction and extension of the oil slicks, are caused by the different atmospheric forcing among the members and the sudden changes of the wind field associated with phase errors in the ensemble (discussed also in section 2.2.2).

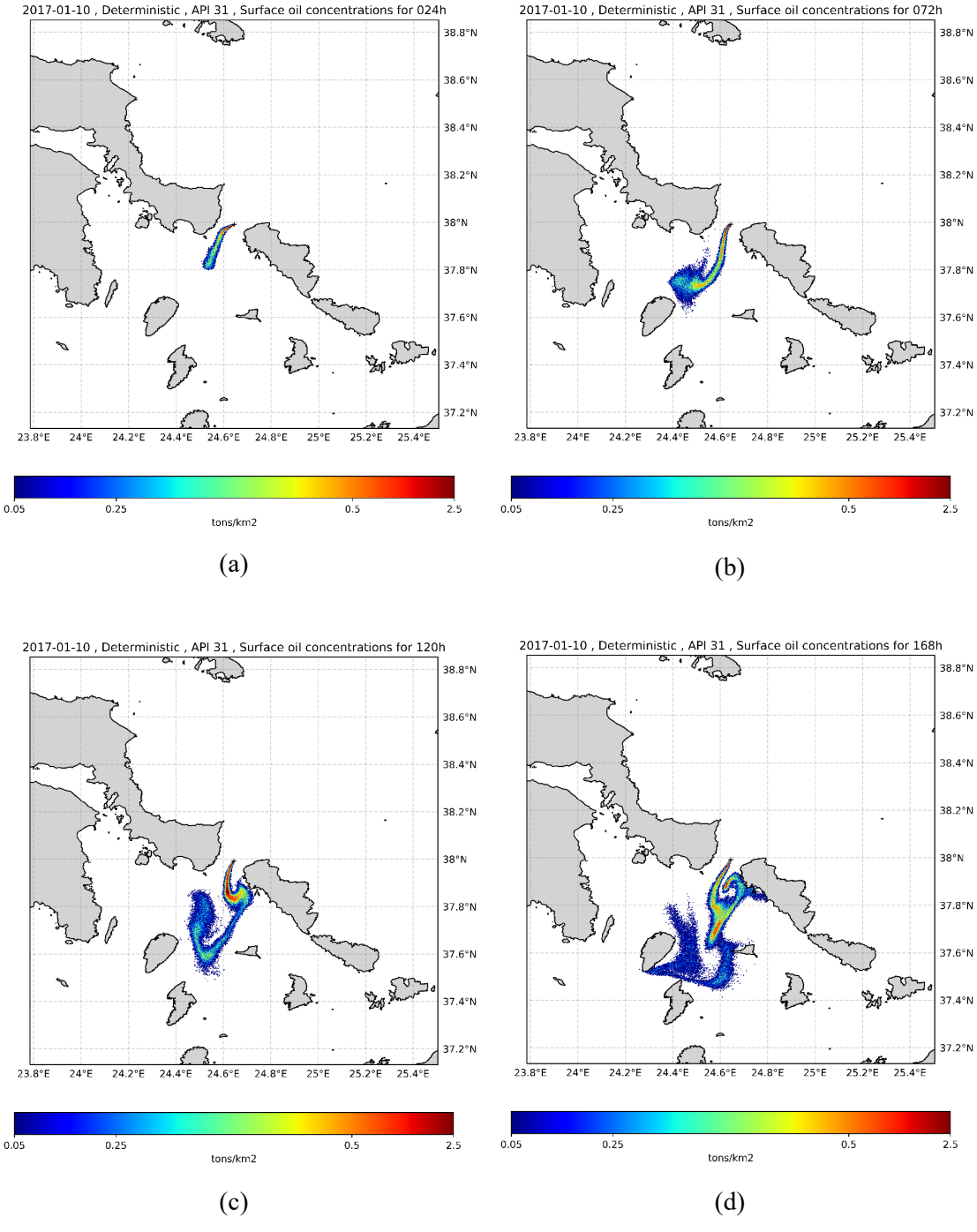

Figure 3.1: Surface oil concentrations of deterministic simulation for winter, 31 API and simulation time of: (a) 24, (b) 72, (c) 120 and (d) 168 hours.

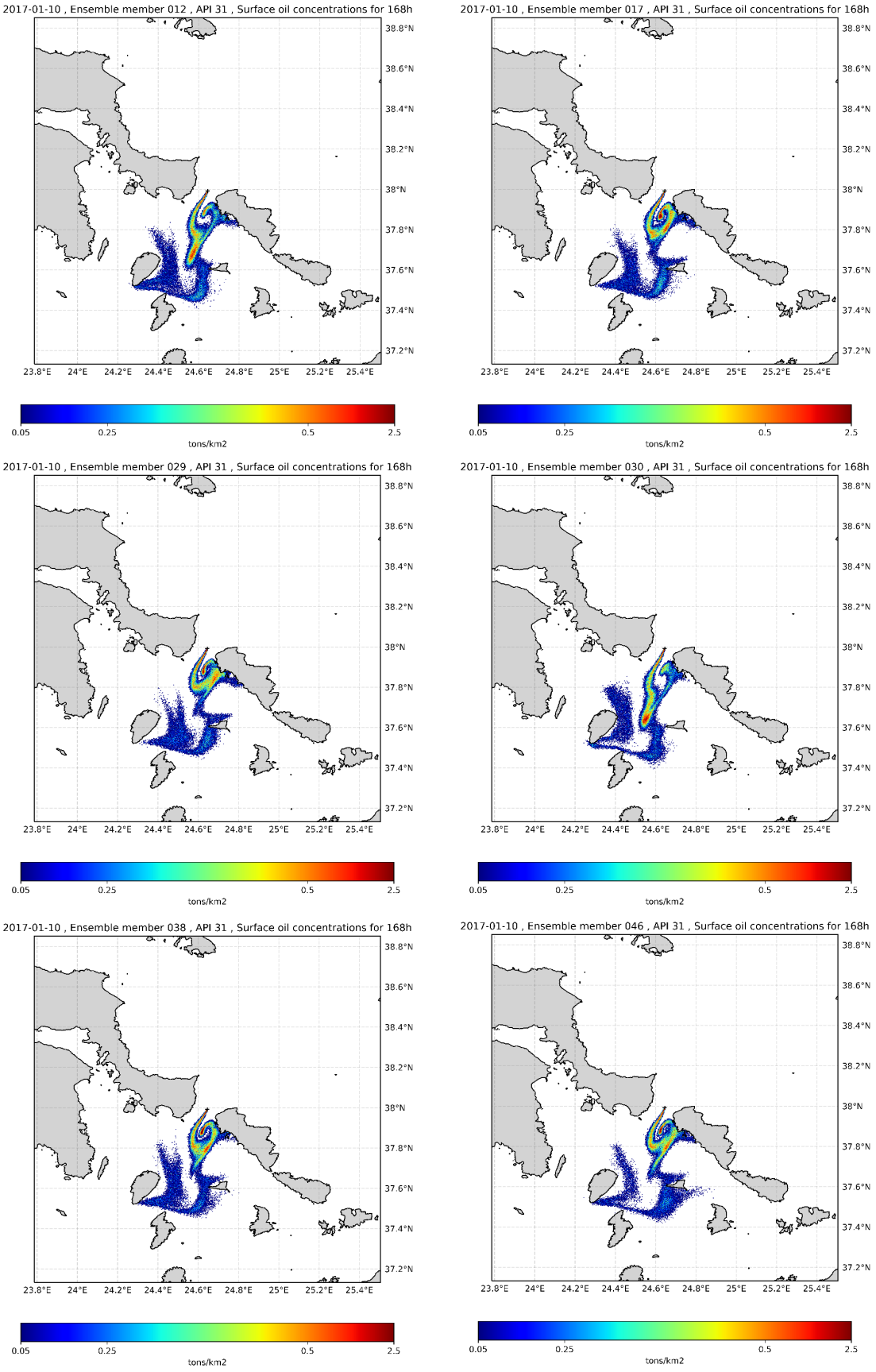

Figure 3.2: Surface oil concentrations of some of the ensemble members for winter, API 31 and simulation time of 168 hours.

Similarly, fig. 3.3 illustrates the surface oil concentrations and spreading of the deterministic simulation for spring and for 24, 72, 120 and 168 hours. The oil slick is transporting southwest for the first day of the simulation according to the marine currents and the wind forcing (fig. 3.3a). Afterwards, due to a change in the direction of the wind, the oil slick transports northeast (fig. 3.3b), in the downwind direction until the 100th hour of the simulation approximately, while also interacting with the coasts of Euboea and Andros. Finally, in the remaining days of the simulation, the oil slick transports southwest as seen in fig. 3.3c and 3.3d. As expected, differences in the oil spill distribution between the deterministic and the ensemble simulations (fig. 3.4) are also present in spring, although on a lesser extent compared to winter, which is mainly attributed to the lower wind spread of the ensemble and the more gradual change of the wind, as described previously on sections 2.2.1 and 2.2.2.

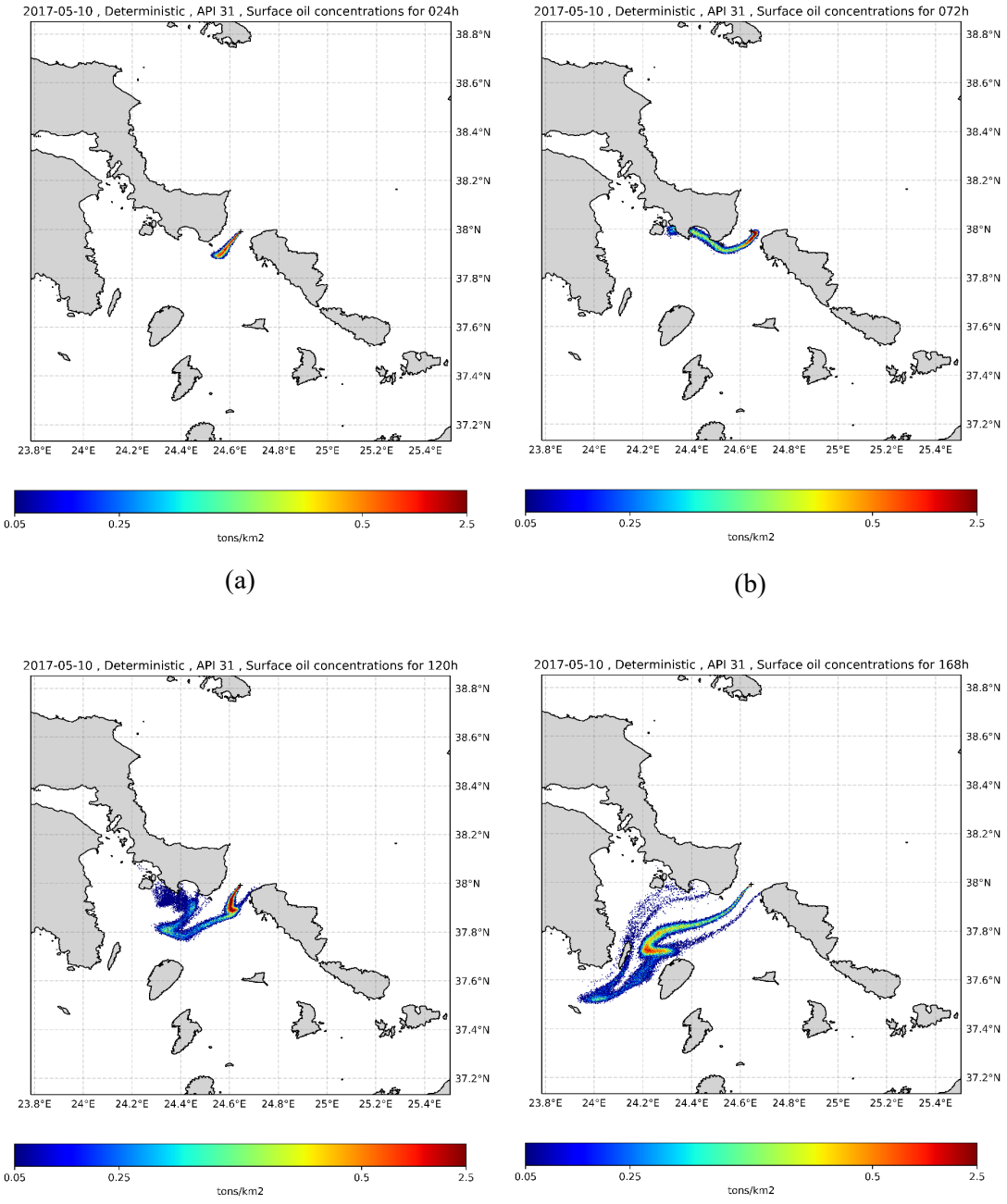

Figure 3.3: Surface oil concentrations of deterministic simulation for spring, 31 API and simulation time of: (a) 24, (b) 72, (c) 120 and (d) 168 hours.

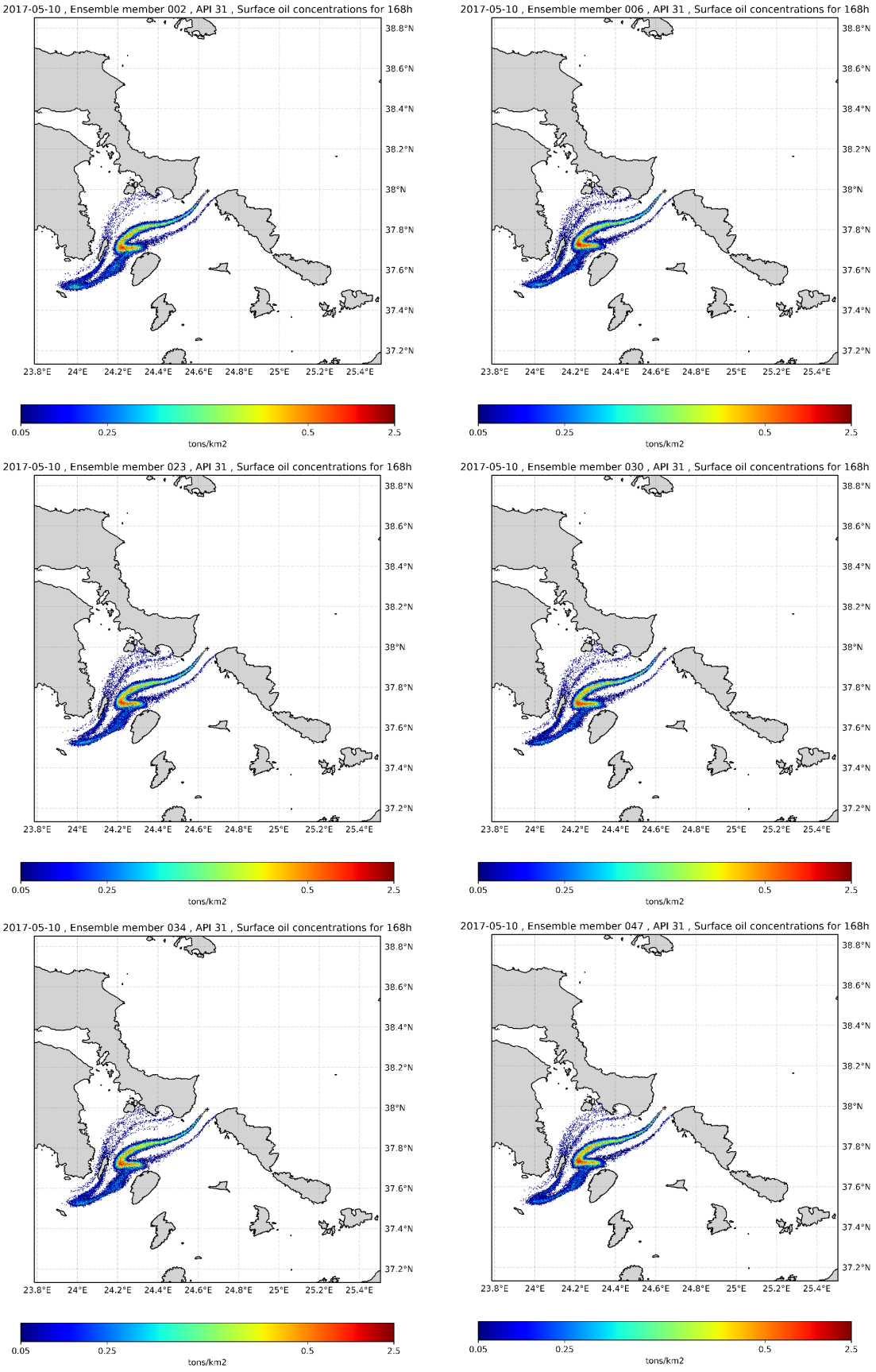

Figure 3.4: Surface oil concentrations of some of the ensemble members for spring, API 31 and simulation time of 168 hours.

3.1.2. Uncertainty assessment for oil spill trajectory and spread

Figure 3.5 presents the convex hull of the deterministic and ensemble members for winter and simulation times of 72 and 168 hours. Both surface and subsurface parcels, as well as those deposited on the coast were used in the computation, to better describe the extent of the oil spills simulated by MEDSLIK II and the extent of the area they affect. As shown in fig. 3.5, the oil spill is advected according to the wind forcing (fig. 2.8a) and the marine currents in the area (fig. 2.2), moving southwest for the first few hours of the simulation and then spreading around the area. Variations in the extent of the area affected by the ensemble oil spills are observed, as shown by the differences in convex hulls (fig. 3.5 b & d).

These variations in the extent of the area affected by the ensemble oil spills are better shown in fig. 3.6, where we present the area of the deterministic convex hull that exceeds the area of each member's convex hull, for the duration of the simulations. This area expressed by the metric A_{exceed} (also discussed in section 2.4.1), increases over time with a maximum of around 370 km^2 for 156 hours. The A_{exceed} spread increases because we continuously force the MEDSLIK II model with different atmospheric forcing per timestep. Also, it is worth noting that there is a rapid increase of A_{exceed} spread around 75 to 114 hours and 125 to 168 hours, linked to the sudden changes in the wind forcing and the possible phase errors in the wind ensembles, as discussed in section 2.2.2. The moment the A_{exceed} spread increases rapidly and the difference in the extent of the oil spills and the area they affect, could prove important knowledge in the formation of the mitigation strategy and the expected length of the deployed booms.

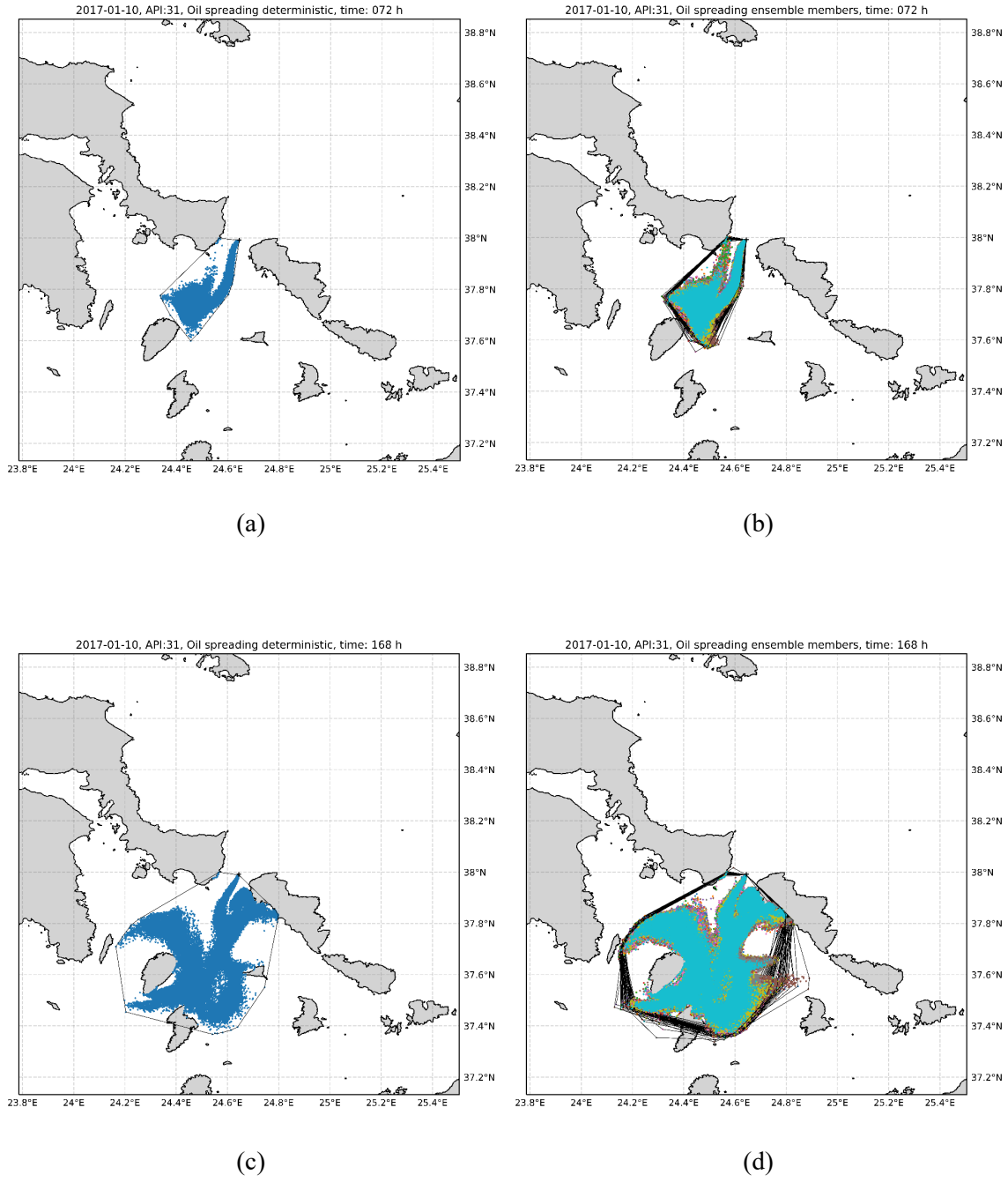

Figure 3.5: Oil spreading of deterministic and ensemble members for winter, oil API: 31 and simulation time of (a - b) 72 hours and (c - d) 168 hours.

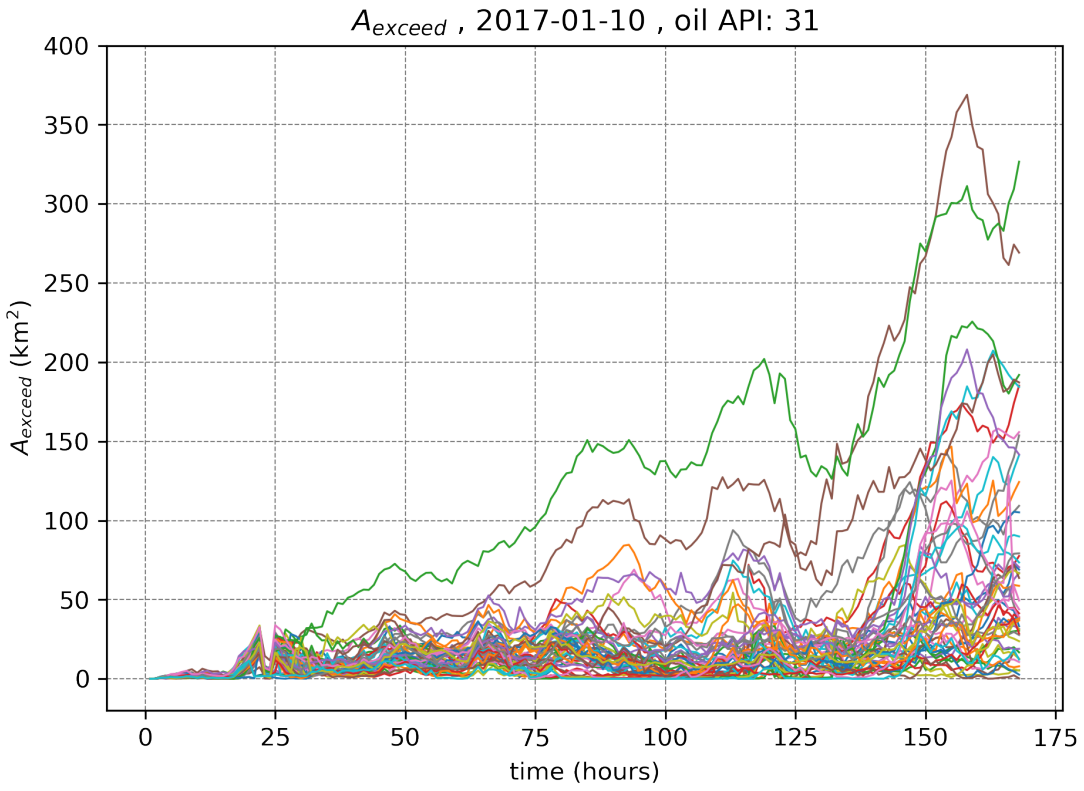

Figure 3.6: Area of deterministic oil spill that exceeds the area of each ensemble member (A_{exceed}), for winter and oil API: 31.

Figure 3.7 illustrates the difference in the extent between the convex hull of the deterministic oil spill and the convex hull of the combined ensemble oil spills, for winter. The convex hull area covered by the whole ensemble (total ensemble convex hull) is larger than the area simulated by the deterministic approach, illustrating that the oil spill may affect a larger area. For example, in fig. 3.7 the total ensemble convex hull indicates a higher risk for the island of Syros (24.91° E, 37.43° N) and the possible appearance of oil if the simulation continued after the time point of 7 days. There is a continuous increase in the difference between the two convex hulls, as shown in fig. 3.8 and denoted by the metric DA (also discussed in section 2.4.1), with a maximum value of about 950 km^2. The rate of increase is higher and more variable in the earlier hours of the simulation as denoted by percentage change (fig. 3.8), with the total ensemble convex hull being greater than the deterministic convex hull by 38% - 102% for the first day of the simulation, while it decreases and stabilizes in the latter hours, with a percentage change of 25% - 30% after the 120 hour mark. The percentage of the additional information offered through the use of the total ensemble convex hull is significantly higher than that of the deterministic in the earlier hours of the simulation and although in the latter hours this percentage drops, the additional information offered

by the total ensemble convex hull is equally or even more important than the earlier hours due to the continuous growth in the extent of the oil spills over time.

For the most part of the simulation, the deterministic convex hull area is enclosed by the whole ensemble, considering all areas spanned by all members, as shown in fig. 3.7 & 3.8. The information for the extent of the oil spills and the extent of the area they affect provided by this approach (ensemble approach), which takes into account the predictability of the atmospheric forcing, is of added value, compared to the deterministic approach.

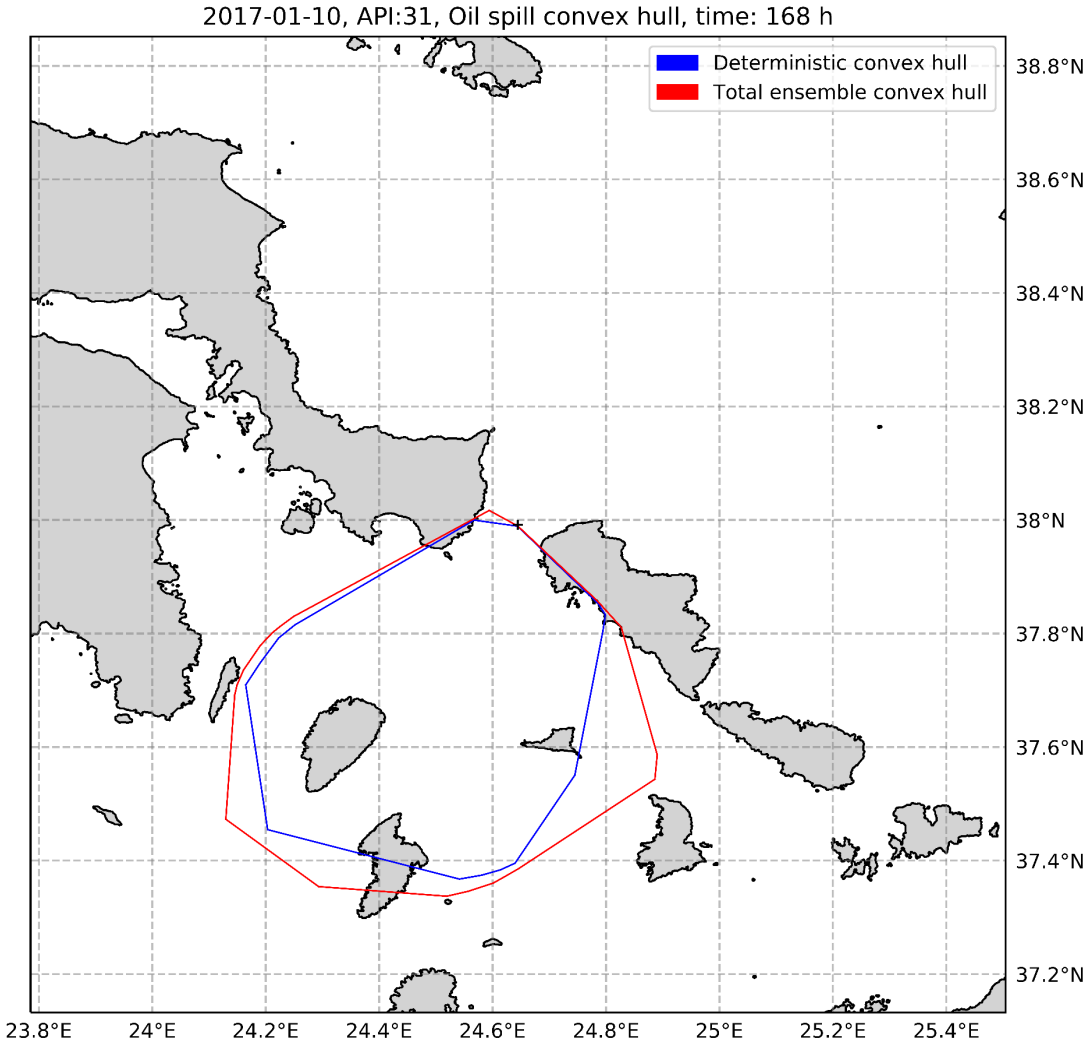

Figure 3.7: Oil spill convex hull for the deterministic and the total ensemble, for winter, oil API: 31 and 168h.

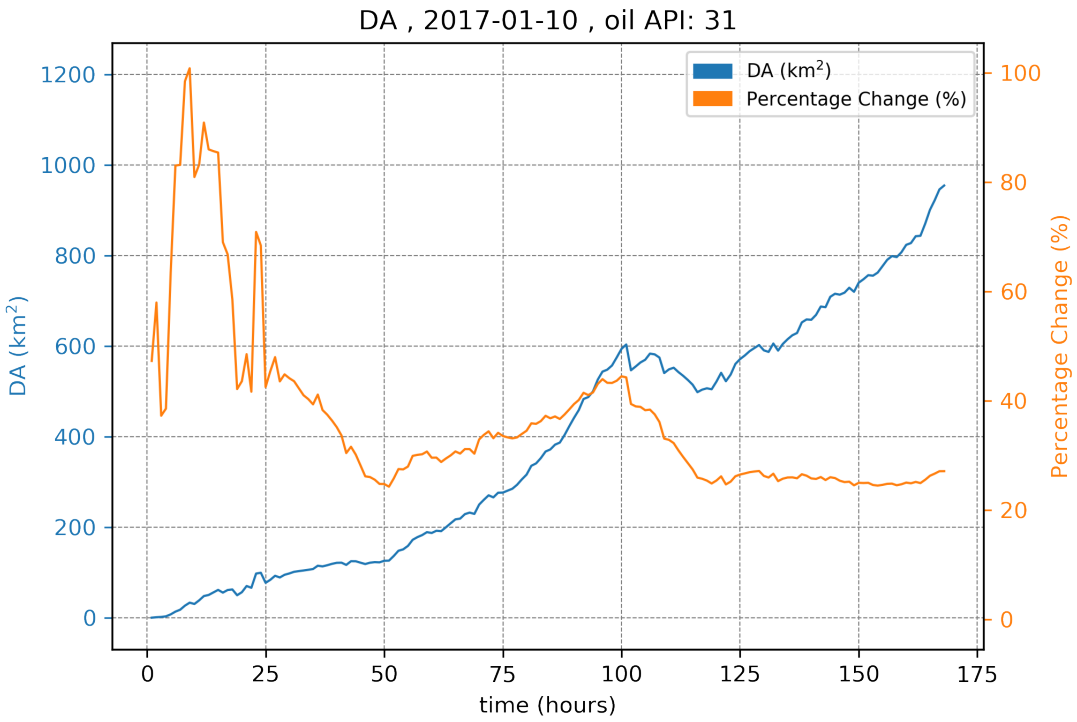

Figure 3.8: Area difference (DA) and percentage change between the deterministic and the total ensemble convex hull, for winter, and oil API: 31.

In spring, as illustrated in fig. 3.9, the oil spill is advected mainly to the southwest and then to the northeast for the first 3-4 days of the simulations, while interacting heavily with the coastline and later to the southwest again following the marine currents in the area (fig. 2.3) and the change in the wind direction, as shown in fig. 2.8b. In contrast to the winter case, differences between the convex hulls are smaller, likely due to the lower intensity of the wind and the more gradual changes in the wind field, associated with lower phase errors in the ensemble (also discussed in section 2.2.2). Also, as shown in fig. 3.10, the A_{exceed} area and A_{exceed} spread are smaller in spring. The rapid increases of A_{exceed} spread around 25 to 50, 75 to 100 and 125 to 150 hours, as shown in the same figure, is most likely due to a change in the direction of the wind. Although the uncertainty in the extent of the oil spill forecasts generated using ensemble wind forcing is smaller in spring, this information is just as important, due to the greater interaction between the oil spill and the shoreline, as opposed to winter with greater spread. Figure 3.11 illustrates the difference in the extent between the convex hull of the deterministic oil spill and the convex hull of the combined ensemble oil spills, for spring. Similarly to the winter case, the convex hull area covered by the whole ensemble is larger than the area simulated by the deterministic approach and for the most part of the simulation, the whole ensemble convex hull area encloses the deterministic convex hull area. Likewise, there is a continuous increase in the difference between the two convex hulls, as shown in fig. 3.12. In contrast to the winter, this difference is lower,

with a maximum value of about 620 km^2. Furthermore, the percentage change, as shown in fig. 3.12, is lower and steadier than the winter, with the total ensemble convex hull being greater than the deterministic convex hull by 35% - 58% for the first day of the simulation and around 20% for the following days.

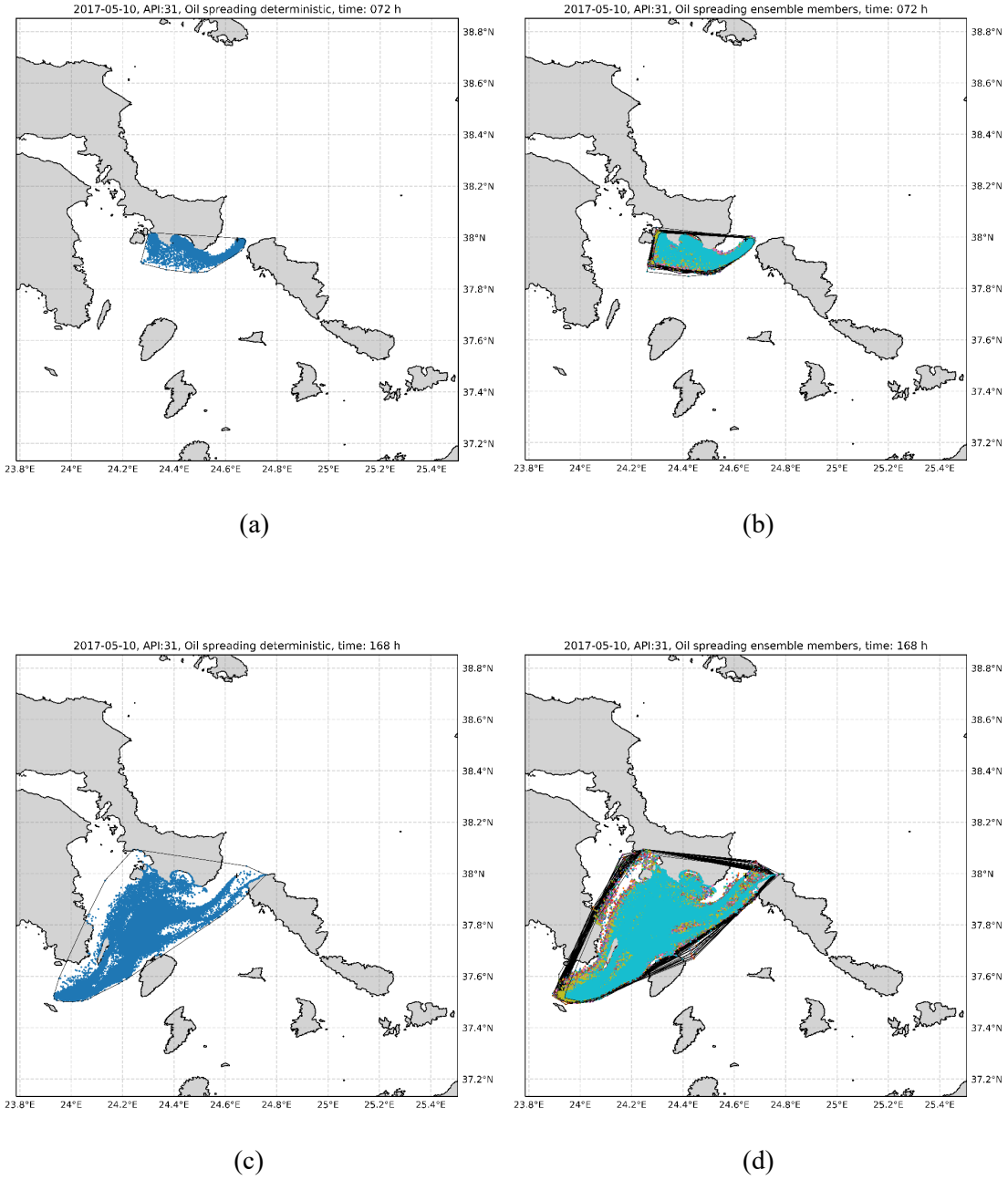

(a) (b)

(c) (d)

Figure 3.9: Oil spreading of deterministic and ensemble members for spring, oil API: 31 and simulation time of (a - b) 72 hours and (c - d) 168 hours.

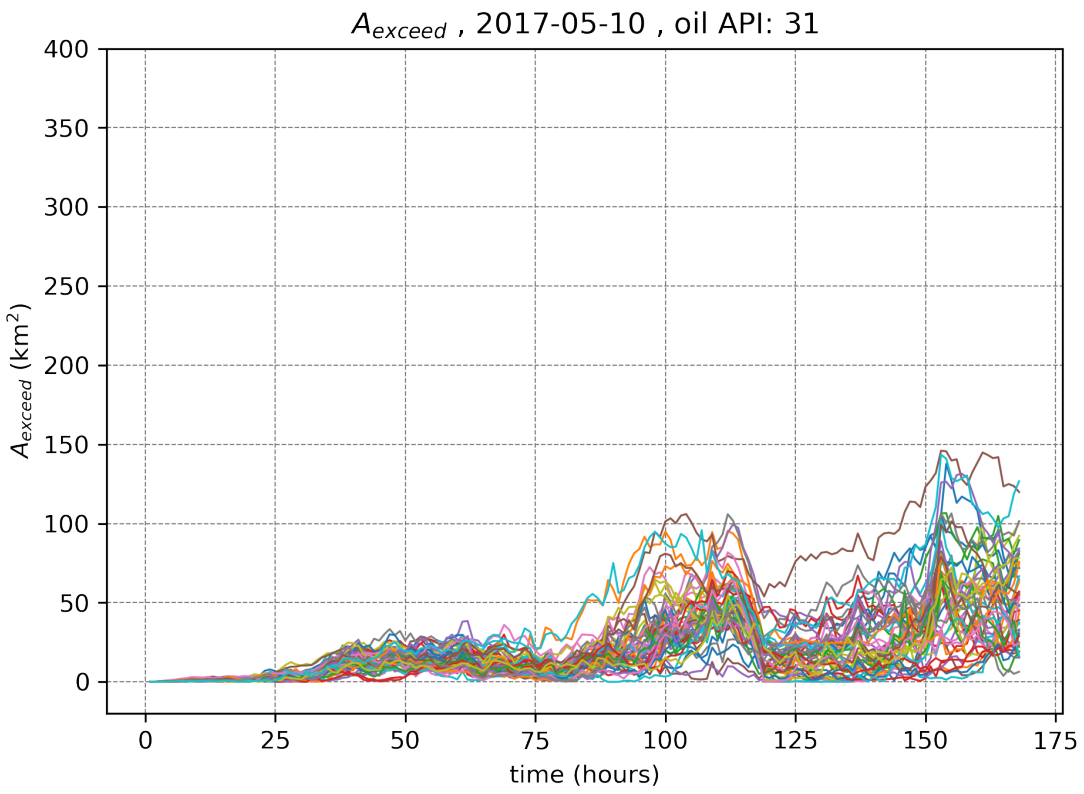

Figure 3.10: Area of deterministic oil spill that exceeds the area of each ensemble member (A_{exceed}), for spring and oil API: 31.

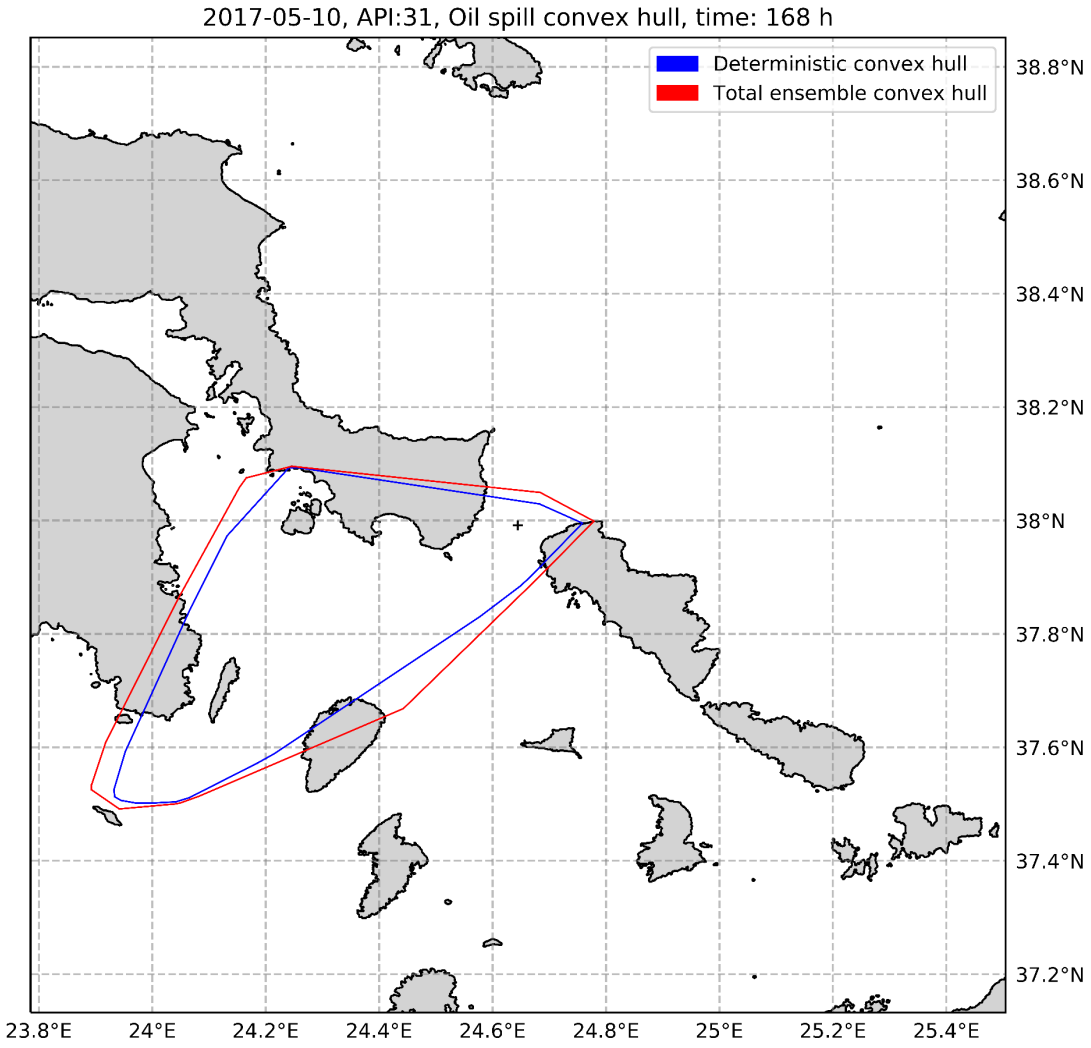

Figure 3.11: Oil spill convex hull for the deterministic and the total ensemble, for spring, oil API: 31 and 168h.

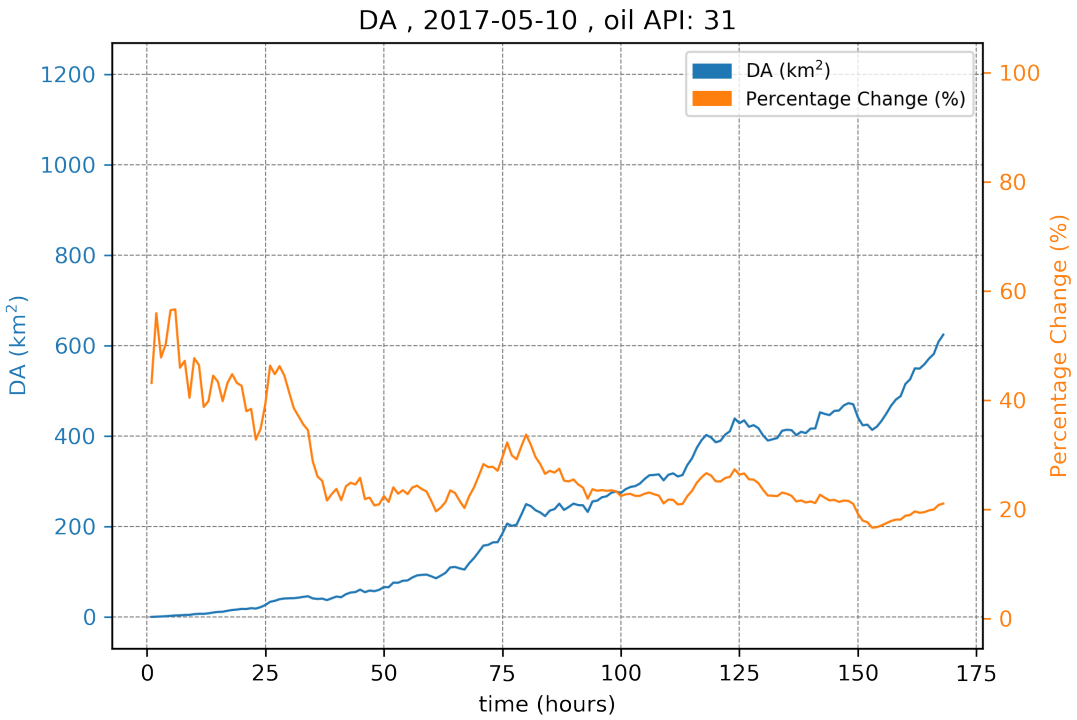

Figure 3.12: Area difference (DA) and percentage change between the deterministic and the total ensemble convex hull, for spring and oil API: 31.

Figure 3.13 shows the trajectories of the simulated parcels' mean of every individual ensemble member with 168 hours forecast lead time, during winter and spring. It is important to investigate the oil spill transport also by means of Lagrangian trajectories, since those trajectories can be considered as a proxy of the most pollutant ocean routes carrying the highest levels of oil concentration. As expected, the trajectory spread increases with time for both cases, displaying a higher spread in winter (fig 3.13a), as a result of the higher wind forcing uncertainty. This uncertainty in the trajectory prediction, generated by the ensembles in both time periods, is an important element to consider in the event of an oil spill.

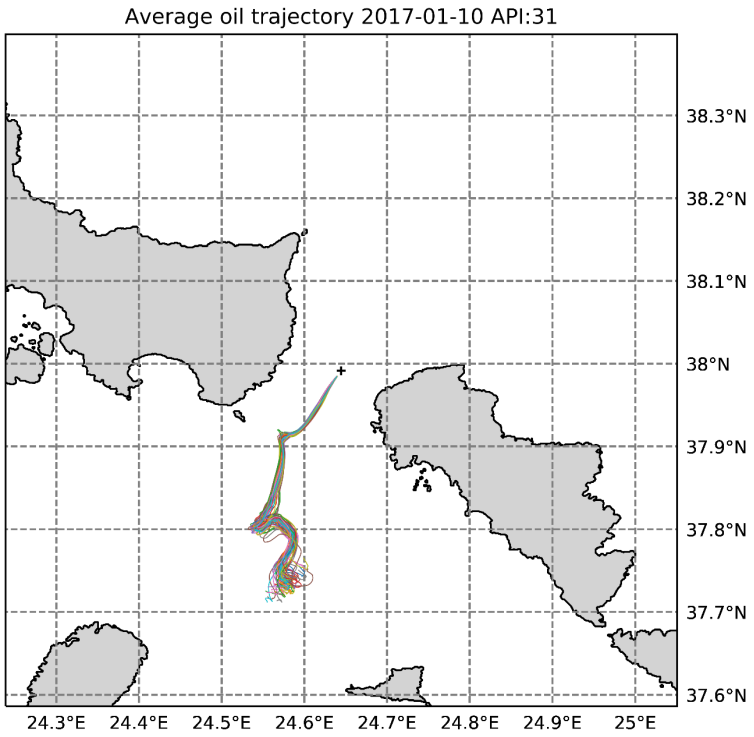

(a)

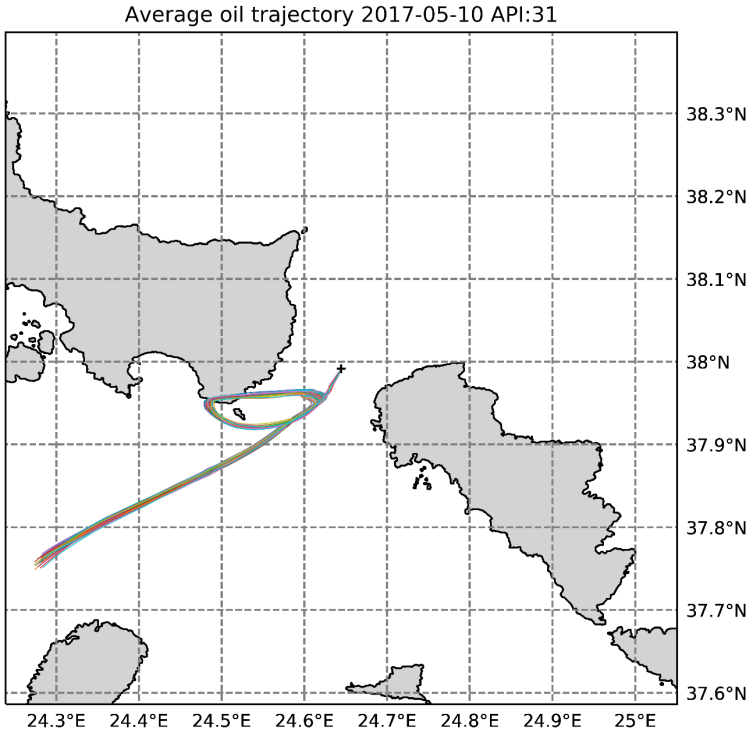

(b)

Figure 3.13: Mean coordinates trajectory of each ensemble member for API 31, simulation time of 168 hours and two time periods: (a) winter, (b) spring.

To further evaluate the uncertainty in the oil spill, focusing now on the mean oil Lagrangian trajectories, we use the RMSE and the uncertainty index s, described in detail in sections 2.4.2 and 2.4.3. As expected, both RMSE and uncertainty index s are increasing with time (fig. 3.14, fig. 3.15), with higher values and a more gradual increase in the winter case. In winter as shown in fig. 3.14a, there is a significant increase in RMSE after the first 125 hours of the simulations, associated with the high spread of the oil spill trajectories (fig. 3.13a) most likely as a result of phase errors in the wind field and the ensemble spread (section 2.2.2). In spring (fig. 3.14b), RMSE displays a discontinuous increase with two significant peaks around 70 and 110 hours, primarily due to the high interaction of the oil spill with the coastline around those two time periods and secondary, as a result of phase errors in the wind field and the ensemble spread. After the first 125 hours, the rate of increase of RMSE appears to be decreasing, most likely due to the stabilization of the wind field (section 2.2.2). Overall the RMSE displays lower values in spring, in agreement with the low trajectory spread (fig. 3.13b) and most likely due to the gradual change of the wind field and the lower ensemble spread as opposed to the winter case (section 2.2.2). The added value of the ensemble oil spill forecasts is shown to be more important when the RMSE is increasing, suggesting that the Lagrangian trajectories of the oil spill members span a larger area than the single trajectory of the deterministic run. The continuous increase of the RMSE over time is attributed to the different atmospheric forcing per member imposed through the whole simulation period.

These observations are supported by uncertainty index s, presented in fig. 3.15. In winter (fig. 3.15a) the uncertainty index s increases over time presenting an almost linear growth. Unlike the winter case, in spring (fig. 3.15b), uncertainty index s displays lower overall values, fluctuations in its growth, and a decrease in its value after the first 120 hours. In this study, the s index is used to show the periods where the contribution of the atmospheric ensemble is most noticeable in terms of increasing the oil spill uncertainty, so as the ensemble prediction to be more useful operationally with respect to the deterministic prediction. We note that this occurs in periods when there is a noticeable increase in the s index, suggesting an increase in the distance of the ensemble Lagrangian trajectory compared with the deterministic. In the opposite case when the s index is decreased, there is a “collapse” of the ensemble envelop with respect to the deterministic simulation, denoting a period with not much contribution in terms of uncertainty.

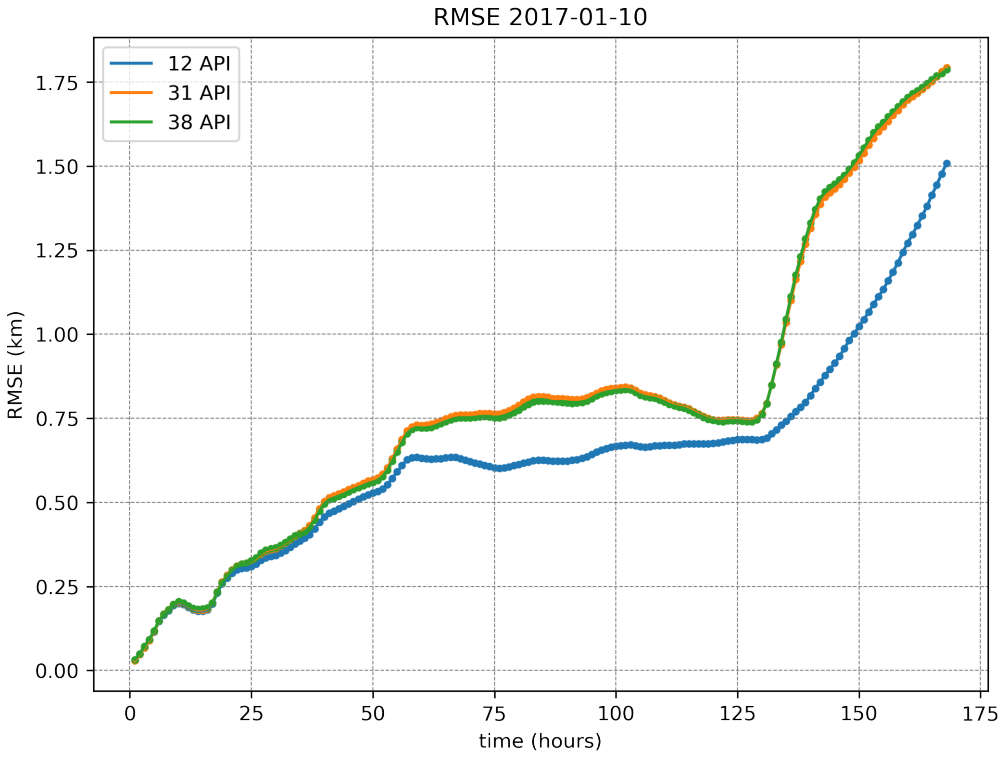

(a)

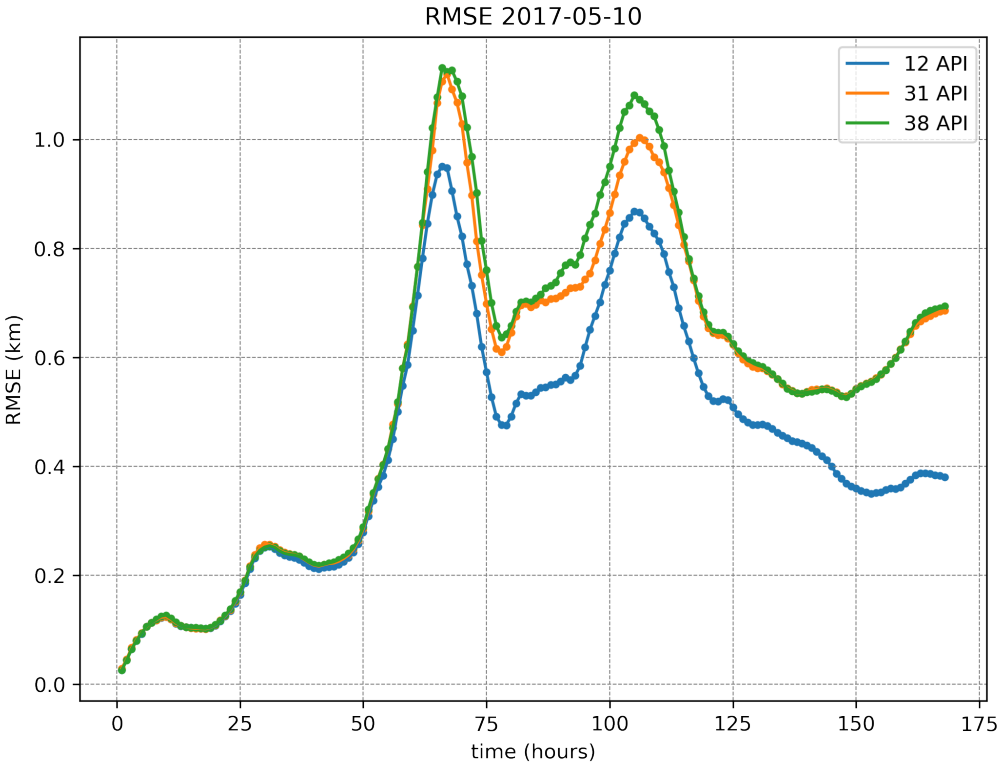

(b)

Figure 3.14: RMSE for each API value and time periods of: (a) winter and (b) spring.

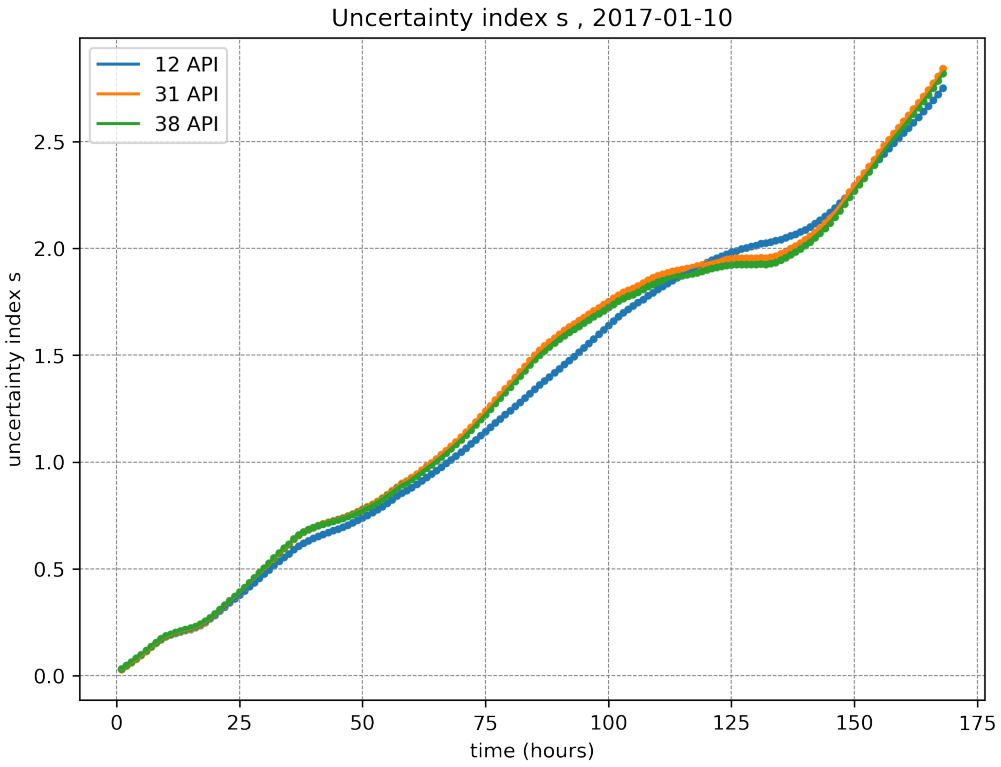

(a)

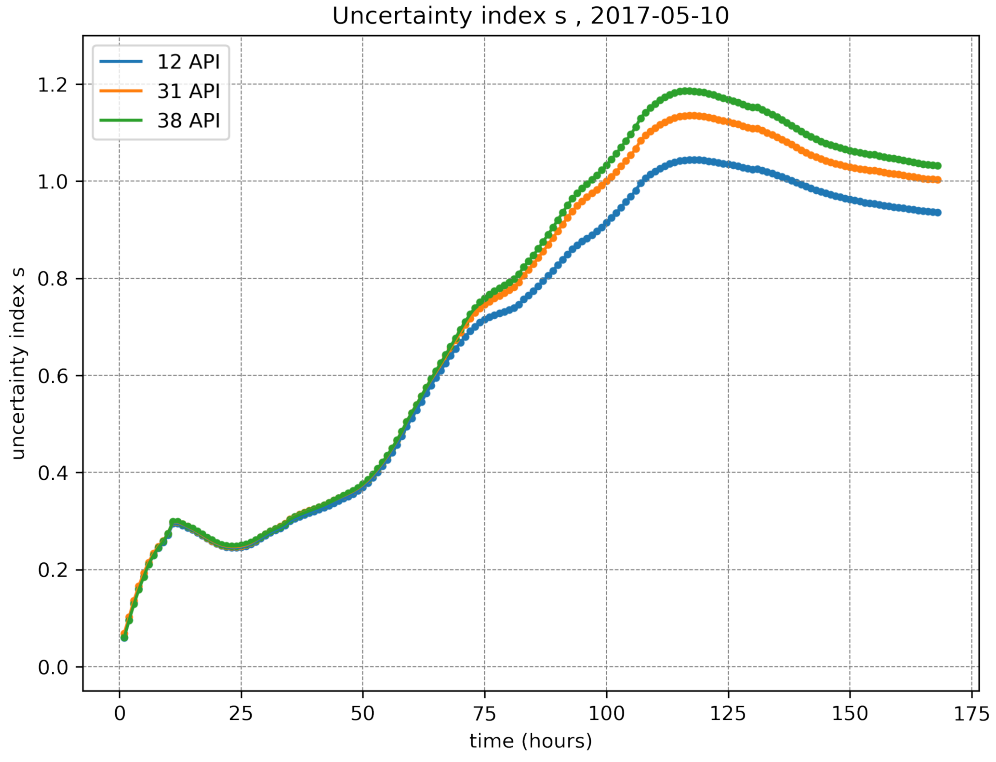

(b)

Figure 3.15 Uncertainty index s for each API value and time periods of: (a) winter and (b) spring.

3.2. Beached oil

"Beaching" is a term commonly used in literature to describe the interaction between the oil and the shoreline and is an essential part of oil spill modelling and impact assessment due to the importance of coastal areas (Samaras et al., 2014). In this section we present the beached oil maps, the total amount of oil beached and fixed on the coast every time step (total fixed oil) and use metrics like oiling probability, in order to determine quantitatively the spatiotemporal uncertainties in beached oil forecasting generated by the wind forcing ensembles. These uncertainties are important to estimate the impact of an oil spill on a coastal area and to better plan the mitigation procedures, including several equally possible oil spill states expressed by our ensemble protocol.

3.2.1. Beached oil maps

Figure 3.16 illustrates the beached oil concentrations of the deterministic simulation for winter and 168 hours forecast lead time (i.e. at the end of the run). The different concentrations of beached oil particles are represented by different colors. The deterministic simulation, predicts a maximum value of 0.47 tons/km. As seen in fig. 3.17, a maximum concentration of 1.44 tons/km (members 017 & 030) is predicted for the presented ensemble members, with significant differences between them, indicating a high degree of uncertainty in the amount of beached oil concentrations. These differences in the beached oil predictions are the result of the differences and uncertainty of the ensemble spread, discussed in section 3.1.

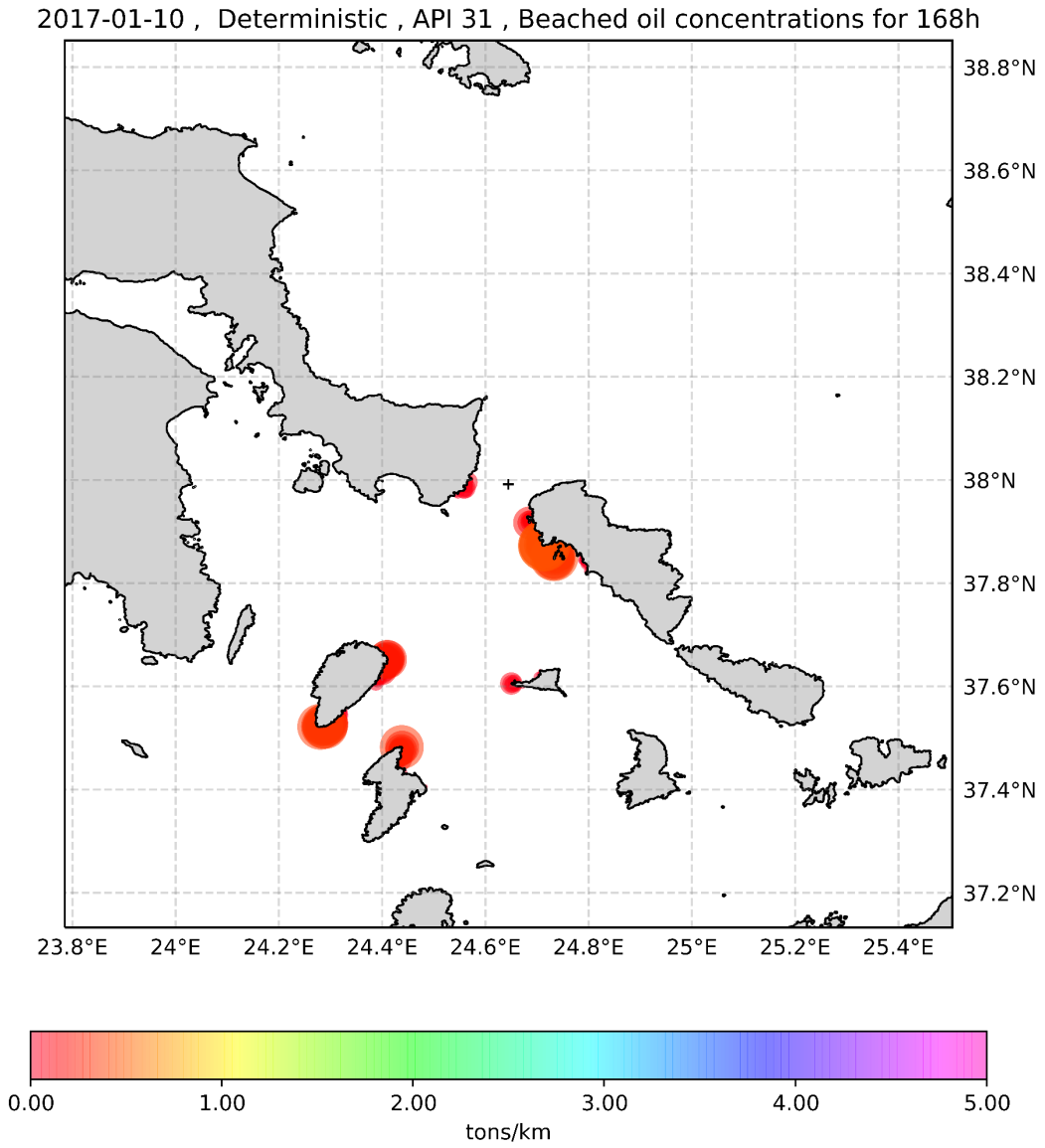

Figure 3.16: Beached oil concentrations of deterministic simulation for winter, simulation time of 168 hours and 31 API.

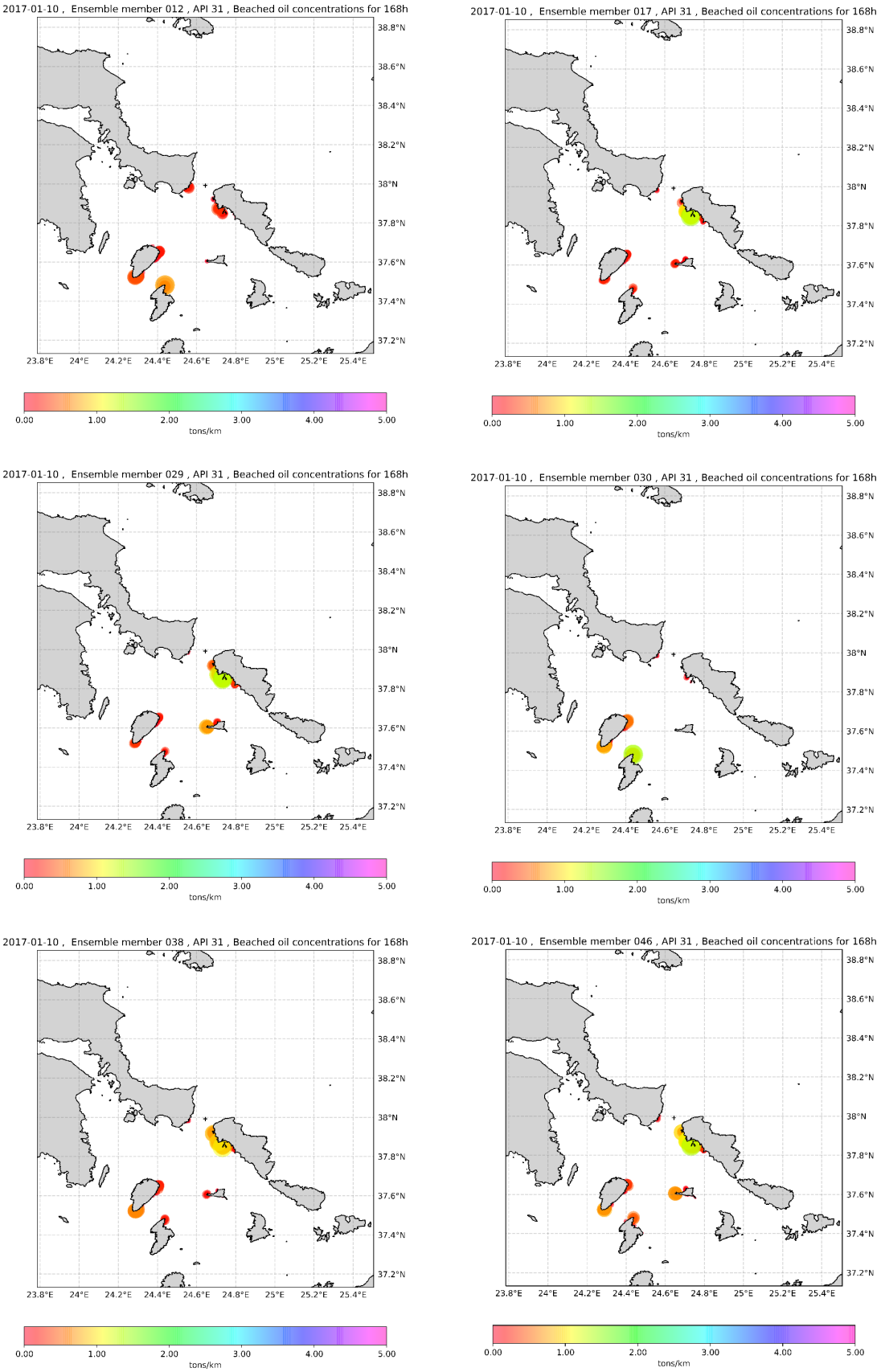

Figure 3.17: Beached oil concentrations of some of the ensemble members for winter, API 31 and simulation time of 168 hours.

Similarly, fig. 3.18 illustrates the beached oil concentrations of the deterministic simulation for spring and 168 hours forecast lead time, with a maximum value of 13.52 tons/km, and fig. 3.19 the beached oil concentrations of a portion of the members, with a maximum value of 18.54 tons/km (ensemble member 034). Although the concentrations of the beached oil in spring are higher than the winter case, differences in the beached oil predictions are lower, as shown in fig. 3.19, due to the lower differences and uncertainty of the MEDSLIK II simulations ensemble spread, discussed in section 3.1. Nevertheless, in both cases, the uncertainties generated by the use of the ensemble approach for the wind forcing and the information about the possible concentration values and hit locations of the beached oil, provide a useful tool to assess the impact on the coastal area and to better prepare, by taking into account the possible scenarios.

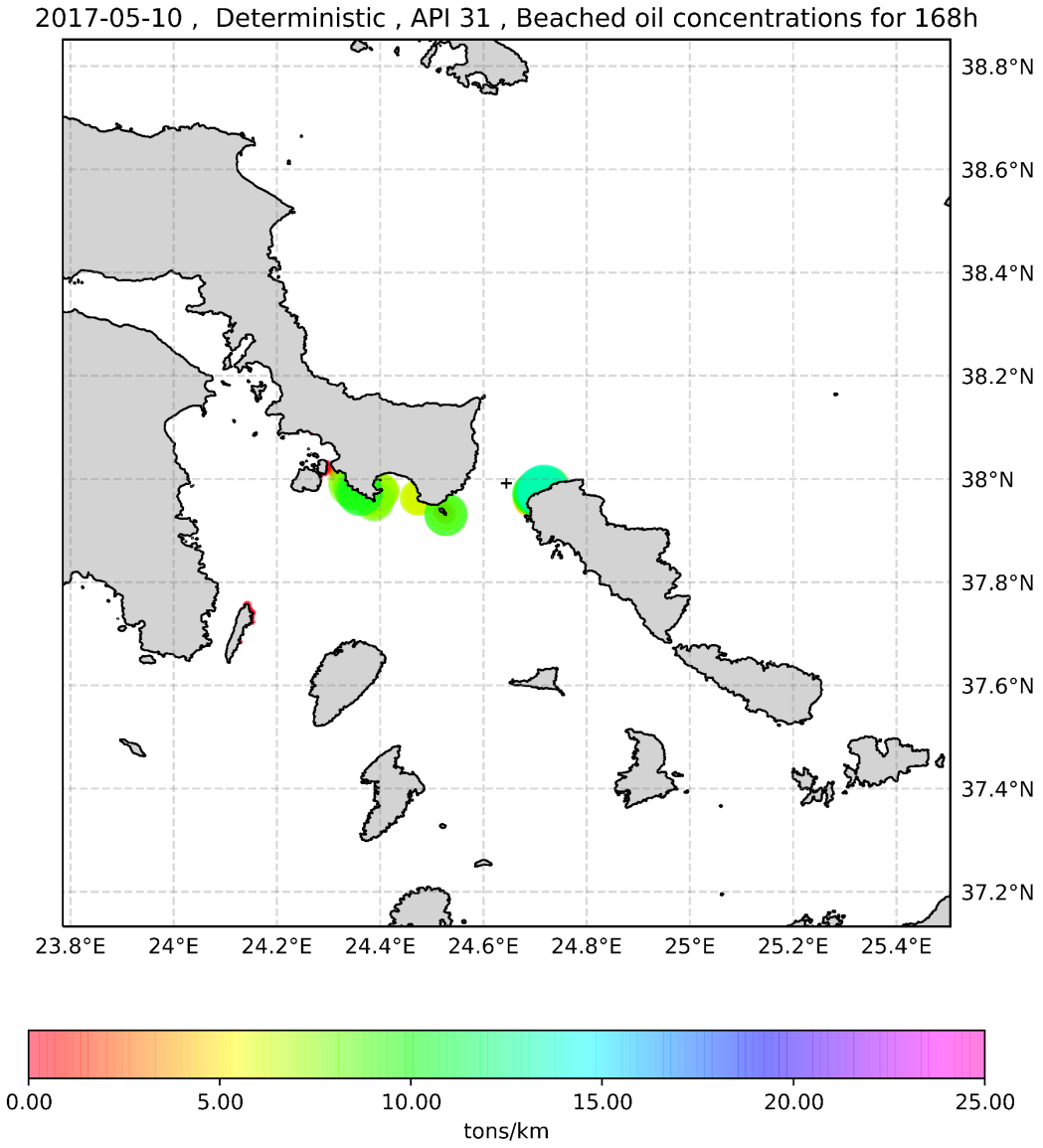

Figure 3.18: Beached oil concentrations of deterministic simulation for spring, simulation time of 168 hours and 31 API.

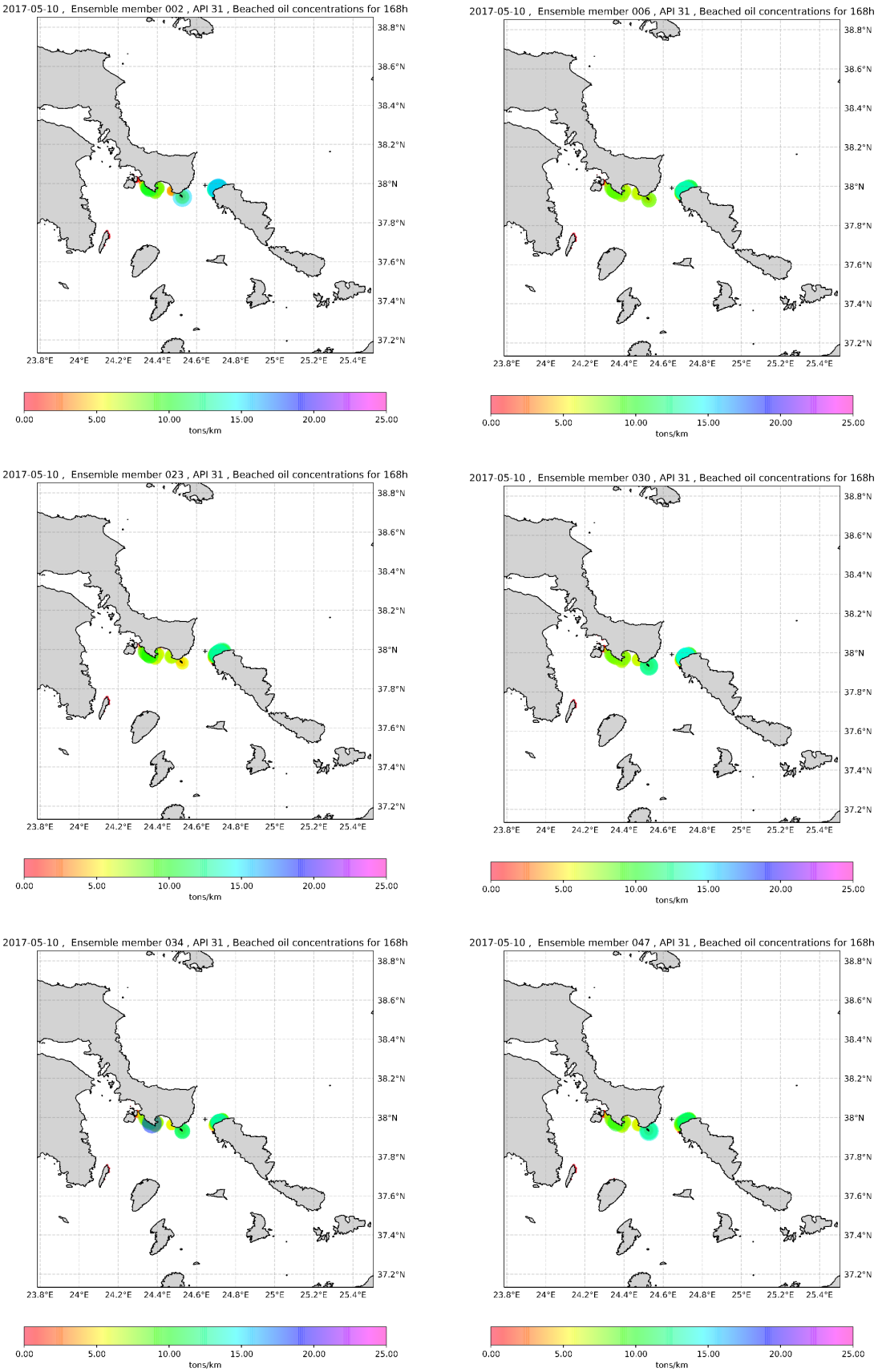

Figure 3.19: Beached oil concentrations of some of the ensemble members for spring, API 31 and simulation time of 168 hours.

3.2.2. Uncertainty assessment for beached oil

The above results can be further verified by looking at the total amount of oil beached and fixed at the coast (total fixed oil) over time. In winter, the variability of the total fixed oil between members is high (fig. 3.20a). This variability can be further expressed as uncertainty, as seen in fig. 3.21, by examining the mean and standard deviation of total fixed oil. The standard deviation is of great magnitude in comparison to the mean, indicating a large distribution about the mean. This high variability is also the reason for the difference in the total fixed oil values between the deterministic and the members' mean (fig. 3.21a & 3.22).

In spring, the variability of the total fixed oil between the members is lower than the winter case, despite the higher quantity of beached oil, as shown in fig. 3.20b. In contrast to the winter case, the smaller magnitude of the standard deviation in comparison to the mean indicates the lower spread of the total fixed oil values around the mean (fig. 3.23). Additionally, the differences in the total fixed oil values between the deterministic and the members' mean, are less important, in comparison to the winter case (fig. 3.23a & 3.24).

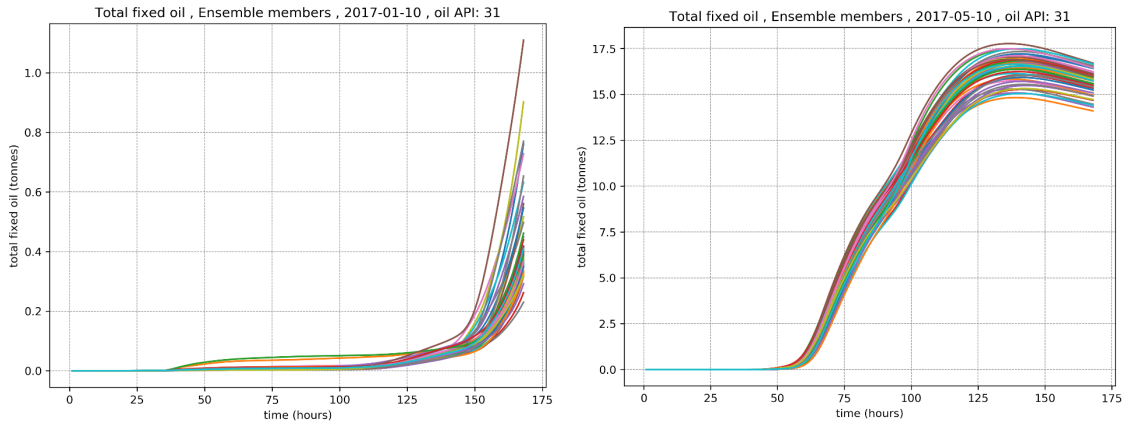

(a) (b)

Figure 3.20: Total fixed oil (beached oil) of each ensemble member for API: 31 and two time periods: (a) winter, (b) spring.

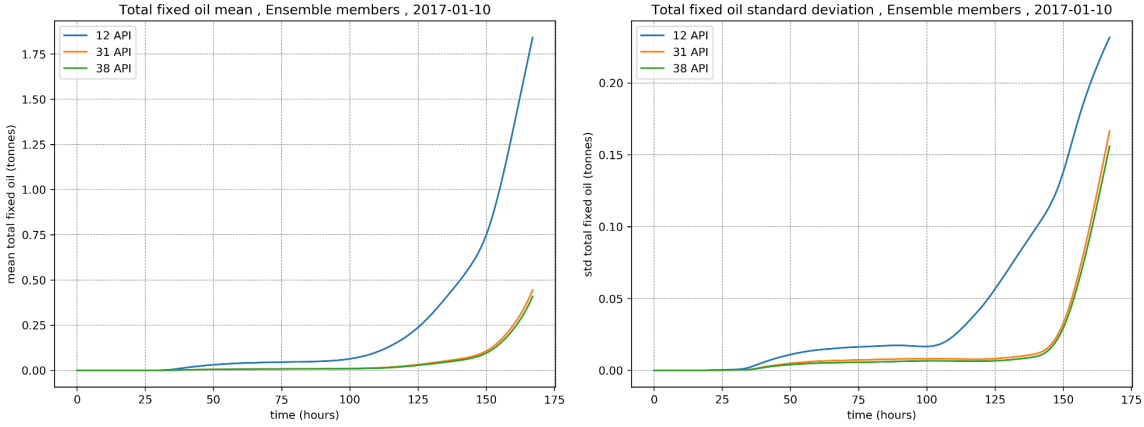

(a) (b)

Figure 3.21: Total fixed oil (a) mean and (b) standard deviation for winter and all oil APIs.

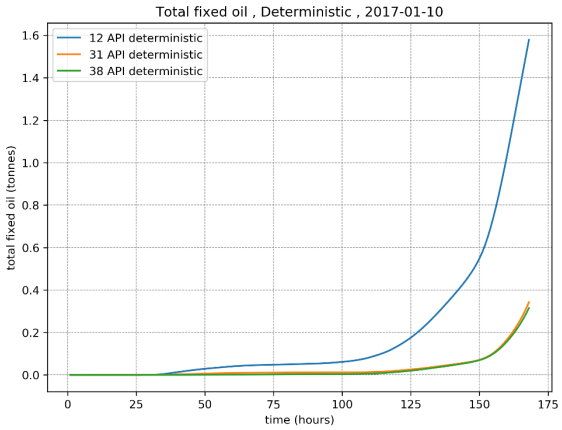

Figure 3.22: Total fixed oil of deterministic simulation for winter and all oil APIs.

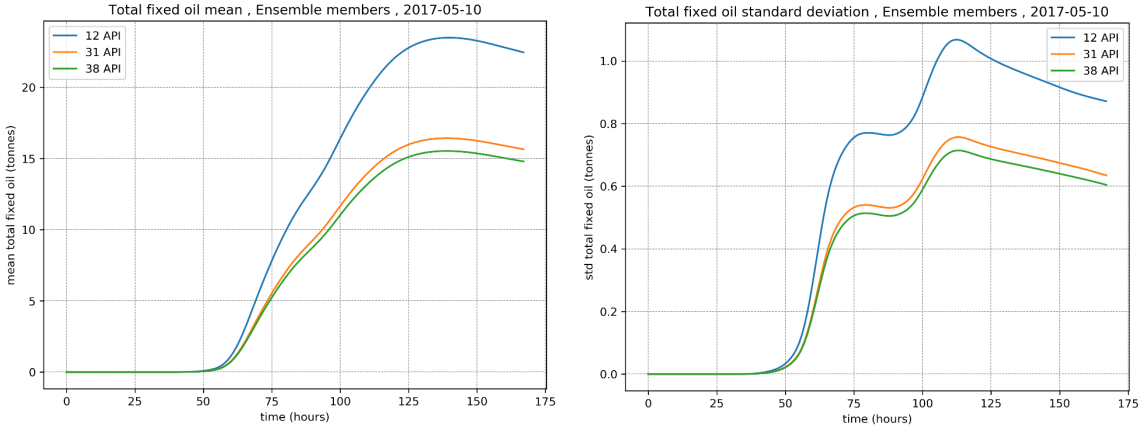

(a) (b)

Figure 3.23: Total fixed oil (a) mean and (b) standard deviation for spring and all oil APIs.

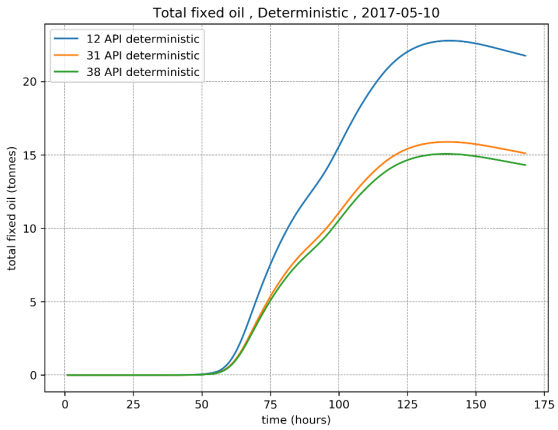

Figure 3.24: Total fixed oil of deterministic simulation for spring and all oil APIs.

For the quantification of temporal uncertainty for the beached oil, we used oiling probability as defined in section 2.4.4, to examine the probability of the presence of fixed oil on the coast, across the 50 ensemble members in total, for every time step. Oiling probability, shows an uncertainty in the hit time for beached oil for the ensemble runs, in contrast to the binary event of a single deterministic run.

In winter, the uncertainty in the temporal window for the beached oil and for the ensemble members for oil API: 31, starts at 21 hours and ends at 36 hours, having a duration of 15 hours, as shown in fig. 3.25a. This means that according to the performed simulations, before the 21 hour time mark and after the 36 hour time mark, the probability of the presence of total fixed oil on the coast (oiling probability) is 0% and 100% respectively, while for the duration between these two time marks the probability varies in time as more members predict oil beaching. This information which takes into account, the predictability of the wind forcing and is translated into oil spill predictability through multiple binary events of beached oil among members, is of added value compared with the binary event shown in fig. 3.25 for the deterministic simulation with a single hit time (at the 25 hour time mark in winter and the 37 hour time mark in spring). In spring, as shown in fig. 3.25b, the uncertainty window for the ensemble members and for oil API: 31 is shorter than in winter, most likely due to the lower ensemble spread of the oil spill, as discussed in previous sections. The duration of this uncertainty temporal window is approximately 8 hours, including the first (at the 33 hour mark) and last members being beached (at the 41 hour mark).

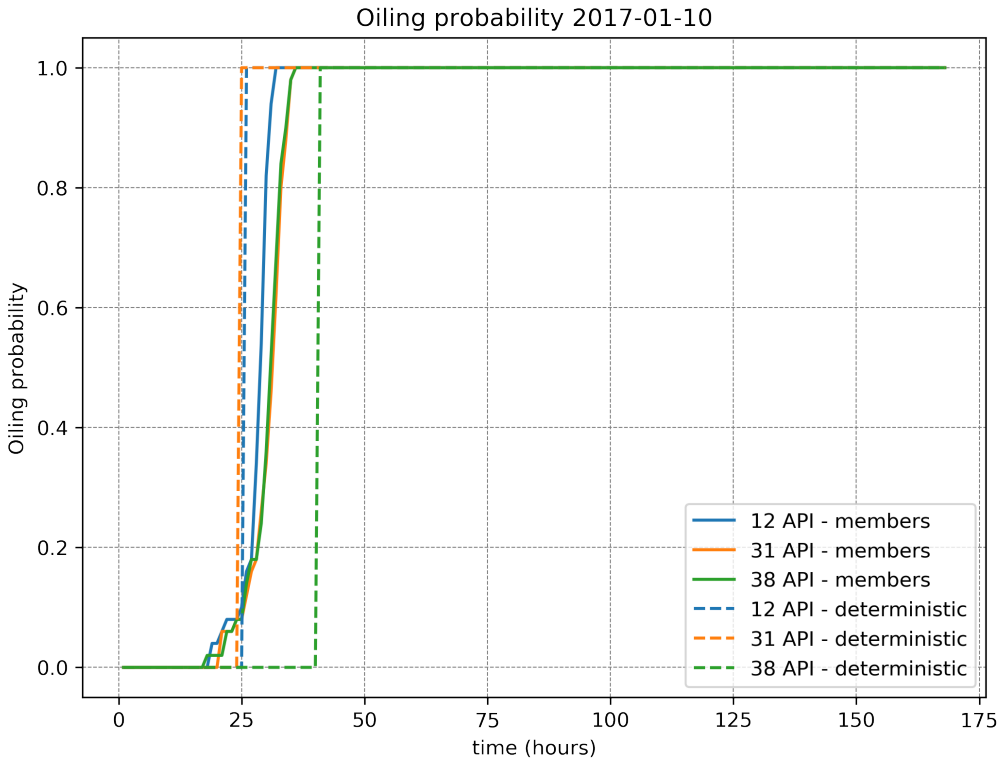

(a)

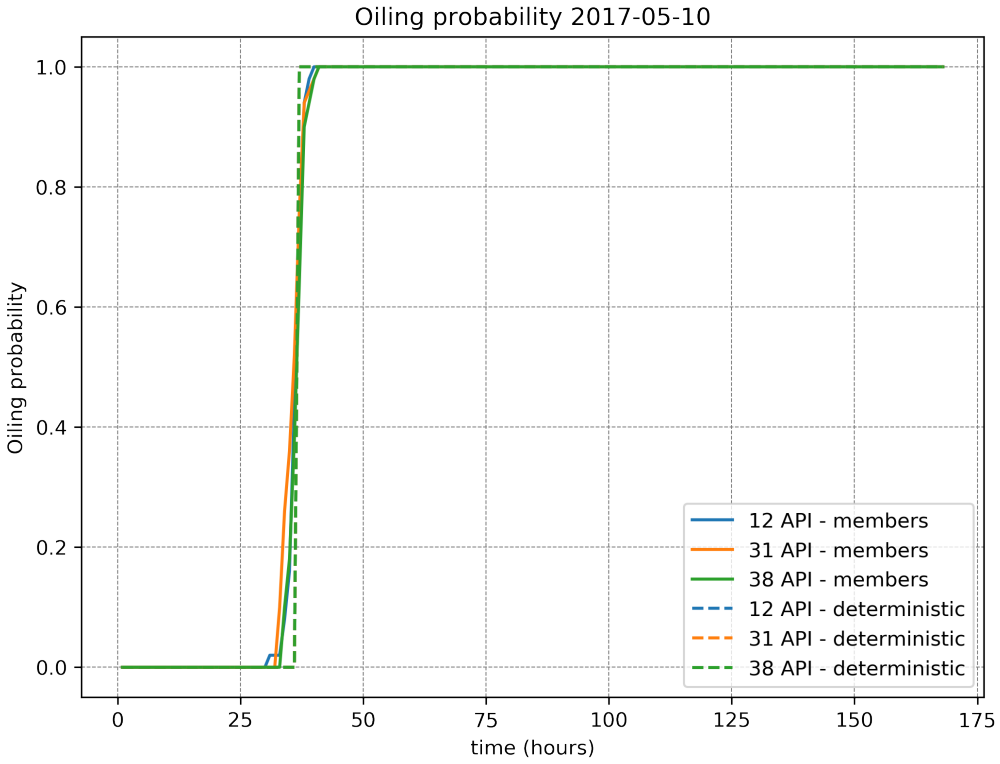

(b)

Figure 3.25: Oiling probability of deterministic and ensemble members for (a) winter and (b) spring.

3.3. Oil trajectory – spreading and beached oil for oil API: 12 & 38

As in sections 3.1 and 3.2, in this part, we discuss concisely about the trajectory and spreading of the oil spills for oil API: 12 and 38, as well as the beached oil maps and the total amount of oil beached and fixed at the coast every time step for these two types of oil, according to the ensemble oil spill simulations, and the uncertainty assessment for these results. For convenience, the figures discussed below are presented in appendices A and B. As expected, the observations discussed in sections 3.1 and 3.2 about the uncertainty generated in the oil spill forecasting by the wind forcing ensembles, are once again seen and verified below.

3.3.1. Oil trajectory – spreading (oil API: 12 & 38)

Figures A.1 to A.8 (appendix A1) illustrate the surface oil concentrations and spreading of the deterministic and ensemble members for winter and spring, with seven days forecast lead time. Oil spill transportation is greatly influenced by the wind forcing. The oil slicks are transporting downwind for both periods, with variations in the transport and the evolution of the shape and size of the oil spills being observed between the ensembles. The lighter oil (API: 38) seems to be more affected by the wind and is transporting further, than the heavier oil (API: 12).

Figures A.9 to A.24 (appendix A2) present the convex hulls of the deterministic and ensemble members for oil API: 12 and oil API: 38, for winter and spring and simulation times of 72 and 168 hours. Also, in this set of figures, we assess the uncertainty in the extent of the ensemble oil spills through the differences between the convex hulls denoted by the metrics A_{exceed} and DA (presented in sections 2.4.1 and 3.1.2). The area difference between the deterministic and the total ensemble convex hull (DA), is higher for the lighter oil (oil API: 38), likely due to the higher influence of the wind in the transportation of the lighter oil slick. However, the spread of the A_{exceed} is higher for oil API: 12 (heavier type of oil), especially in spring, indicating higher variations in the extent of the ensemble oil spills for this type of oil. This is likely due to the interaction between the oil spill and the shoreline, which is also higher in spring. The uncertainty and the variability in the extent of the oil spill ensembles, generated by the wind forcing ensembles, is higher for heavy types of oil (e.g. oil API: 12) if the oil spill interacts heavily with the coast (beached oil) in the duration of the simulation, as suggested by our results. This indicates the importance of the ensemble approach for the wind forcing in the oil spill simulations, for heavier types of oil spills in nearshore areas.

Figures A.25 and A.26 show the trajectories of the simulated parcels' mean of every individual ensemble member for 168 hours and oil API: 12 and 38, during winter and spring. The trajectory spread increases with time for all cases and a more significant transport is observed for the lighter oil.

In fig. 3.14 and 3.15 (presented in section 3.1.2), RMSE and uncertainty index s are used to further evaluate the uncertainty in the oil spill. RMSE displays higher values for lighter types of oil (oil API: 38) in both winter and spring. This observation is also supported by the uncertainty index s metric, which weights the average of the separation distances between the simulated deterministic and ensemble members by the length of the deterministic trajectory. According to uncertainty index s, the uncertainty in the oil spill generated by the ensemble wind forcing displays higher values for lighter types of oil (oil API: 38).

3.3.2. Beached oil (oil API: 12 & 38)

Figures B.1 to B.8 illustrate the beached oil concentrations of the deterministic and the ensemble simulations for winter and spring, with seven days forecast lead time. The deterministic simulation in the winter predicts a maximum value of 3.36 tons/km for oil API: 12 (fig. B.1) and 0.52 tons/km for oil API: 38 (fig. B.3). For the presented ensemble members in winter, a maximum value of 5.63 tons/km (member 046) is predicted for oil API: 12 (fig. B.2) and 1.39 tons/km (member 017) for oil API: 38 (fig. B.4). In spring the concentrations of the beached oil are higher than the winter case and the deterministic simulation predicts a maximum value of 20.83 tons/km for oil API: 12 (fig. B.5) and 12.44 tons/km for oil API: 38 (fig. B.7), while the presented ensemble members predict a maximum value of 39.74 tons/km (member 034) for oil API: 12 (fig. B.6) and 14.27 tons/km (member 002) for oil API: 38 (fig. B.8).

Figures B.9 and B.10 present the total amount of oil beached and fixed at the coast (total fixed oil) over time, for oil API: 12 and 38, in winter and spring. The variability of total fixed oil is higher for heavier oils (oil API: 12), an important consideration especially in spring, where the amount of total fixed oil is higher than the winter case. The higher uncertainty and spread of the ensemble for heavier types of oil can be further expressed by examining the standard deviation of the total fixed oil as shown in fig. 3.21 and 3.23 (presented in section 3.2.2). The magnitude of the standard deviation is higher for oil API: 12 (heavy type of oil) for both winter and spring.

Finally, as shown in fig. 3.25 (presented in section 3.2.2), the uncertainty window for the ensemble members and for oil API: 12 is shorter in the winter than the uncertainty window for oil API: 38 and higher in spring.

4. Conclusions and Recommendations for Further Work

4.1. Summary and Main Conclusions

This study aims at evaluating the impact of the atmospheric forcing uncertainty on the performance of the oil spill modelling and the dispersion of the pollutants in the marine environment of the Aegean Sea, following a probabilistic approach for the simulation of the oil spill. Ensemble wind predictions generated via the ECMWF EPS were used for the required atmospheric forcing and generated an ensemble of oil spill forecasts using oil spill model MEDSLIK II, in order to better represent the predictability of the atmospheric forcing. We examined uncertainties like the spreading and transport of the oil slick, the extent of the oil spill, including both surface and subsurface as well as the oil beached on the coast, the amount of total fixed oil on the coast and finally temporal uncertainties regarding the oil beaching time. Our final goal was to ascertain whether the uncertainty information generated by the ensembles is important, and therefore, if an ensemble approach for the atmospheric forcing can improve the information provided by the oil spill forecasting and provide the decision makers with a picture of the outcomes closer to the reality in the event of an oil spill. An ensemble of 50 members and the deterministic simulation was used for the atmospheric forcing in the oil spill simulations, for two time periods (winter and spring) and 3 different types of oil with a 168 hours lead time.

Wind forcing influences heavily the oil transportation in the study area. The sensitivity analysis performed indicates the importance of the wind on the performance of the oil spill modelling especially in nearshore areas. All the ensemble oil slicks simulated by MEDSLIK II, spread mainly in the downwind direction, but there are variations in the transport and the evolution of the shape and size of the oil spills between the ensembles. Oil spill ensemble spread increases over time, representing the uncertainty generated in the oil spill forecasting by the ECMWF EPS ensembles. This increase displays higher values and more significant increases for a highly variable wind forcing, with high wind intensity, sudden changes in the wind field, and the possible presence of phase errors in the wind ensembles used. The extent of the area affected by the ensemble oil spills in total, is found to be greater than the area only affected by the deterministic simulation, providing additional information (of the order of 15% - 35% in the latter hours of the simulation, depending on the time period and the type of oil) with respect to the deterministic approach. For a highly variable wind forcing, the spread and uncertainty generated by the atmospheric ensembles are higher for lighter types of oil (higher API values). However, for a lower variable wind forcing with a higher interaction between the oil spill and the coast and a greater amount of beached oil, the

spread and the uncertainty generated by the atmospheric ensembles appear to be higher for heavier types of oil (lower API values).

Our results show that as time goes on and the uncertainty increases, a deterministic approach for the wind forcing can presumably limit the accuracy and the information provided by the oil spill model forecasts, regardless of how good the forecast model is. Thus, the use and the added value of a probabilistic approach for the wind forcing that takes into account the predictability of the atmospheric forcing, in relation to the deterministic, and the simulation of ensemble oil spill forecasts that predict several equally possible oil spill states becomes more important as time goes on. In conclusion, the ensemble approach as described above has great potential benefits and seems to improve the possibilities of the oil spill modelling, by predicting the possible trajectories of the oil spill transport, the volume and location of the beached oil, by giving a better estimate for the possible extent of the oil spill and the area it may affect and by providing a possible time window for the appearance of oil in the coastal area. This knowledge could prove an important tool to better plan and direct the available resources for the control and mitigation procedures, in the event of an oil spill.

4.2. Recommendations for Further Work

- MEDSLIK II calculates the wave-induced velocity (Stokes drift) using an empirical formulation that depends on wind amplitude (De Dominicis et al., 2013a). Future studies could fruitfully explore this issue further by using complex numerical wave models to calculate the Stokes drift and examine the potential effects it may have on the ensemble approach for the atmospheric forcing.
- We believe that hazard maps could possibly be created based on the ensemble methodology we described in our study, to better present our results.
- Also, it will be important that future research verify our results against observations.

5. References

Al Shami, A., Harik, G., Alameddine, I., Bruschi, D., Garcia, D. A., & El-Fadel, M. (2017). Risk assessment of oil spills along the Mediterranean coast: A sensitivity analysis of the choice of hazard quantification. *Science of The Total Environment*, *574*, 234–245. https://doi.org/10.1016/j.scitotenv.2016.09.064

Amir-Heidari, P., Arneborg, L., Lindgren, J. F., Lindhe, A., Rosén, L., Raie, M., … Hassellöv, I.-M. (2019). A state-of-the-art model for spatial and stochastic oil spill risk assessment: A case study of oil spill from a shipwreck. *Environment International*, *126*(February), 309–320. https://doi.org/10.1016/j.envint.2019.02.037

Amir-Heidari, P., & Raie, M. (2019). A new stochastic oil spill risk assessment model for Persian Gulf: Development, application and evaluation. *Marine Pollution Bulletin*, *145*(May), 357–369. https://doi.org/10.1016/j.marpolbul.2019.05.022

Cheung, J., Hally, A., Heijstek, J., Marsman, A., & Brenguier, J. L. (2015). Recommendations on trajectory selection in flight planning based on weather uncertainty. *SESAR Innovation Days*, (January).

Clementi, E., Pistoia, J., Escudier, R., Delrosso, D., Drudi, M., Grandi, A.,Lecci R., Cretí S., Ciliberti S., Coppini G., Masina S., Pinardi, N. (2019). Mediterranean Sea Analysis and Forecast (CMEMS MED-Currents, EAS4 system) [Data set]. *Copernicus Monitoring Environment Marine Service (CMEMS).* https://doi.org/https://doi.org/10.25423/CMCC/MEDSEA_ANALYSIS_FORECAST_PHY_006_013_EAS4

De Dominicis, M., Pinardi, N., Zodiatis, G., & Archetti, R. (2013b). MEDSLIK-II, a Lagrangian marine surface oil spill model for short-term forecasting – Part 2: Numerical simulations and validations. *Geoscientific Model Development*, *6*(6), 1871–1888. https://doi.org/10.5194/gmd-6-1871-2013

De Dominicis, M., Pinardi, N., Zodiatis, G., & Lardner, R. (2013a). MEDSLIK-II, a Lagrangian marine surface oil spill model for short-term forecasting – Part 1: Theory. *Geoscientific Model Development*, *6*(6), 1851–1869. https://doi.org/10.5194/gmd-6-1851-2013

EMSA. (2019). *Annual Overview of Marine Casualties and Incidents 2019*.

GEBCO Compilation Group. (2014). *GEBCO 2014 Grid*. Retrieved from https://www.gebco.net/

Goldman, R., Biton, E., Brokovich, E., Kark, S., & Levin, N. (2015). Oil spill contamination probability in the southeastern Levantine basin. *Marine Pollution Bulletin*, *91*(1), 347–356. https://doi.org/10.1016/j.marpolbul.2014.10.050

Jiménez Madrid, J. A., García-Ladona, E., & Blanco-Meruelo, B. (2016). Oil Spill Beaching Probability for the Mediterranean Sea. In *Handbook of Environmental Chemistry* (Vol. 5, pp. 305–324). https://doi.org/10.1007/698_2016_37

Jorda, G., Comerma, E., Bolaños, R., & Espino, M. (2007). Impact of forcing errors in the CAMCAT oil spill forecasting system. A sensitivity study. *Journal of Marine Systems*, *65*(1–4), 134–157. https://doi.org/10.1016/j.jmarsys.2005.11.016

Khade, V., Kurian, J., Chang, P., Szunyogh, I., Thyng, K., & Montuoro, R. (2017). Oceanic ensemble forecasting in the Gulf of Mexico: An application to the case of the Deep Water Horizon oil spill. *Ocean Modelling*, *113*, 171–184. https://doi.org/10.1016/j.ocemod.2017.04.004

Lardner, R., Zodiatis, G., Hayes, D., Pinardi, N. (2006). Application of the MEDSLIK oil spill model to the Lebanese Spill of July 2006. *European Group of Experts on Satellite Monitoring of Sea Based Oil Pollution. European Communities*.

Lardner, R., Zodiatis, G., Loizides, L., & Demetropoulos, A. (1998). An operational oil spill model for the Levantine Basin(Eastern Mediterranean Sea. *International Symposium on Marine Pollution*.

Liu, Y., & Weisberg, R. H. (2011). Evaluation of trajectory modeling in different dynamic regions using normalized cumulative Lagrangian separation. *Journal of Geophysical Research*, *116*(C9), C09013. https://doi.org/10.1029/2010JC006837

Liubartseva, S., De Dominicis, M., Oddo, P., Coppini, G., Pinardi, N., & Greggio, N. (2015). Oil spill hazard from dispersal of oil along shipping lanes in the Southern Adriatic and Northern Ionian Seas. *Marine Pollution Bulletin*, *90*(1–2), 259–272. https://doi.org/10.1016/j.marpolbul.2014.10.039

Mackay, D., Paterson, S., Trudel, B. (1980). A mathematical model of oil spill behaviour. *Report to Research and Development Division, Environment Emergency Branch, Environmental Impact Control Directorate, Environmental Protection Service, Environment Canada, Ottawa*.

MarineTraffic – Global Ship Tracking Intelligence (www.marinetraffic.com).

NITTIS, K., & PERIVOLIOTIS, L. (2002). Circulation and hydrological characteristics of the North Aegean Sea: a contribution from real-time buoy measurements. *Mediterranean Marine Science*, *3*(1), 21. https://doi.org/10.12681/mms.255

Olita, A., Fazioli, L., Tedesco, C., Simeone, S., Cucco, A., Quattrocchi, G., … Sorgente, R. (2019). Marine and Coastal Hazard Assessment for Three Coastal Oil Rigs. *Frontiers in Marine Science*, *6*(May), 1–8. https://doi.org/10.3389/fmars.2019.00274

Portman, M. E. (2016). Principles of Integration for Oceans and Coasts. In *Environmental Planning for Oceans and Coasts* (pp. 61–77). https://doi.org/10.1007/978-3-319-26971-9_4

Poulos, S. E., Drakopoulos, P. G., & Collins, M. B. (1997). Seasonal variability in sea surface oceanographic conditions in the Aegean Sea (Eastern Mediterranean): an overview. *Journal of Marine Systems*, *13*(1–4), 225–244. https://doi.org/10.1016/S0924-7963(96)00113-3

Price, J. M., Johnson, W. R., Marshall, C. F., Ji, Z.-G., & Rainey, G. B. (2003). Overview of the Oil Spill Risk Analysis (OSRA) Model for Environmental Impact Assessment. *Spill Science & Technology Bulletin*, *8*(5–6), 529–533.

https://doi.org/10.1016/S1353-2561(03)00003-3

Samaras, A. G., De Dominicis, M., Archetti, R., Lamberti, A., & Pinardi, N. (2014). Towards improving the representation of beaching in oil spill models: A case study. *Marine Pollution Bulletin*, *88*(1–2), 91–101. https://doi.org/10.1016/j.marpolbul.2014.09.019

Sepp Neves, Antonio A., Pinardi, N., Navarra, A., & Trotta, F. (2020). A General Methodology for Beached Oil Spill Hazard Mapping. *Frontiers in Marine Science*, *7*(February), 1–10. https://doi.org/10.3389/fmars.2020.00065

Sepp Neves, Antonio Augusto, Pinardi, N., & Martins, F. (2016). IT-OSRA: applying ensemble simulations to estimate the oil spill risk associated to operational and accidental oil spills. *Ocean Dynamics*, *66*(8), 939–954. https://doi.org/10.1007/s10236-016-0960-0

Snow, B. J., Moulitsas, I., Kolios, A. J., & De Dominicis, M. (2014). CranSLIK v1.0: stochastic prediction of oil spill transport and fate using approximation methods. *Geoscientific Model Development*, *7*(4), 1507–1516. https://doi.org/10.5194/gmd-7-1507-2014

UN/MAP. (2017). Mediterranean Quality Status Report. *Mediterranean Action Plan Barcelona Convention*, 539. Retrieved from https://www.medqsr.org/sites/default/files/inline-files/2017MedQSR_Online_0.pdf

UNEP/MAP. (2012). UNEP/MAP: State of the Mediterranean Marine and Coastal Environment. *Barcelona Convention, Athens, 2012*. https://doi.org/10.13140/RG.2.1.3013.2648

Zodiatis, G., Lardner, R., Hayes, D., Georgiou, G., Pinardi, N., De Dominicis, M., Panayidou, X. (2008). The Mediterranean oil spill and trajectory prediction model in assisting the EU response agencies. *Congreso Nacional de Salvamento En La Mar, Cadiz, 2-4 October, Libro de Actas*, 535–547.

Zodiatis G., Lardner R., Georgiou G., Kallos G., P. N. (2005). Operational oil spill modeling predictions in the Mediterranean. *4th EuroGOOS Conference: European Operational Oceanography Present and Future, Brest, 6-9 June*, 131–132.

Zodiatis, G., Coppini, G., Perivoliotis, L., Lardner, R., Alves, T., Pinardi, N., … Sepp Neves, A. A. (2017). Numerical Modeling of Oil Pollution in the Eastern Mediterranean Sea. In A. Carpenter & A. G. Kostianoy (Eds.), *Handbook of Environmental Chemistry* (Vol. 83, pp. 215–254). https://doi.org/10.1007/698_2017_131

Zodiatis, G., Lardner, R., Alves, T. M., Krestenitis, Y., Perivoliotis, L., Sofianos, S., & Spanoudaki, K. (2017). Oil spill forecasting (prediction). *Journal of Marine Research*, *75*(6), 923–953. https://doi.org/10.1357/002224017823523982

Appendix A: Oil trajectory – spreading (oil API: 12 & 38)

A1 Surface oil concentration maps

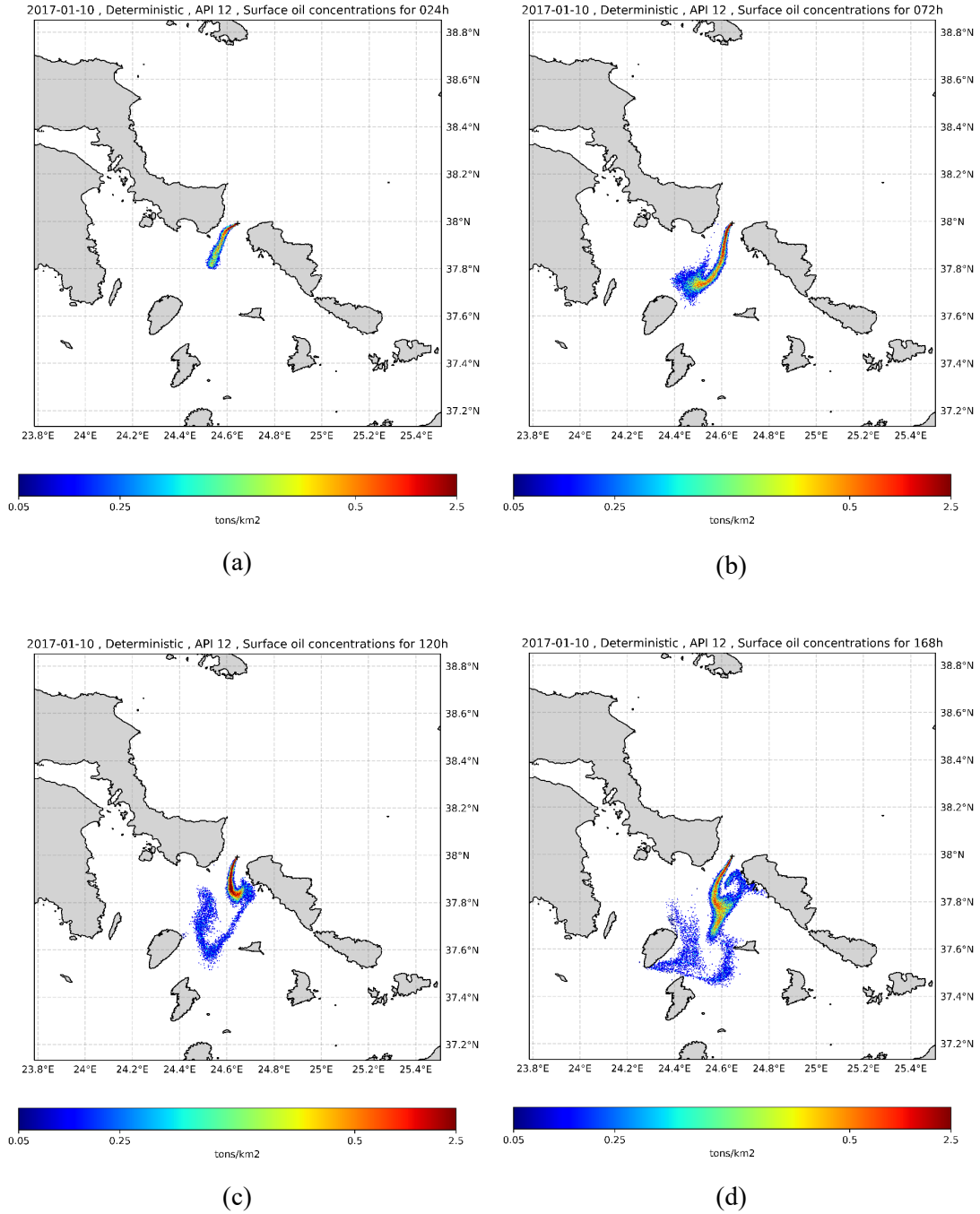

Figure A.1 : Surface oil concentrations of deterministic simulation for winter, 12 API and simulation time of: (a) 24, (b) 72, (c) 120 and (d) 168 hours.

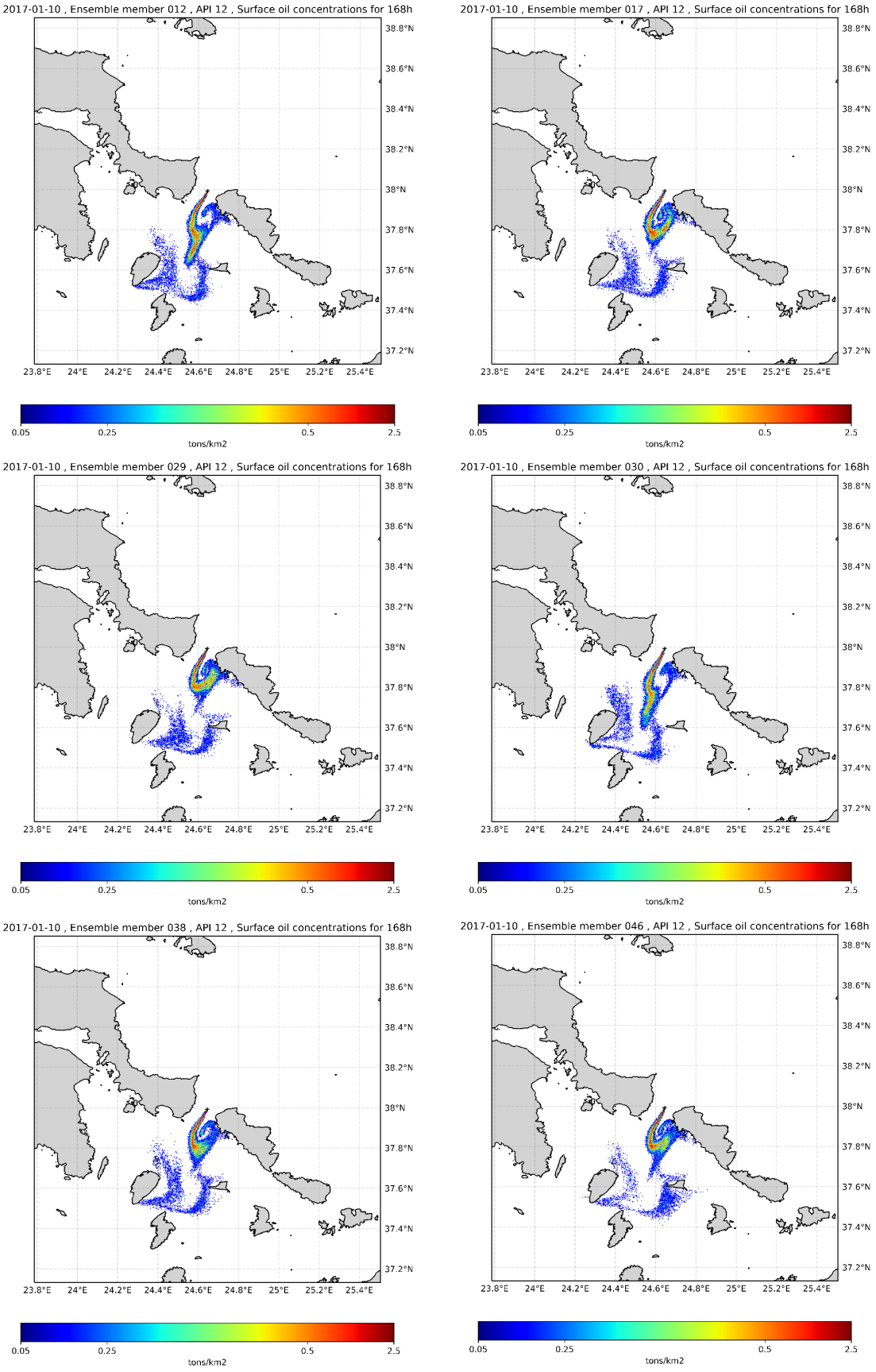

Figure A.2: Surface oil concentrations of some of the ensemble members for winter, API 12 and simulation time of 168 hours.

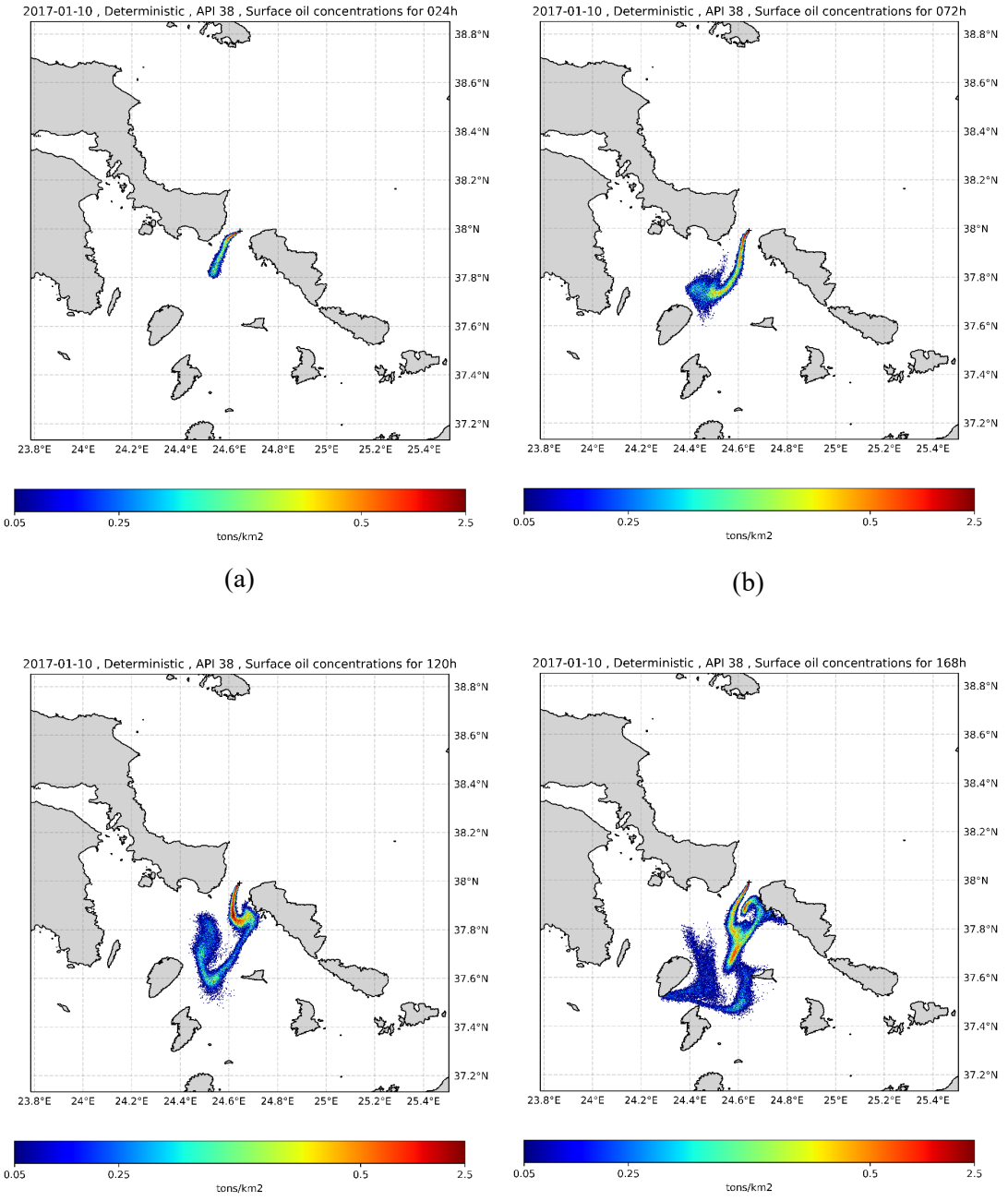

Figure A.3: Surface oil concentrations of deterministic simulation for winter, 38 API and simulation time of: (a) 24, (b) 72, (c) 120 and (d) 168 hours.

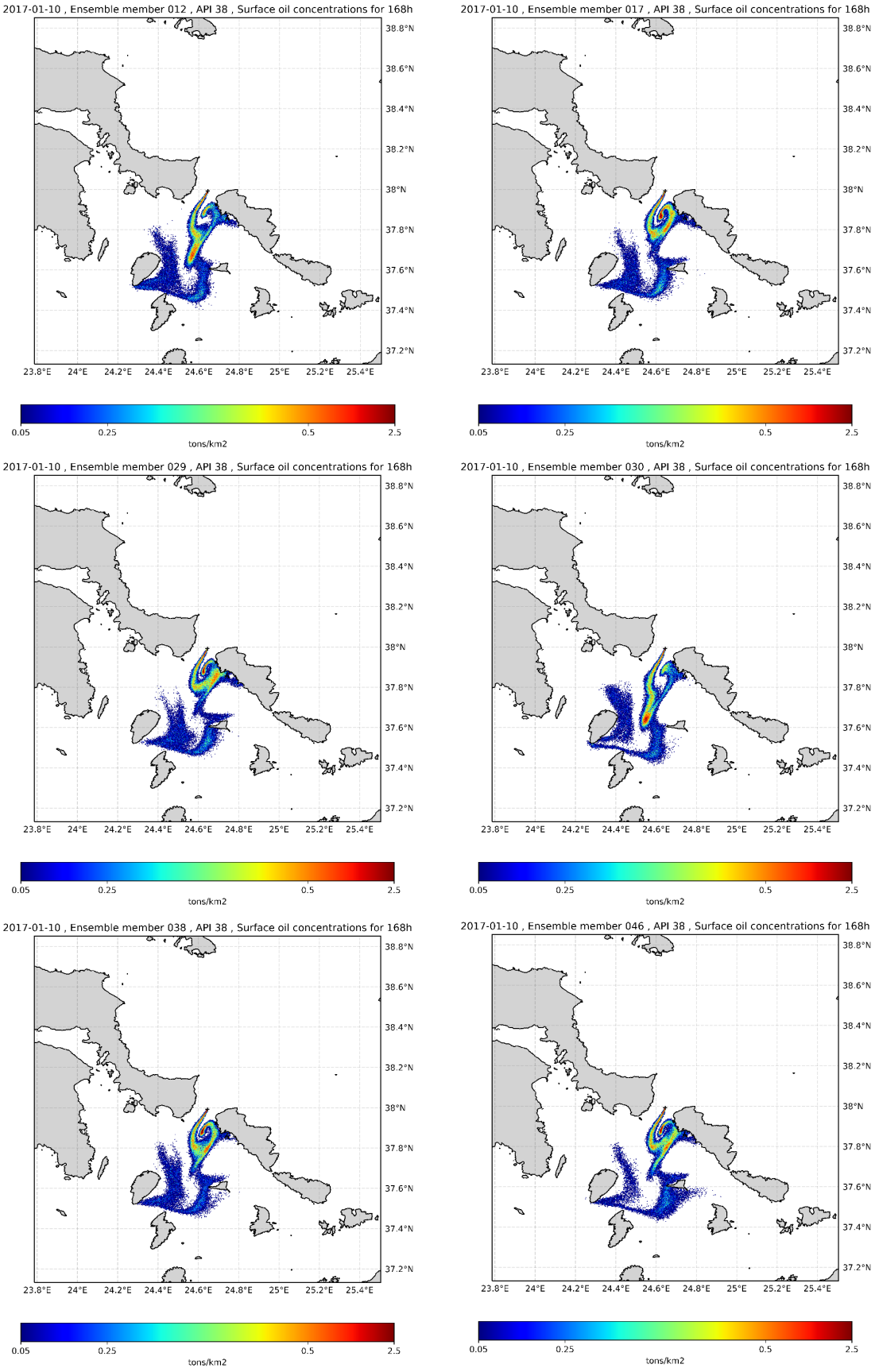

Figure A.4: Surface oil concentrations of some of the ensemble members for winter, API 38 and simulation time of 168 hours.

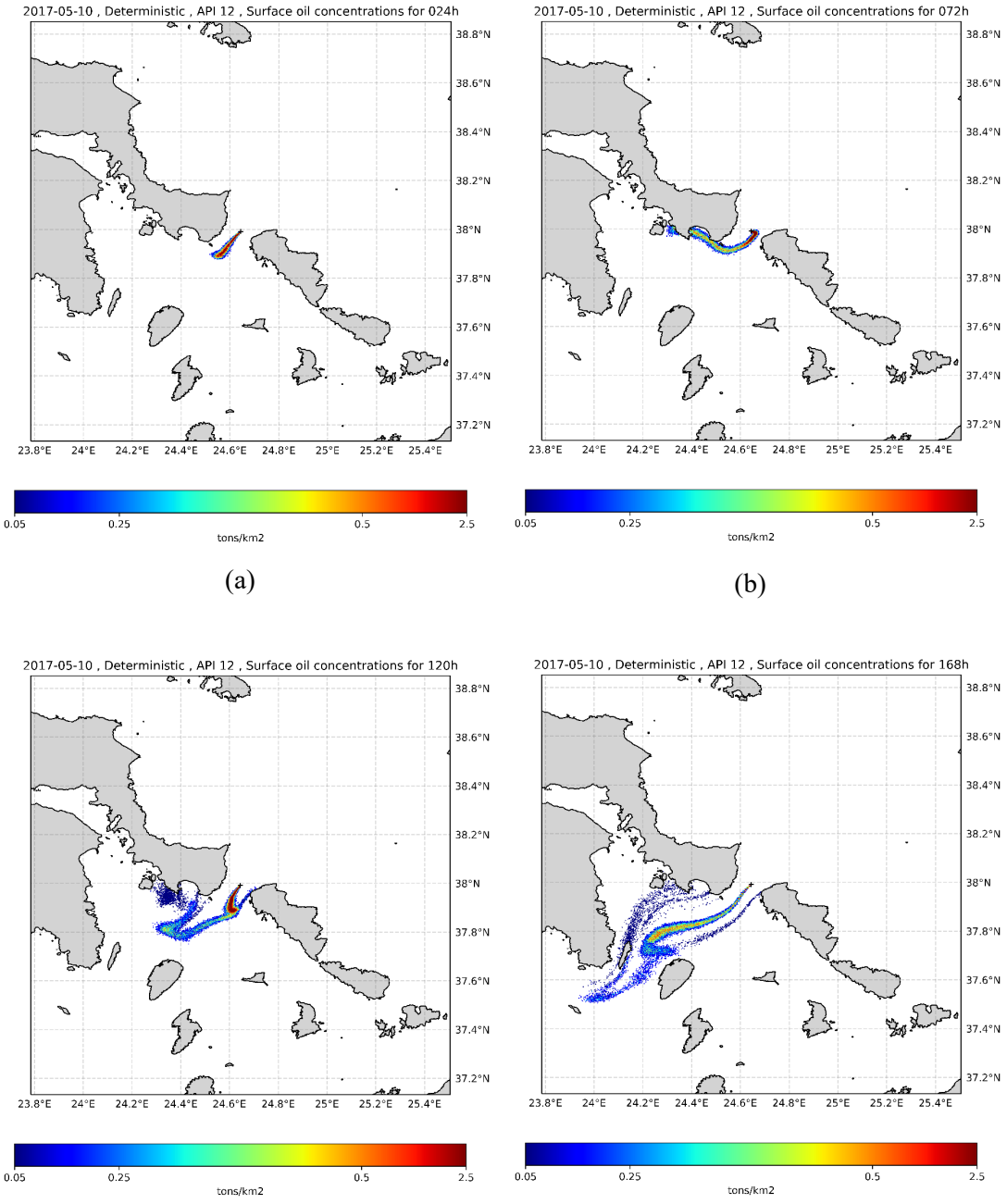

Figure A.5: Surface oil concentrations of deterministic simulation for spring, 12 API and simulation time of: (a) 24, (b) 72, (c) 120 and (d) 168 hours.

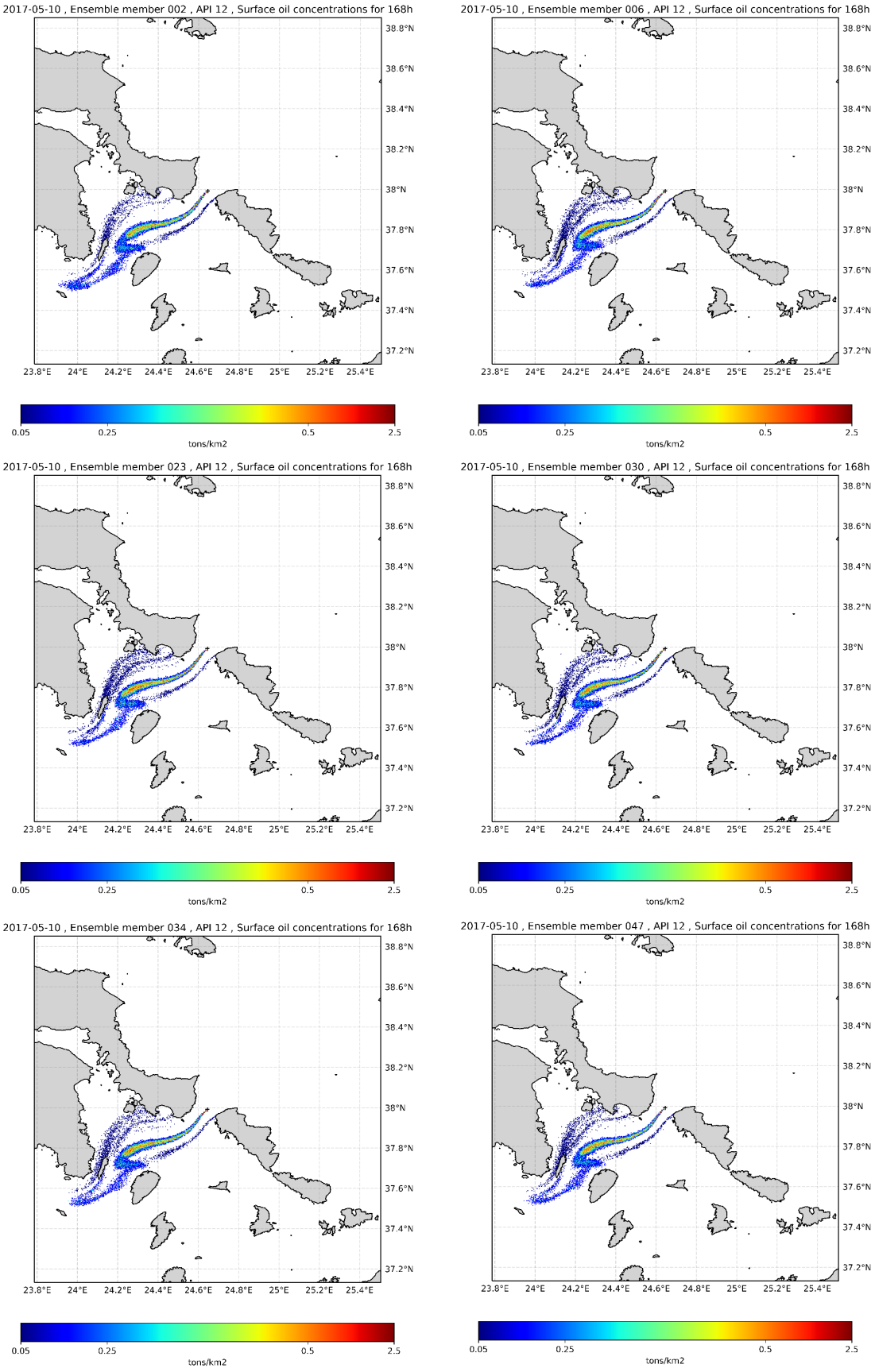

Figure A.6: Surface oil concentrations of some of the ensemble members for spring, API 12 and simulation time of 168 hours.

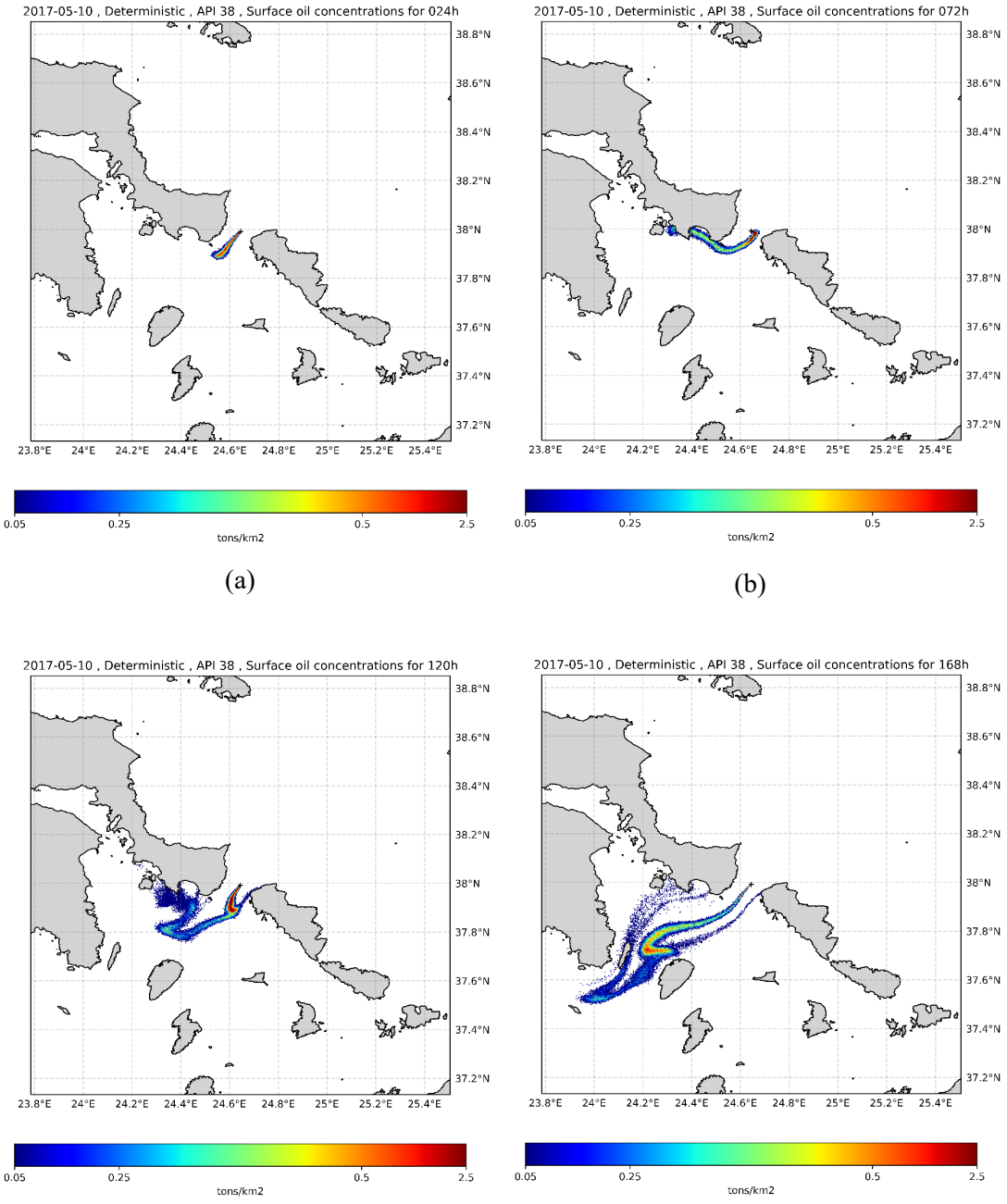

Figure A.7: Surface oil concentrations of deterministic simulation for spring, 38 API and simulation time of: (a) 24, (b) 72, (c) 120 and (d) 168 hours.

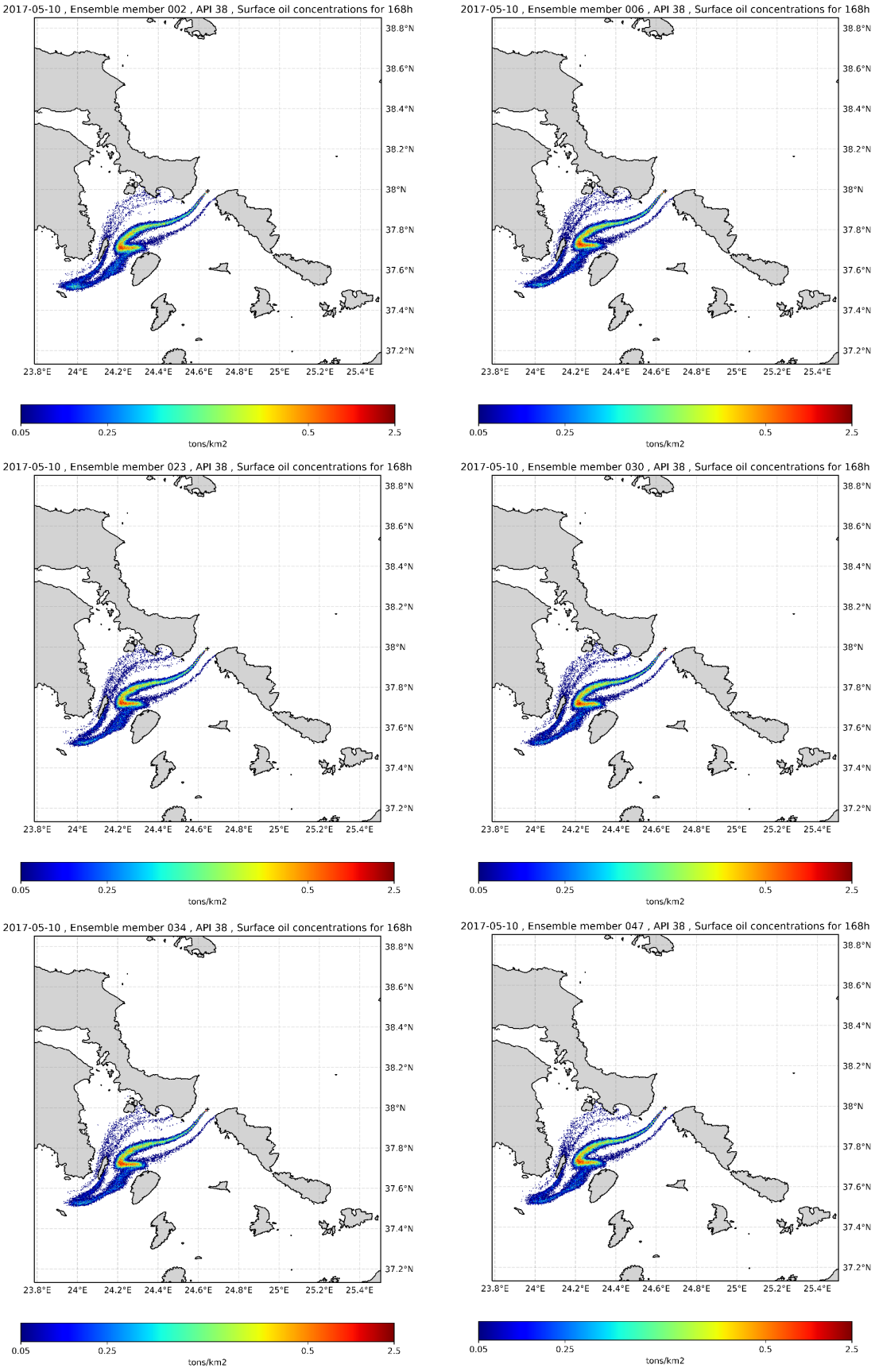

Figure A.8: Surface oil concentrations of some of the ensemble members for spring, API 38 and simulation time of 168 hours.

A2 Uncertainty assessment for oil spill trajectory and spread

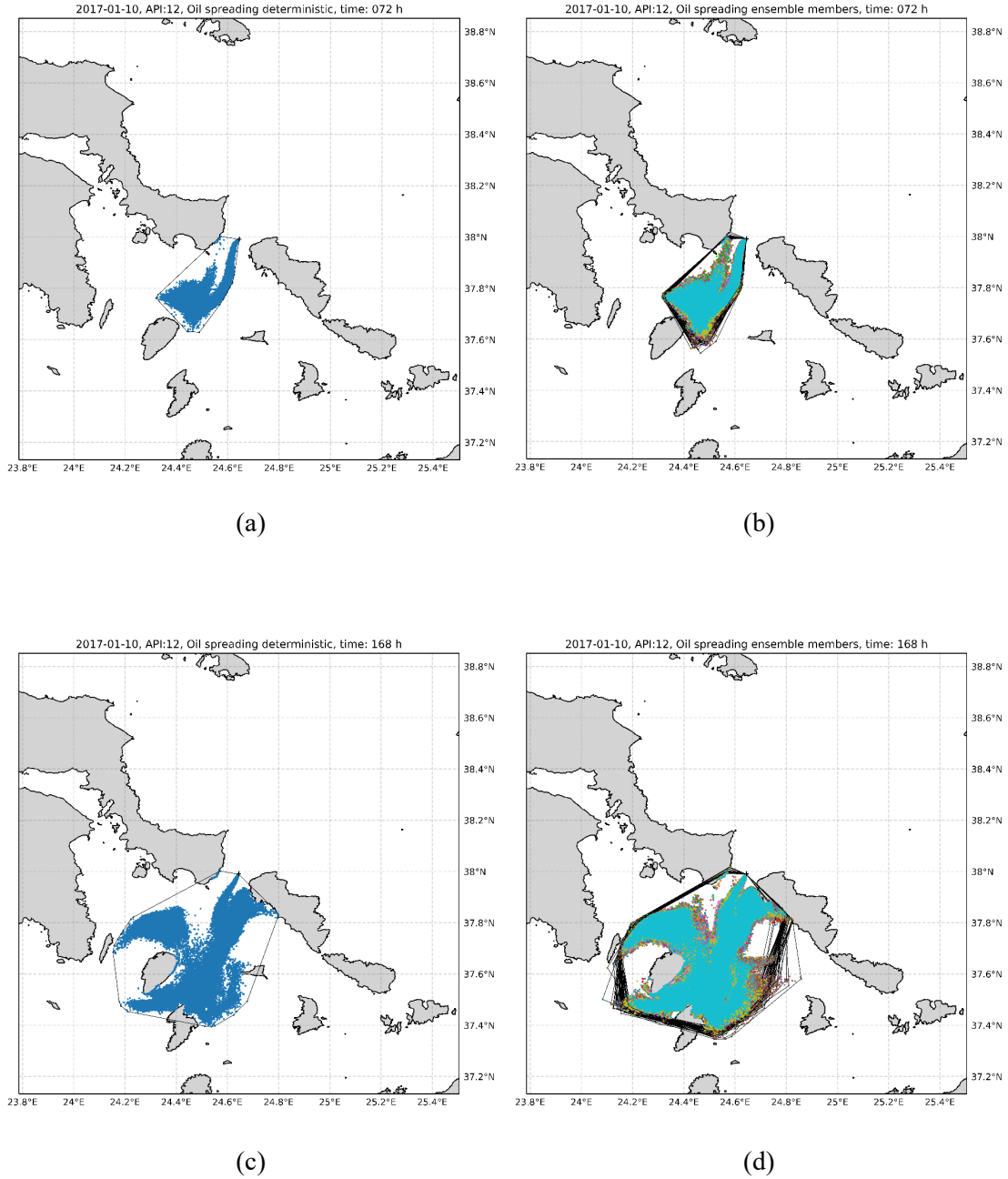

(a) (b)

(c) (d)

Figure A.9: Oil spreading of deterministic and ensemble members for winter, oil API: 12 and simulation time of (a - b) 72 hours and (c - d) 168 hours.

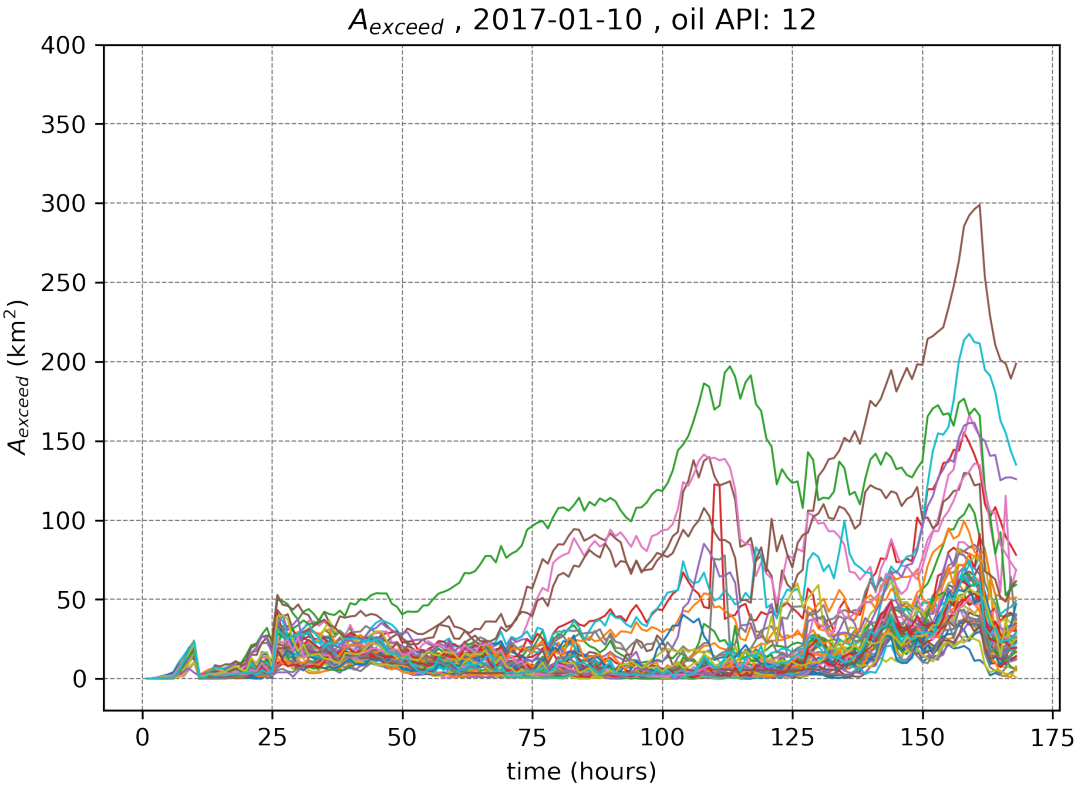

Figure A.10: Area of deterministic oil spill that exceeds the area of each ensemble member (A_{exceed}), for winter and oil API: 12.

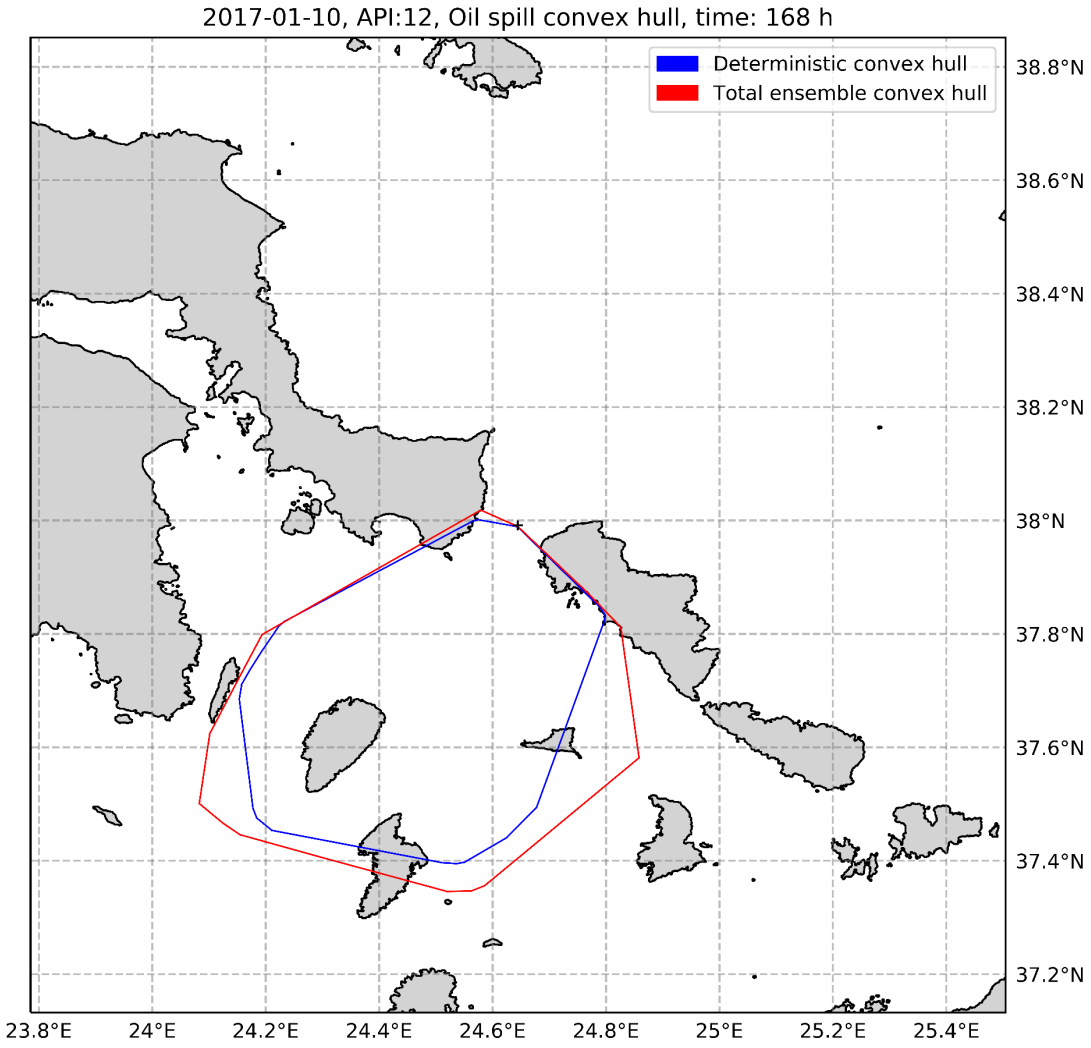

Figure A.11: Oil spill convex hull for the deterministic and the total ensemble, for winter, oil API: 12 and 168h.

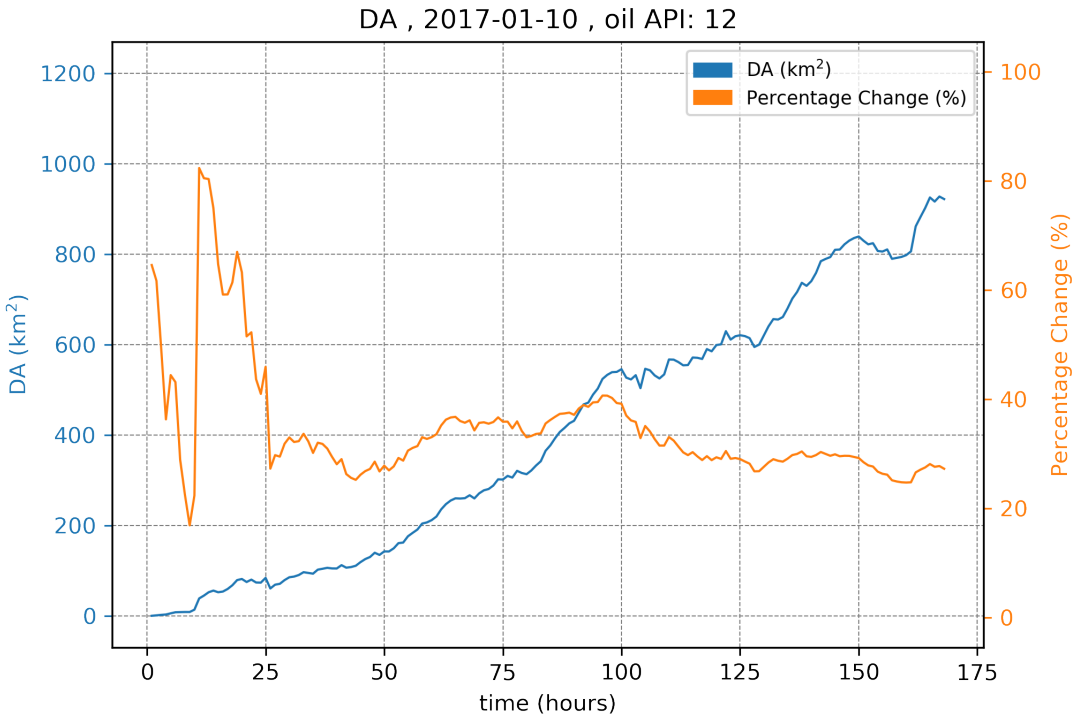

Figure A.12: Area difference (DA) and percentage change between the deterministic and the total ensemble convex hull, for winter, and oil API: 12.

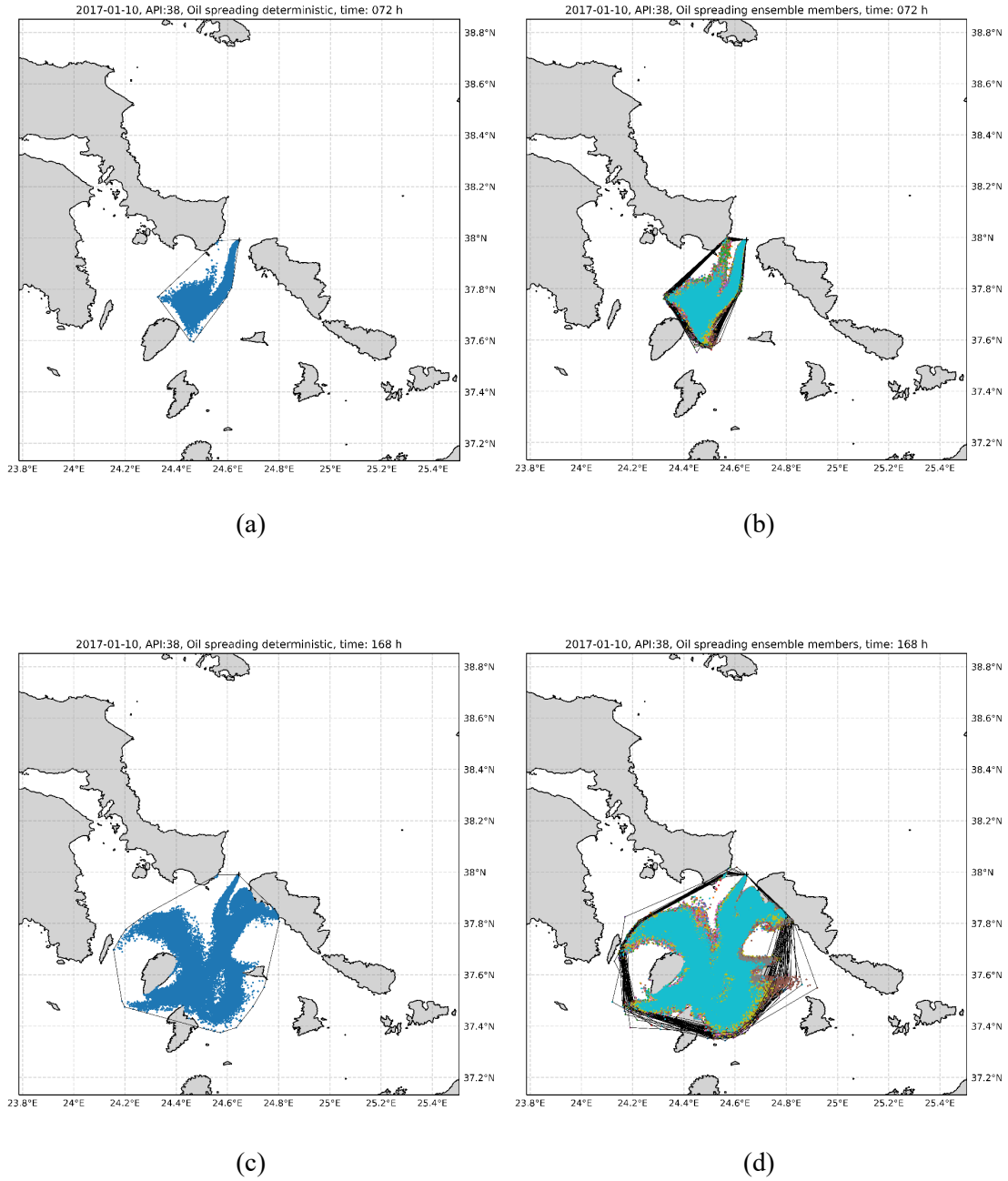

Figure A.13: Oil spreading of deterministic and ensemble members for winter, oil API: 38 and simulation time of (a - b) 72 hours and (c - d) 168 hours.

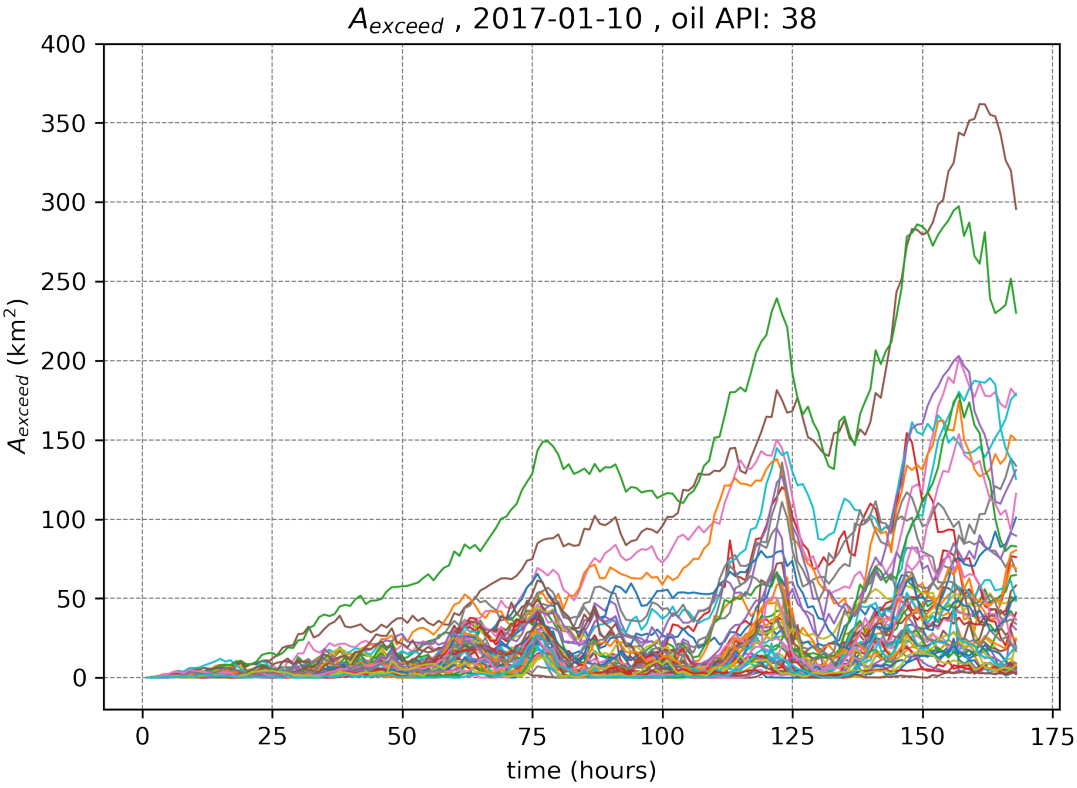

Figure A.14: Area of deterministic oil spill that exceeds the area of each ensemble member (A_{exceed}), for winter and oil API: 38.

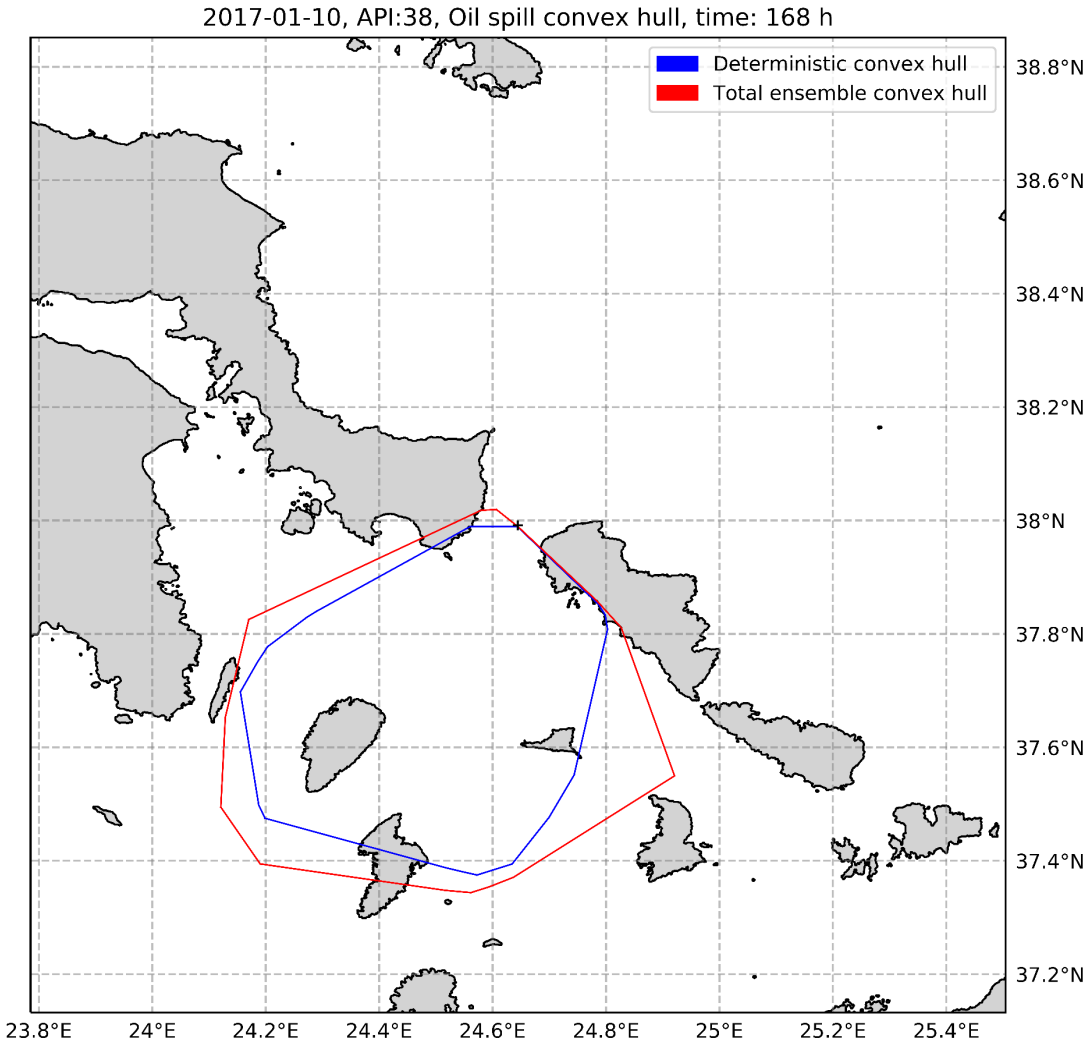

Figure A.15: Oil spill convex hull for the deterministic and the total ensemble, for winter, oil API: 38 and 168h.

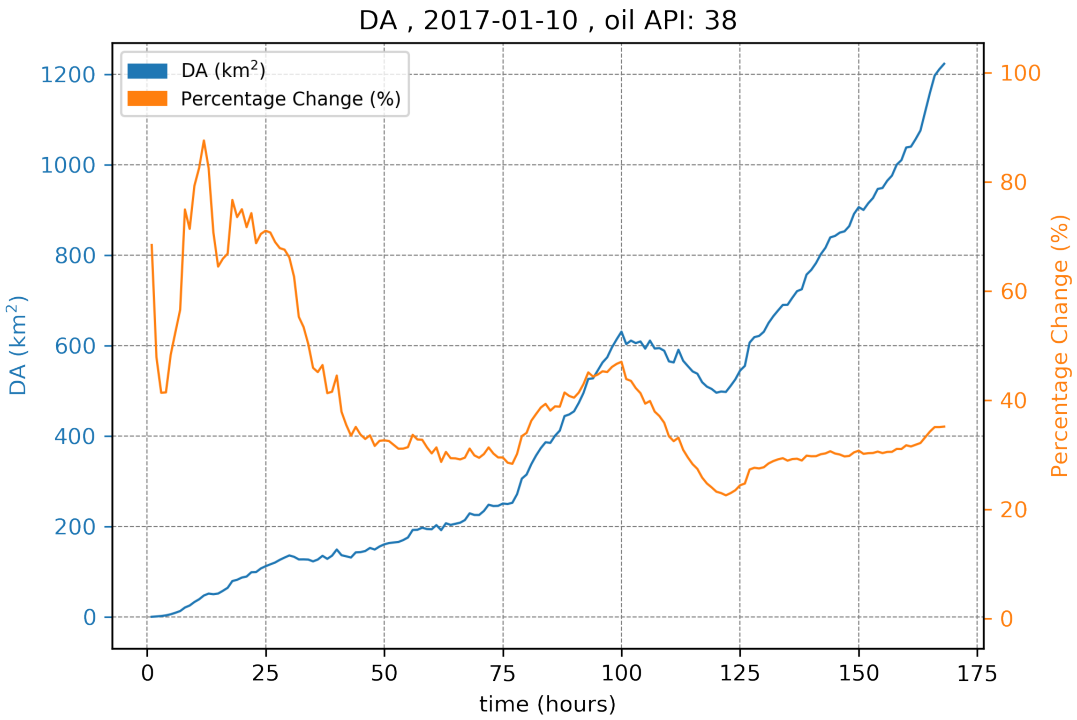

Figure A.16: Area difference (DA) and percentage change between the deterministic and the total ensemble convex hull, for winter, and oil API: 38.

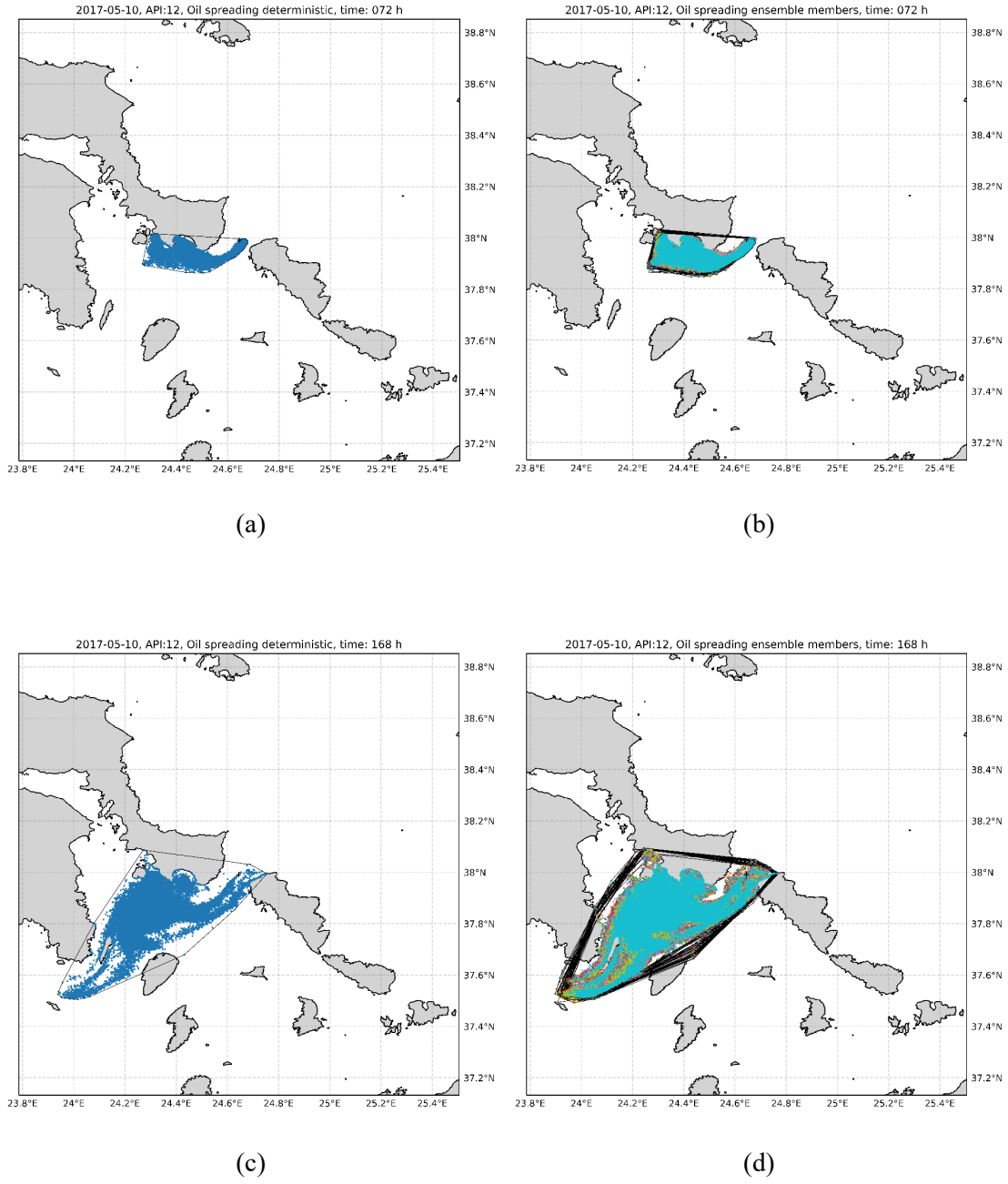

Figure A.17: Oil spreading of deterministic and ensemble members for spring, oil API: 12 and simulation time of (a - b) 72 hours and (c - d) 168 hours.

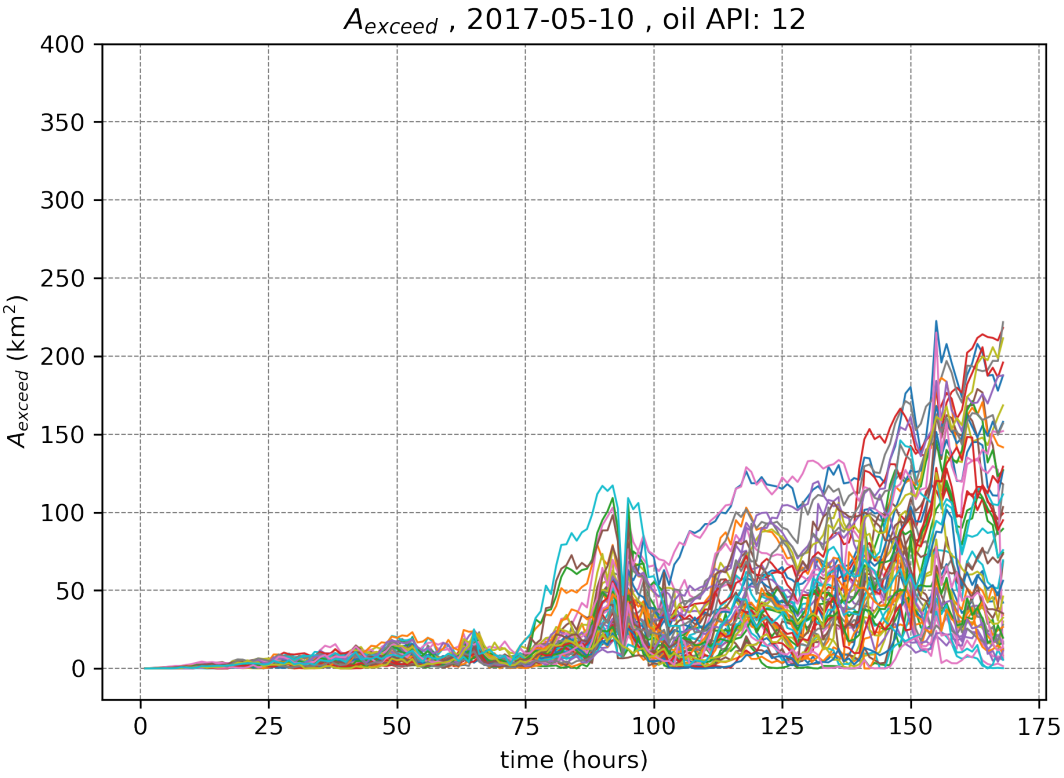

Figure A.18: Area of deterministic oil spill that exceeds the area of each ensemble member (A_{exceed}), for spring and oil API: 12.

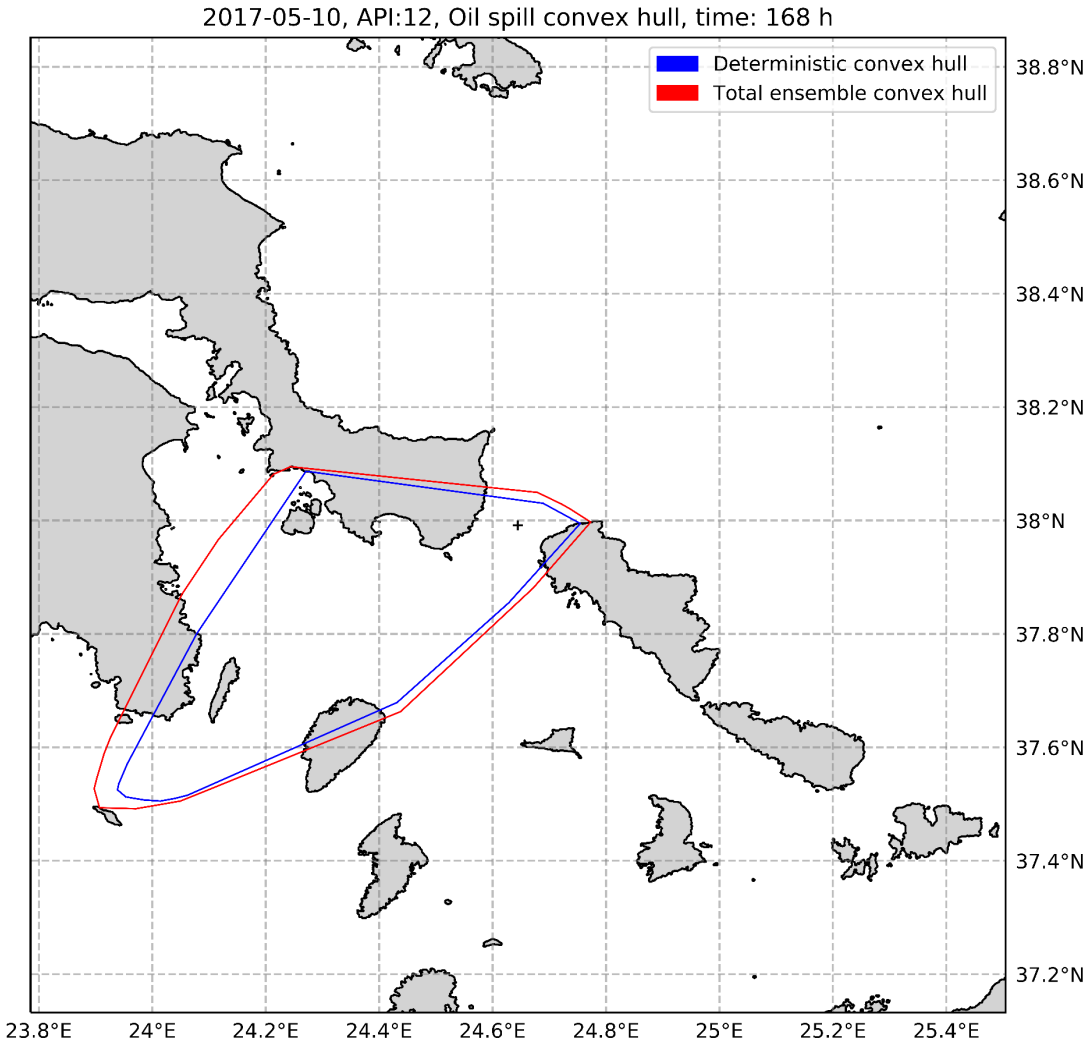

Figure A.19: Oil spill convex hull for the deterministic and the total ensemble, for spring, oil API: 12 and 168h.

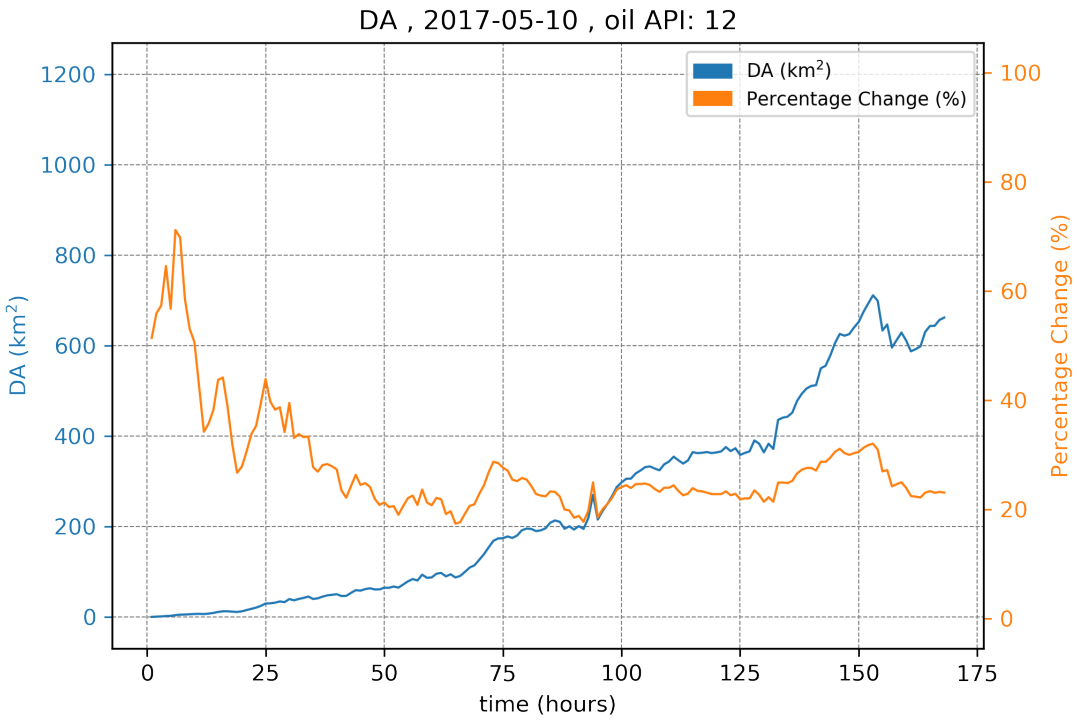

Figure A.20: Area difference (DA) and percentage change between the deterministic and the total ensemble convex hull, for spring, and oil API: 12.

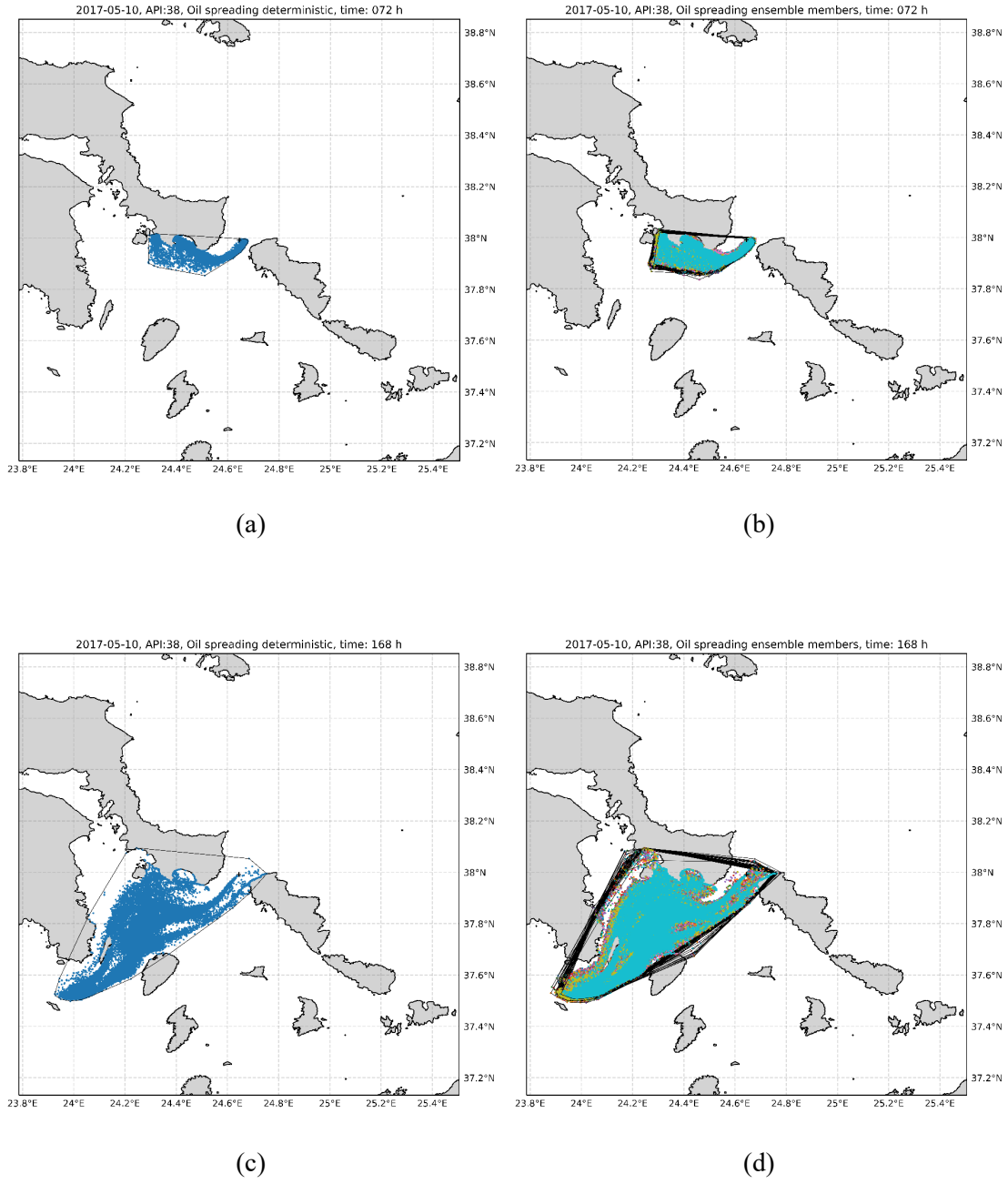

Figure A.21: Oil spreading of deterministic and ensemble members for spring, oil API: 38 and simulation time of (a - b) 72 hours and (c - d) 168 hours.

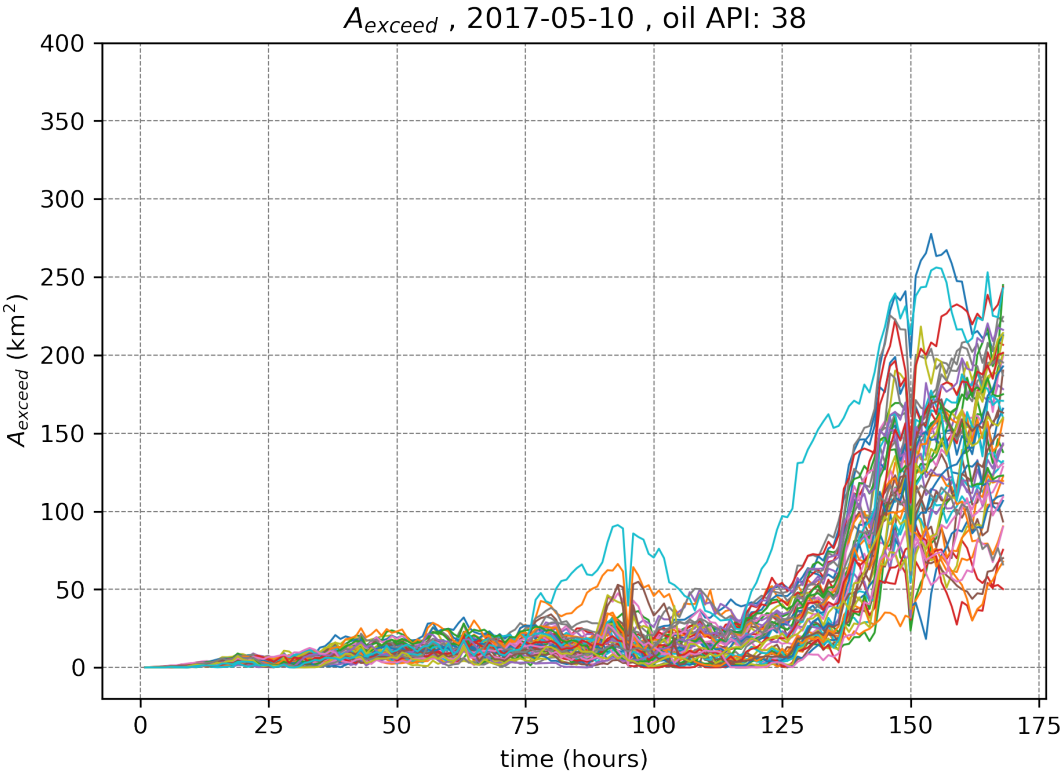

Figure A.22: Area of deterministic oil spill that exceeds the area of each ensemble member (A_{exceed}), for spring and oil API: 38.

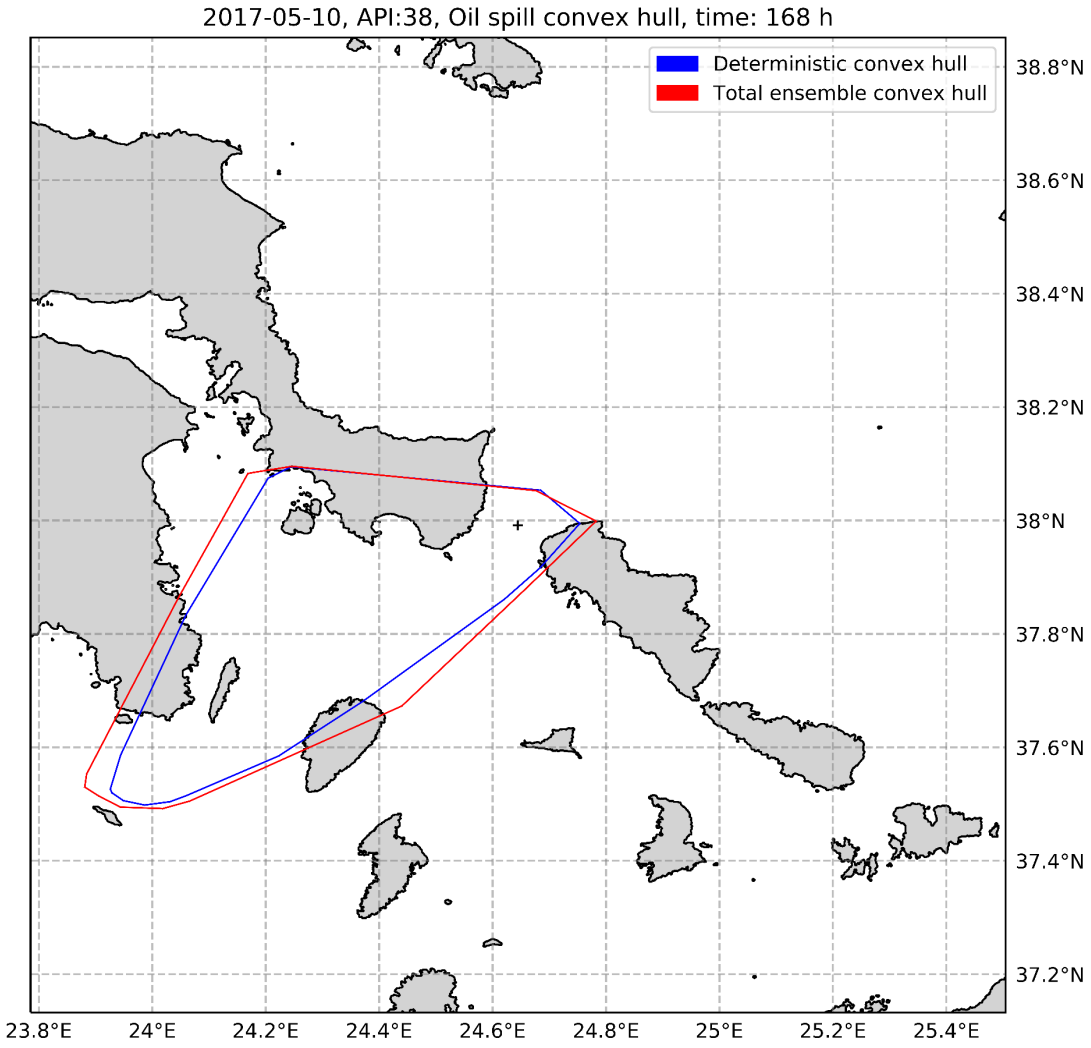

Figure A.23: Oil spill convex hull for the deterministic and the total ensemble, for spring, oil API: 38 and 168h.

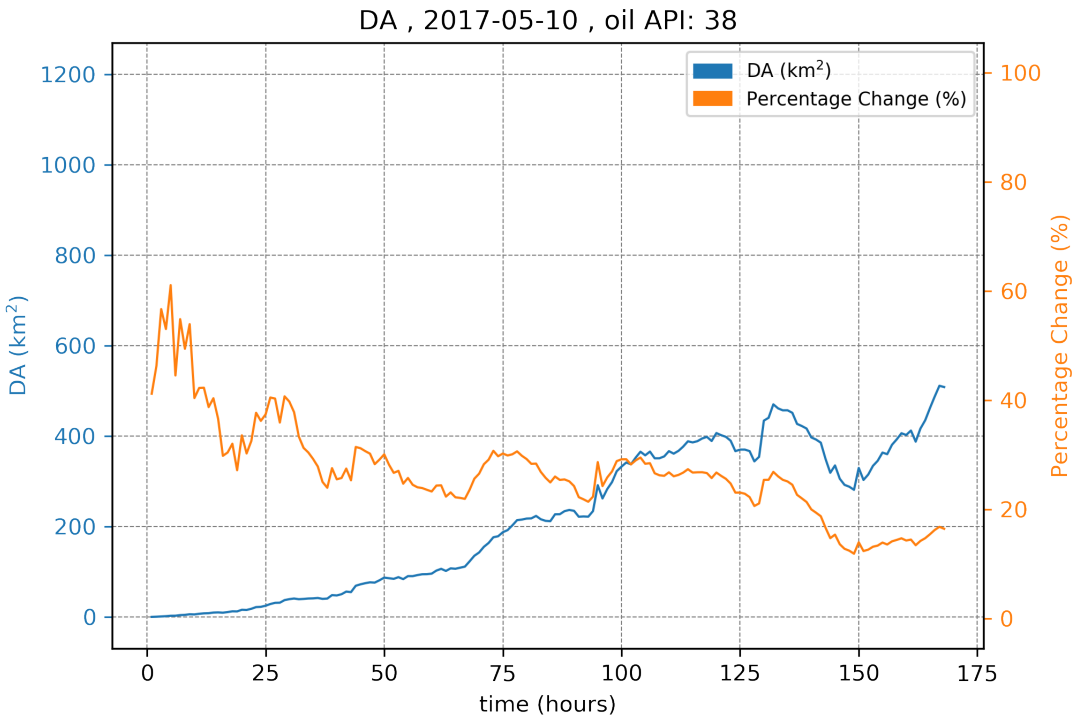

Figure A.24: Area difference (DA) and percentage change between the deterministic and the total ensemble convex hull, for spring, and oil API: 38.

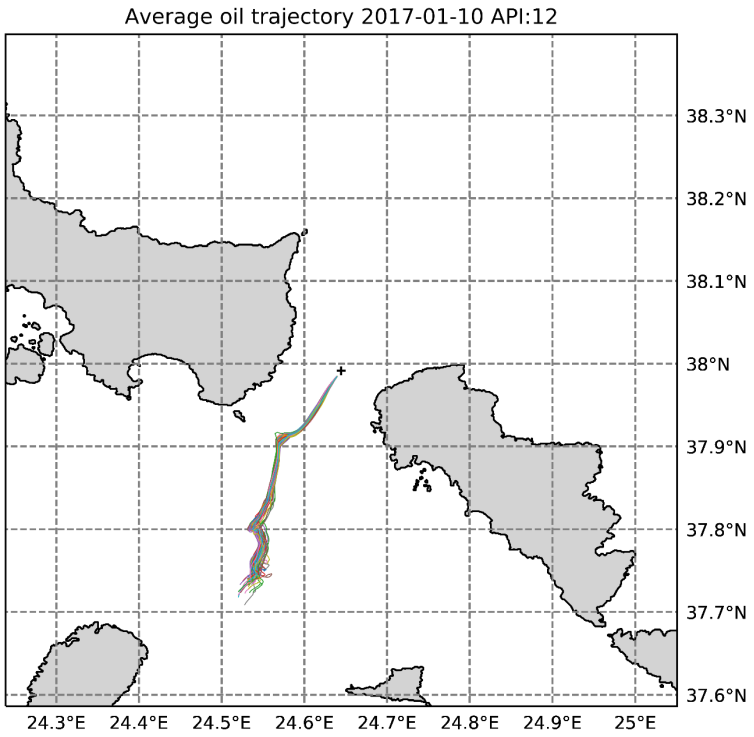

(a)

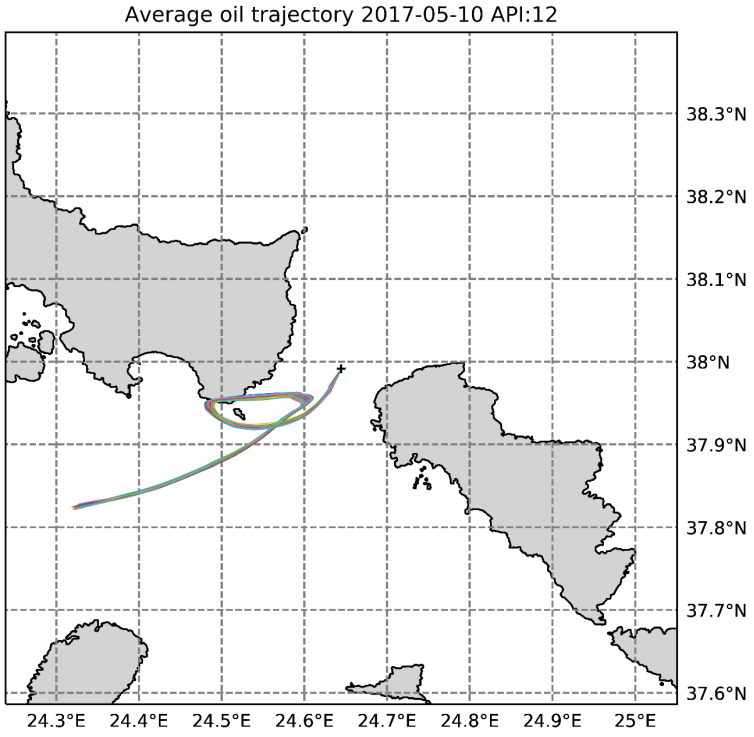

(b)

Figure A.25: Mean coordinates trajectory of each ensemble member for API 12, simulation time of 168 hours and two time periods: (a) winter, (b) spring.

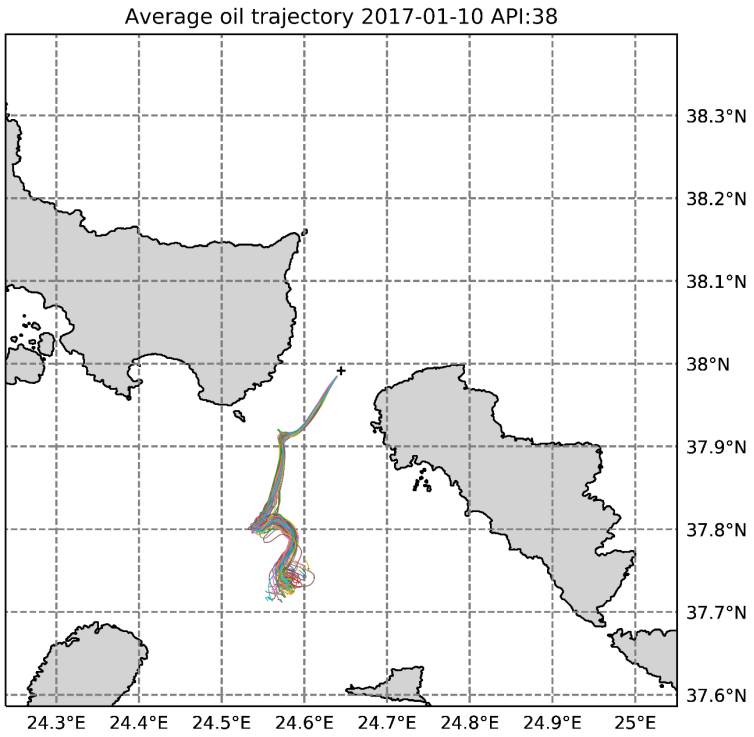

(a)

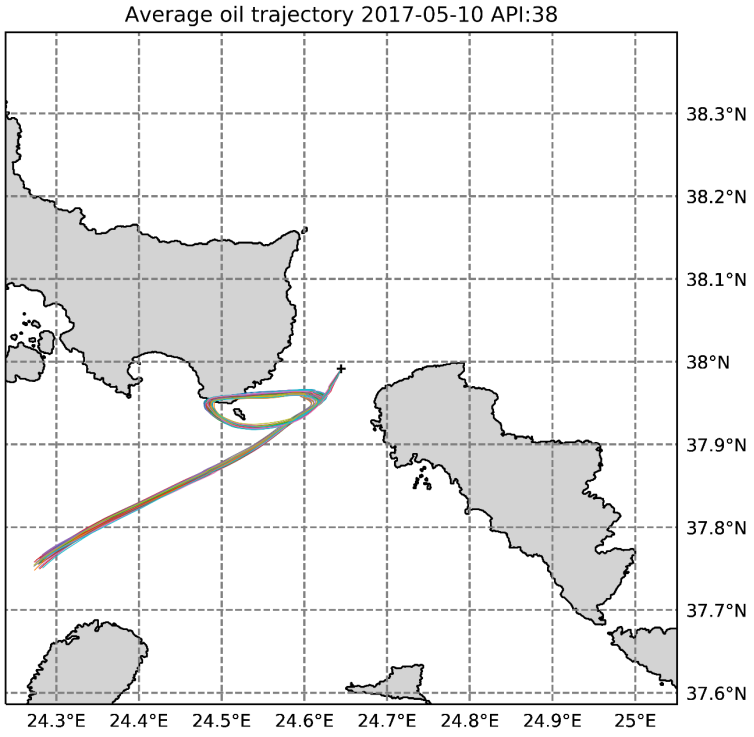

(b)

Figure A.26: Mean coordinates trajectory of each ensemble member for API 38, simulation time of 168 hours and two time periods: (a) winter, (b) spring.

Appendix B: Beached oil (oil API: 12 & 38)

B1 Beached oil maps

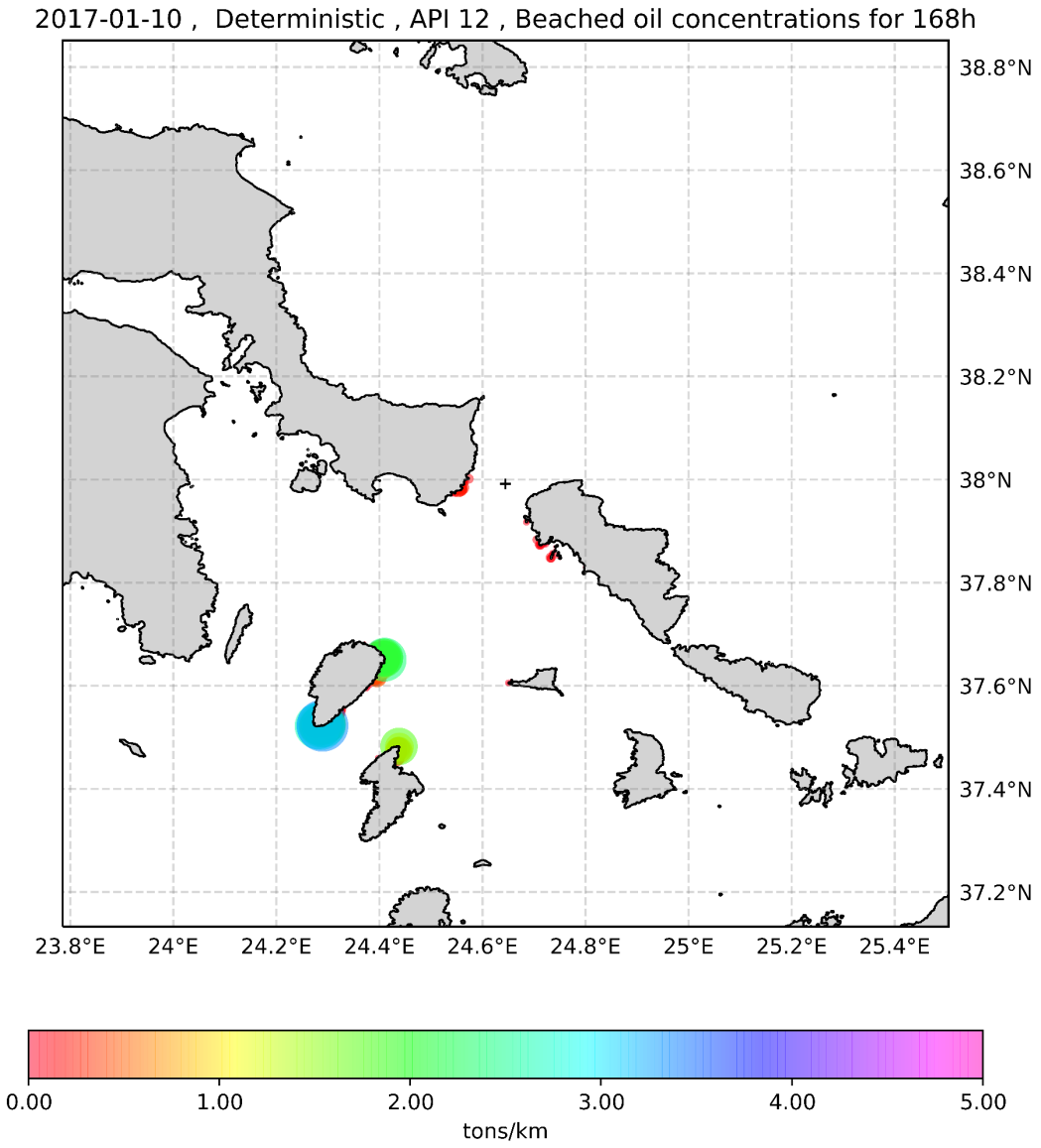

Figure B.1: Beached oil concentrations of deterministic simulation for winter, simulation time of 168 hours and 12 API.

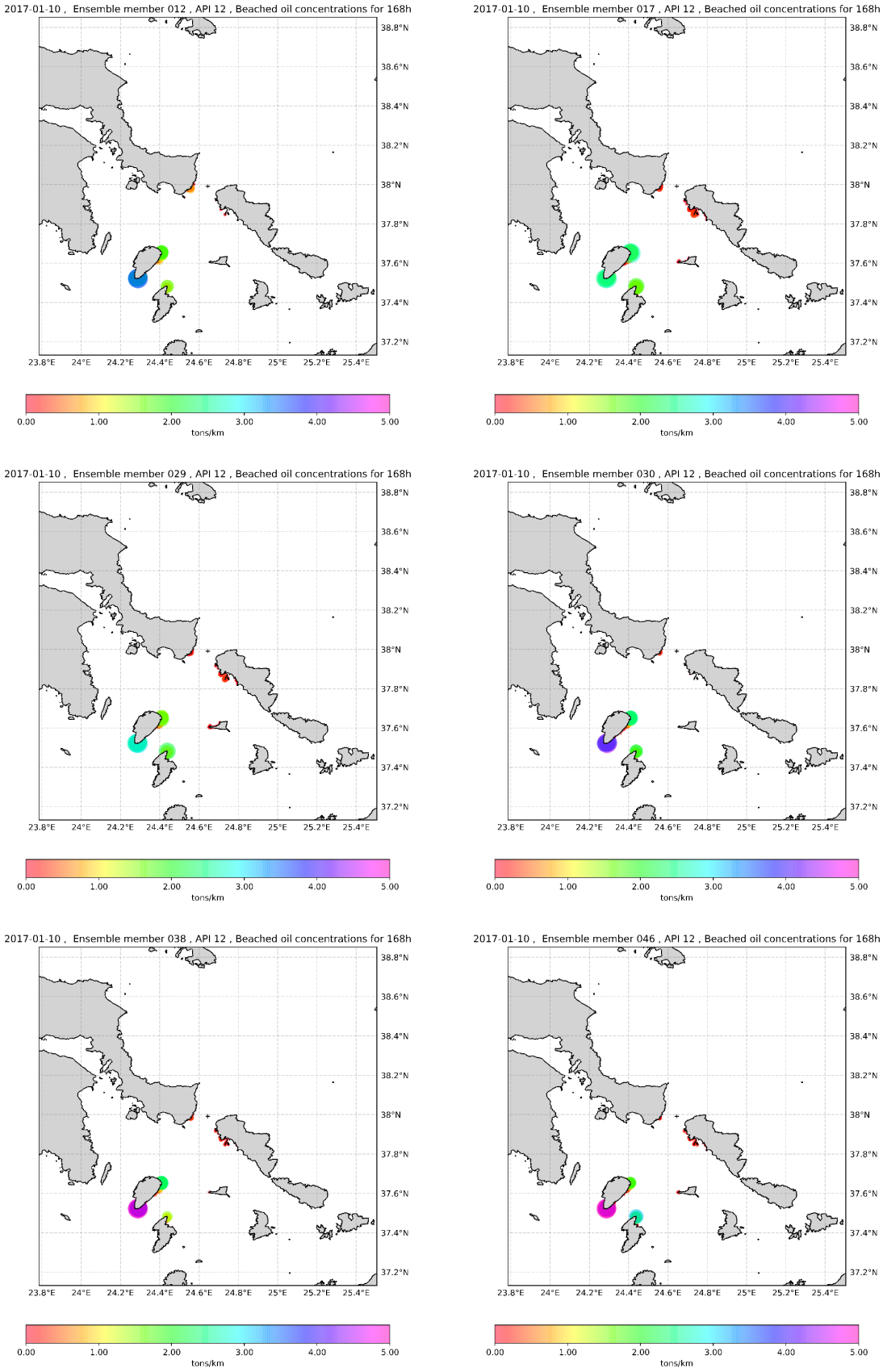

Figure B.2: Beached oil concentrations of some of the ensemble members for winter, API 12 and simulation time of 168 hours.

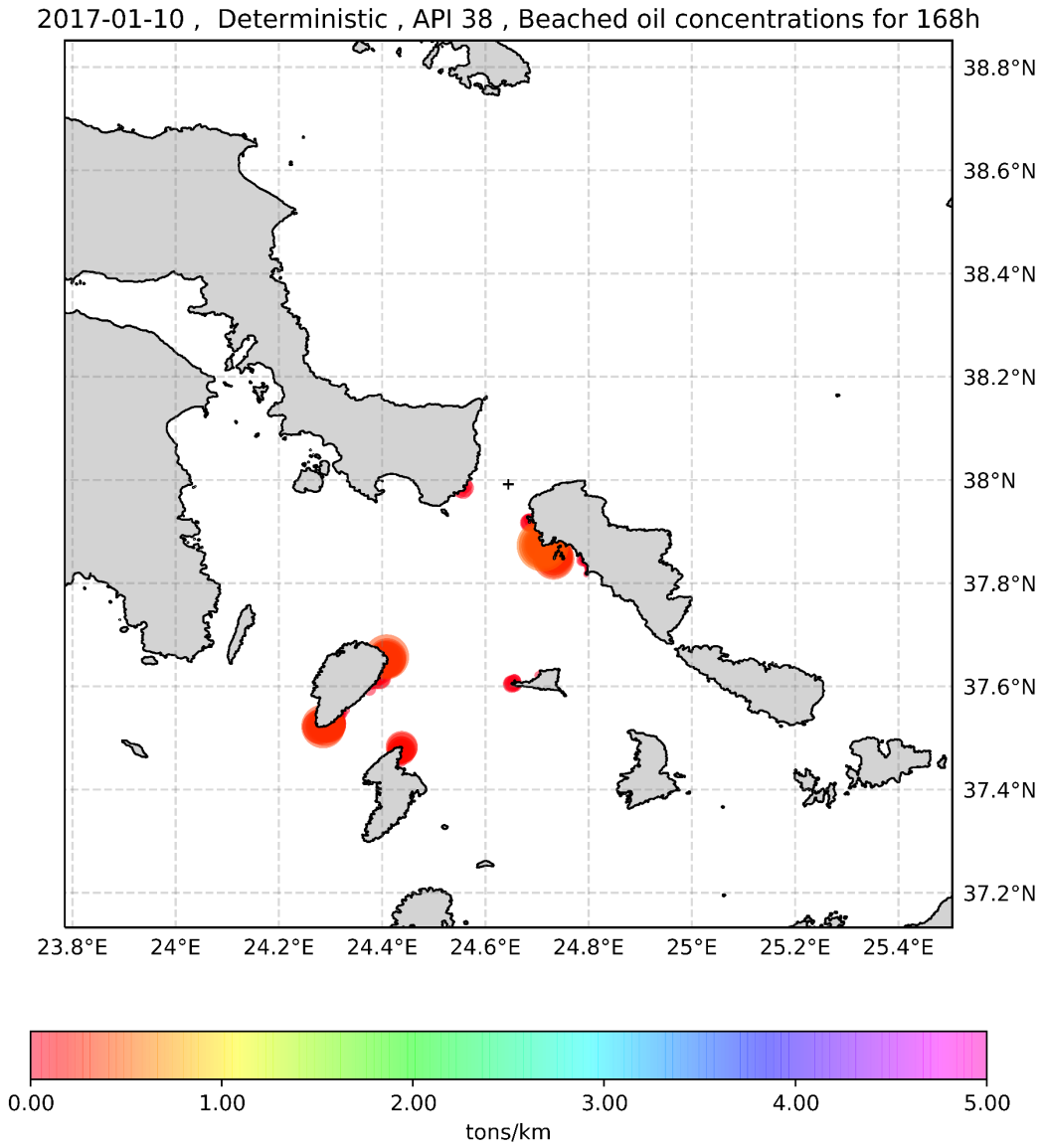

Figure B.3: Beached oil concentrations of deterministic simulation for winter, simulation time of 168 hours and 38 API.

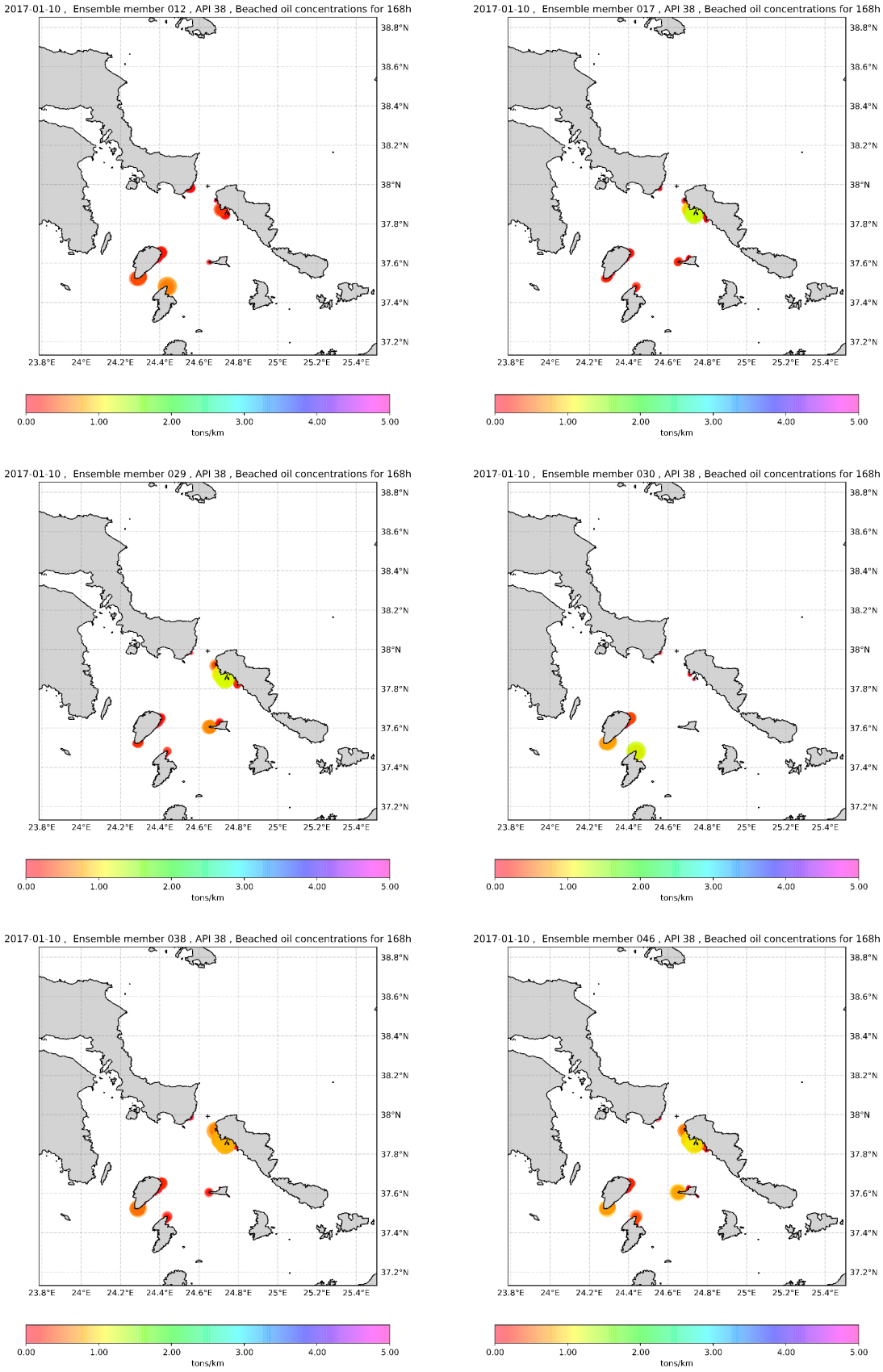

Figure B.4: Beached oil concentrations of some of the ensemble members for winter, API 38 and simulation time of 168 hours.

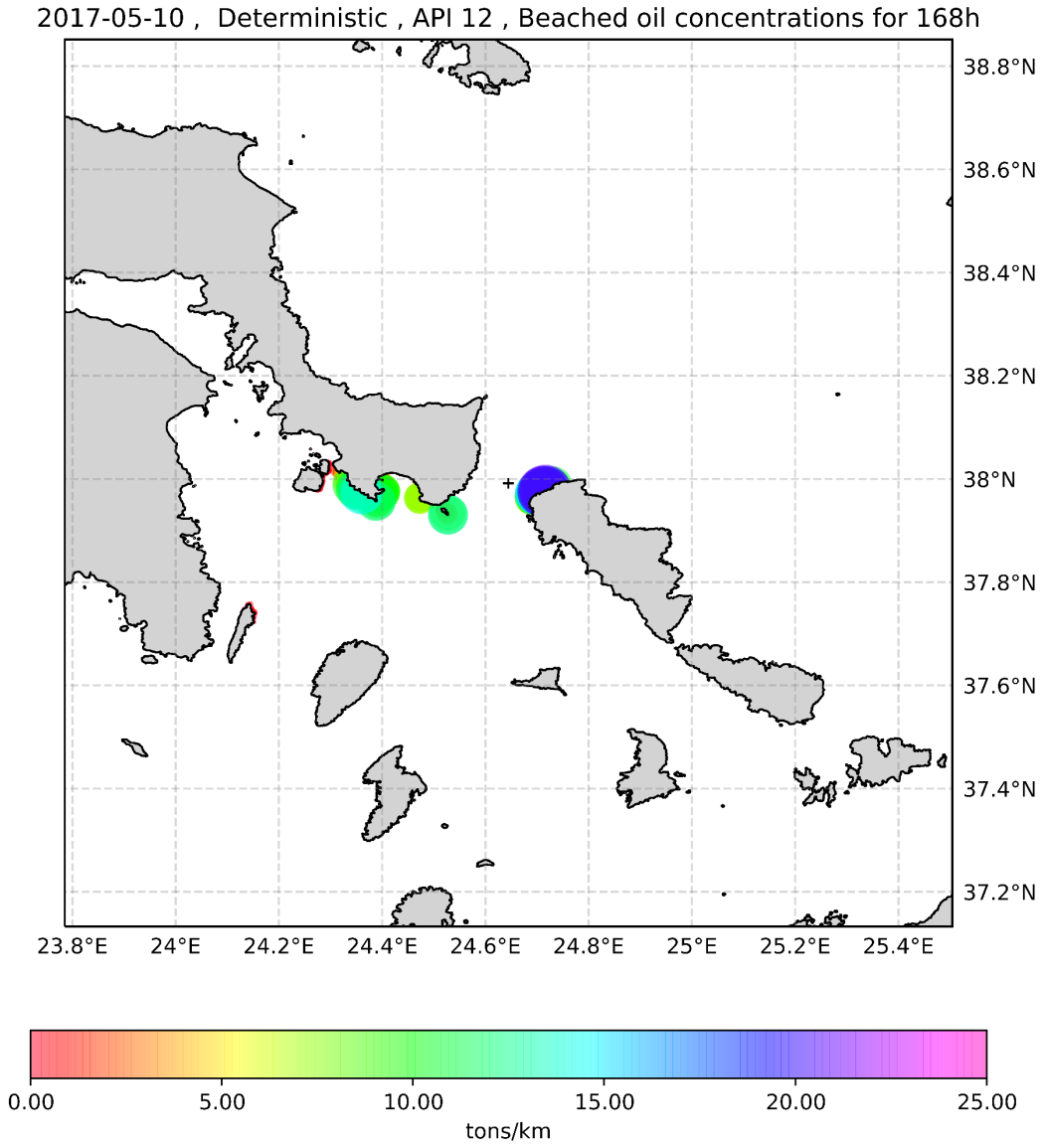

Figure B.5: Beached oil concentrations of deterministic simulation for spring, simulation time of 168 hours and 12 API.

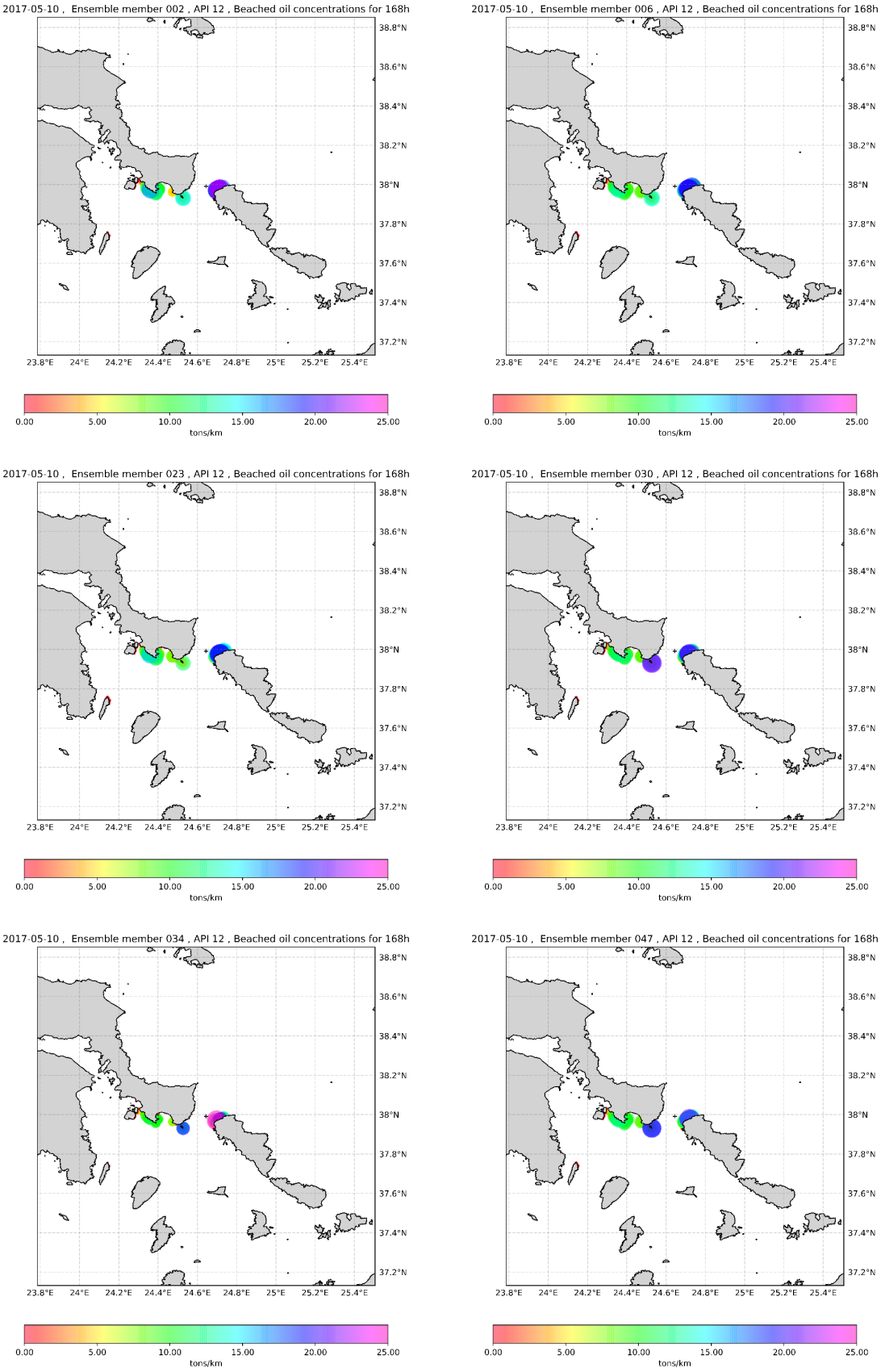

Figure B.6: Beached oil concentrations of some of the ensemble members for spring, API 12 and simulation time of 168 hours.

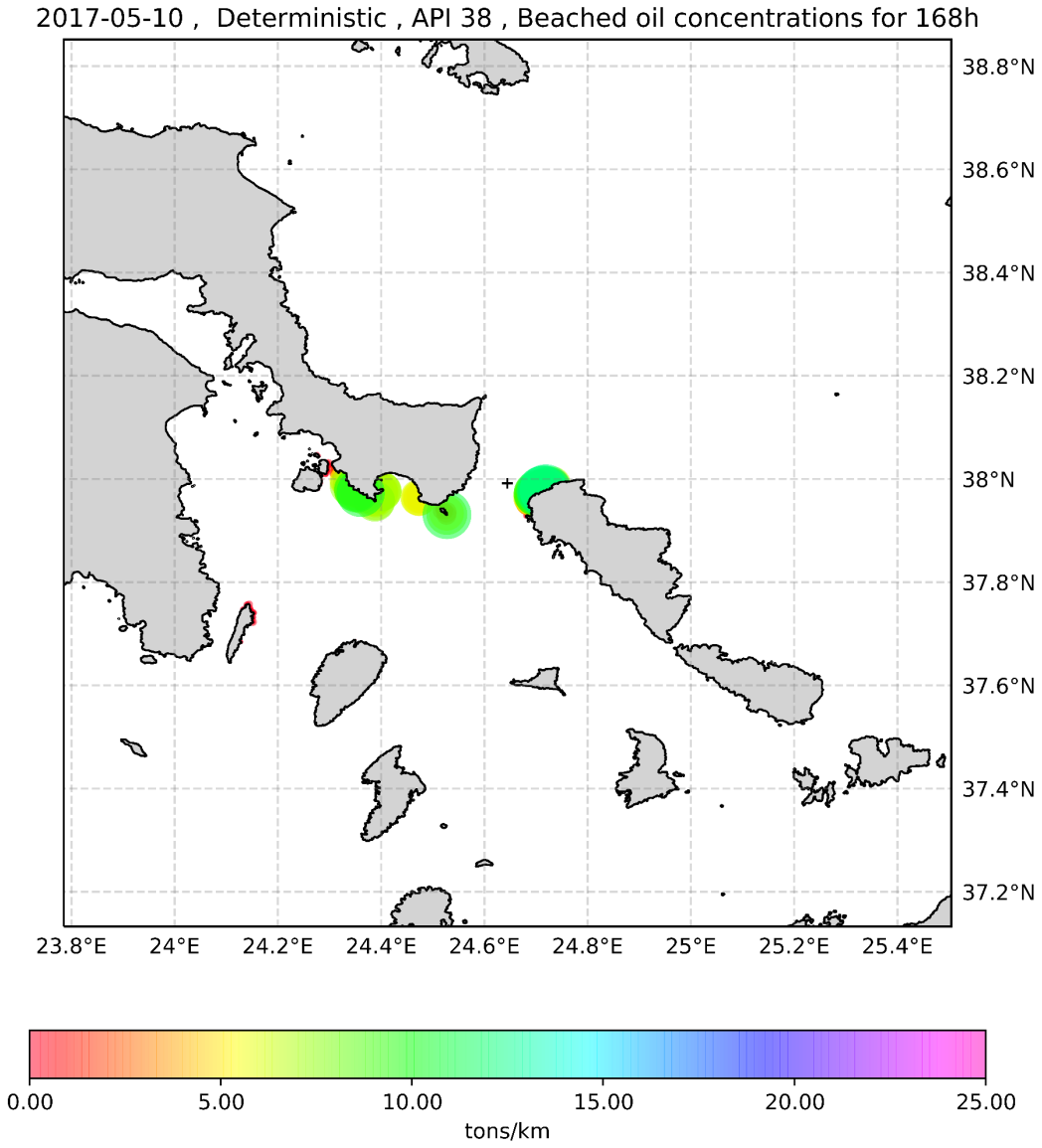

Figure B.7: Beached oil concentrations of deterministic simulation for spring, simulation time of 168 hours and 38 API.

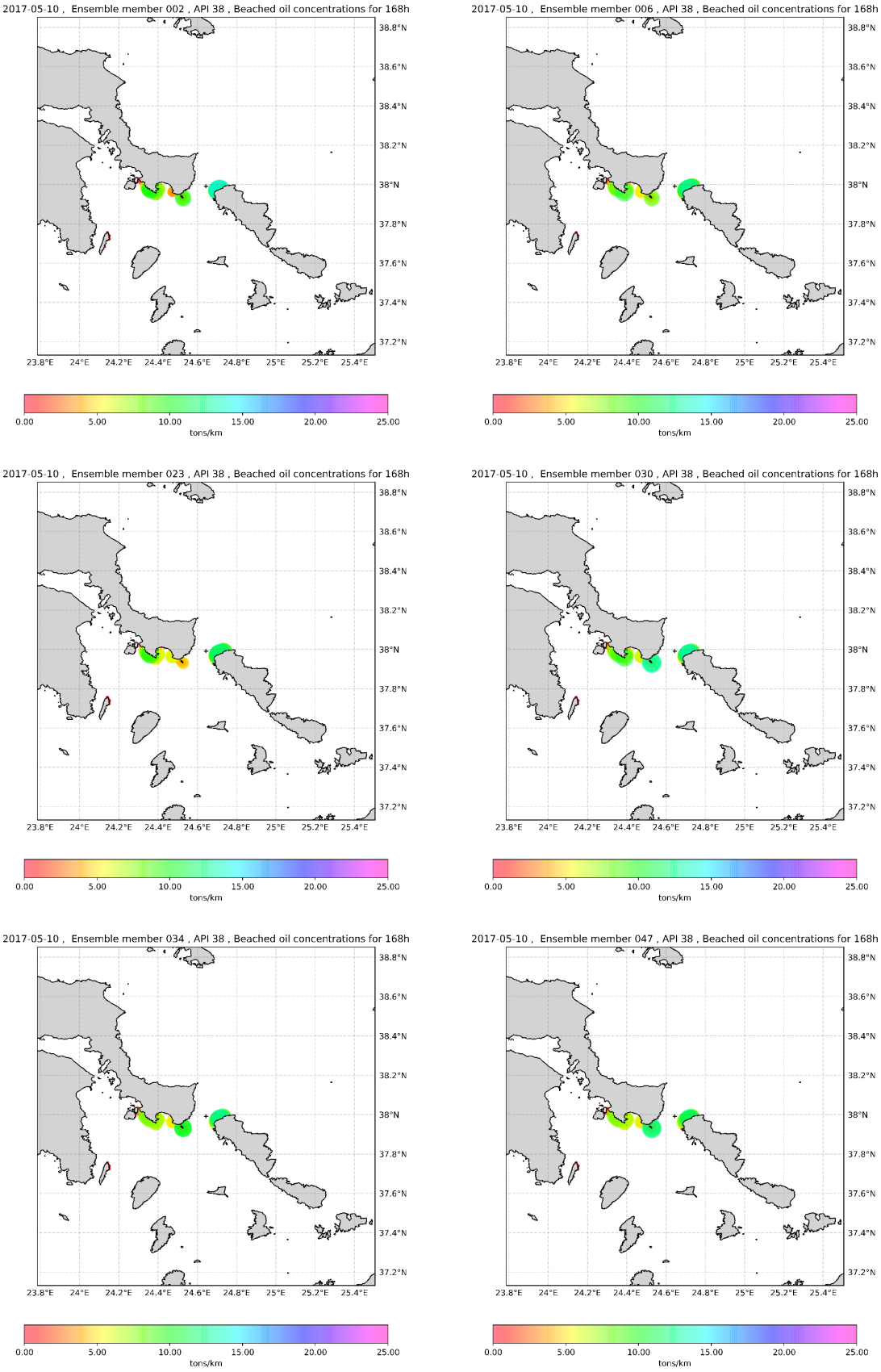

Figure B.8: Beached oil concentrations of some of the ensemble members for spring, API 38 and simulation time of 168 hours.

B2 Uncertainty assessment for beached oil

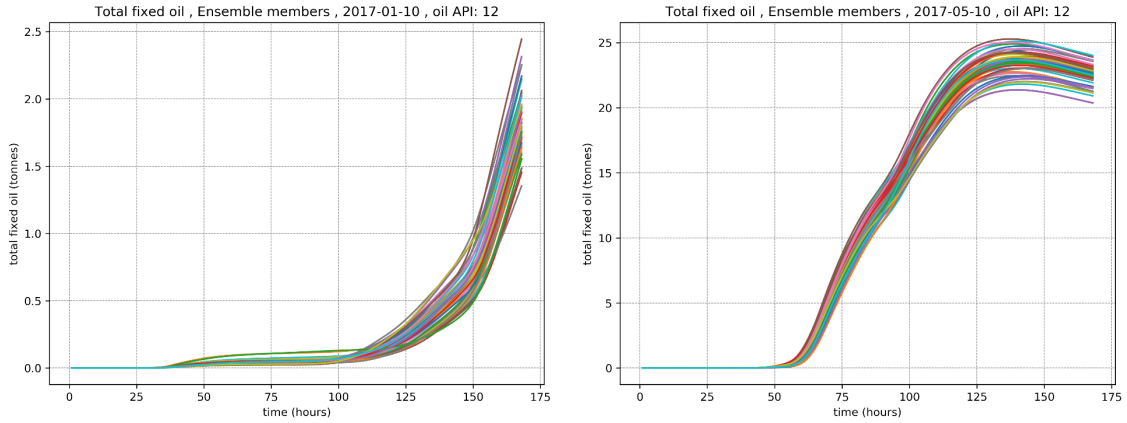

(a) (b)

Figure B.9: Total fixed oil of each ensemble member for API: 12 and two time periods: (a) winter, (b) spring.

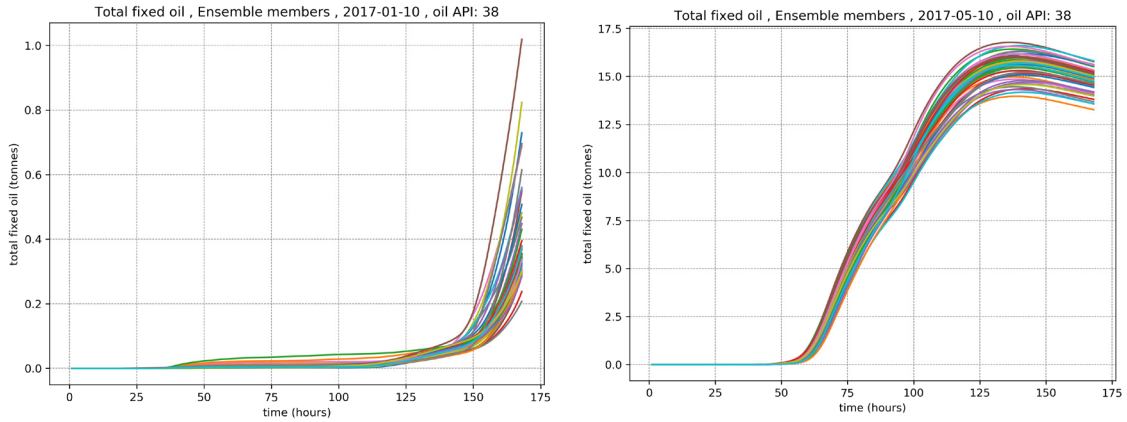

(a) (b)

Figure B.10: Total fixed oil of each ensemble member for API: 38 and two time periods: (a) winter, (b) spring.